Effect of Radiation and Immune Checkpoint Blockade (ICB) on Tumor Metastasis

by

Lam Sai Kit

Medical Physics Program
Duke Kunshan University and Duke University

Date:_____
Approved:

_____
Gregory M. Palmer, Co-Supervisor

_____
Mark W. Dewhirst, Co-Supervisor

_____
David Huang

A thesis submitted in partial fulfillment of the requirements for the degree of
Master of Science in the Medical Physics Program
in Duke Kunshan University and Duke University

2017

ABSTRACT

Effect of Radiation and Immune Checkpoint Blockade (ICB) on Tumor Metastasis

by

Lam Sai Kit

Medical Physics Program
Duke Kunshan University and Duke University

Date:_____
Approved:

_____
Gregory M. Palmer, Co-supervisor

_____
Mark W. Dewhirst, Co-supervisor

_____
David Huang

An abstract of a thesis submitted in partial fulfillment of the requirements for
the degree of Master of Science in Medical Physics Program
in Duke Kunshan University and Duke University

2017

Copyright © 2017 by Lam Sai Kit

Abstract

Background: PD-L1 (Programmed Death Ligand 1) is an immune checkpoint molecule that is commonly expressed on the surface of cancer cells. When it interacts with its receptor – the PD-1 molecule, which is commonly expressed on the surface of immune cells, such as T-cells, it will then deliver a negative signal which in turn inactivates the T-cell function, depresses the T-cell expansion, and dampens the overall tumor response. Anti-PD-L1 antibody blocks the direct interaction between the PD-L1 and PD-1 molecules, thus inhibits the PD-L1 signaling pathways, enabling the immune system, and hence the anti-tumor immunity, to eliminate the cancer cells. We refer to these mechanisms as the Immune Checkpoint Blockade (ICB).

Methods and Materials: In the current study, we report the effects of combination treatment of radiation and ICB on tumor metastasis. A single radiation dose of 10 Gy was used to irradiate the dorsal fat pad region of mice, into which the E0771-luc breast cancer cells were injected. For the ICB treatment, anti-PD-L1 antibody was used. We established a spontaneous metastatic model using E0771-luc breast cancer cells. As the tumor grew, primary tumor growth was monitored using calipers. We then examined the metastatic lung lesions by using In-Vivo Imaging System (IVIS), the signals from IVIS were then quantified in terms of total photon flux (photons/second). An India-Ink Assay was also employed to further verify the lung mass formations. In addition,

variation of primary tumors' hemoglobin saturation levels and total hemoglobin levels were recorded before and after treatments using zenascope, for the sake of assessing the vascular oxygenation and vascularity information, respectively.

Principal Findings: Data from calipers' measurement showed that the RT-alone group did not show any effects on tumor growth. Tha anti-PD-L1-alone group showed a slightly delayed tumor growth. The combination treatment showed that 3 out of 5 mice showed tumor growth delay, while the tumor regrew after 20 days. Furthermore, survival curves indicated that there is no significant difference among all groups, indicating that radiation treatment or anti-PD-L1 antibody or the combination of both treatments did not affect the time at which the mice reach their endpoints (tumor volume ≥ 1500mm^3). In addition, data from the IVIS indicated that the total photon flux emitted from primary tumors varied dramatically among experimental subjects within the same group. There were also extremely low or no luciferase signals from the lung. Statistically, two-way ANOVA for IVIS data showed that there are no significant differences between the RT-alone or anti-PD-L1-alone or RT + anti-PD-L1 group and the control group, for both primary tumors and lung tissue, suggesting that all kinds of treatments used in the current study neither helped eliminate the primary tumor cells nor reduced the burden of metastatic cancer cells in lungs, compared to the control group. Interestingly, results from the India-ink Assay showed that grossly visible lung

nodules were **not** observed in all lungs of the mice, suggesting that the primary tumors in the dorsal fat pad region did not result in grossly visible lung metastases in any groups. Furthermore, analysis for the Zenascope data showed that there was a gradual increase in Hb-Sat(%) in mice for the control group, while a gradual decrease in Hb-Sat(%) for the anti-PD-L1-alone group. The RT-alone group did not show a clear response of change in Hb-Sat. For the combination treatment group, 3 out of 4 mice demonstrated a relatively flat response of change in Hb-Sat(%). Lastly, the total Hb levels in the control group, the anti-PD-L1-alone group and the combination treatment group remained relatively stable over the treatment time. For the RT-alone group, 3 out of 5 mice showed almost no changes, while the other two demonstrated a huge increase in total Hb levels on day 0, and day 2, respectively, but the levels went back to almost the pre-treatment values after day 3.

Conclusions: The combination treatment of 10 Gy of radiation and anti-PD-L1 antibodyimmunotherapy did not show significant effects on E0771 primary tumor growth when using an orthotopic tumor model. The time required for the tumor volume to exceed an endpoint of 1500mm^3 was not significantly affected by all of the treatment methods used in the current study. The results from the IVIS and the India-ink Assay suggest that E0771 might not a good model for lung metastasis. However, the treatment response and the E0771 model were affected by a number of technical problems that render the evaluation inconclusive. Solutions to some of these technical problems have

been provided, enabling future reseachers to replicate and improve on this study and futher determine the treatment response and the usefulness of the E0771 model. Regarding the zenascope measurement, the changes in Hb-Sat(%) may be correlated with the blood vessel growth within the primary tumors, while the changes in total Hb were almost negligible. Nevertheless, several limitions when performing the zenascope measurement have been listed, including the pigmentation and fur of the skin of mice, the motion of the mice and/or the operator's hands, as well as the uncertainties in placing the optical probe onto the tumor. Further research is needed to uncover the promise of this combined therapy and to further verify the correlation among the changes in Hb-Sat(%), the changes in total Hb levels, and the tumor physiological characteristics.

Contents

Abstract iv

List of Tables xi

List of Figures xiiii

Acknowledgements xivv

1. Introduction 1

1.1 Challenges of the Conventional Cancer Treatments and Some Kinds of Immune Therapies 1

1.2 Emerging Hallmark of Cancer – Evading Immune Destruction and the Solution to Deal with It 1

1.3 Immune Checkpoints 2

1.4 Immune Checkpoint Blockade (ICB) 3

1.5 Combination of ICB and Radiation 4

1.5.1 Pre-clinical studies in animal models 5

1.5.2 Clinical Trials in patients 5

1.6 Rationales for Targeting PD-L1 6

2. Methods and Materials 8

2.1 Cell Culture 8

2.2 Luciferase Assay 8

2.3 Animals and Cell Implantation 8

2.4 Radiation Therapy for Orthotopically Transplanted Tumors 9

2.5 Tumor Volume Measurement 12

2.6 Zenalux Biomedical Zenascope 12
2.7 In-Vivo Imaging System (IVIS) on the day of euthanasia 13
2.8 India-Ink Assay 14
2.9 Drugs 14
2.10 Statistical Analysis 15
3. Results 16
3.1 Primary Tumor Growth 16
3.1.1 Control Group 16
3.1.2 Radiation-alone Group 17
3.1.3 Anti-PD-L1-alone Group 17
3.1.4 Radiation and Anti-PD-L1 Group 18
3.1.5 Comparison among Different Groups 18
3.2 Survival Curves 21
3.3 IVIS Data - Primary Tumors and Lung Metastases 26
3.4 India-Ink Assay 34
3.5 Zenascope Measurement 34
3.5.1 Changes in Hemoglobin Saturation (Hb-Sat) Levels 34
3.5.2 Changes in Total Hemoglobin (Hb) Levels 36
4. Discussion 38
4.1 Primary Tumor Growth and Survival Curves 43
4.1.1 Caliper Measurement and Survival Plots 43
4.1.2 In-Vivo Imaging System (IVIS) 46

4.2 Lung Metastases 47
4.2.1 In-Vivo Imaging System (IVIS) 48
4.2.2 India-ink Assay 52
4.3 Zenascope Measurement 52
4.4 Future Study 53
5. Conclusions 56
6. Appendix A 57
7. Appendix B 97
8. References 99

List of Tables

Table 3.1.1: A table shows amount of days required for each tumor to reach the limit of volume ≥1500mm^3. 20

Table 3.2.1: A table shows a comparison of survival curves among all 4 groups. 22

Table 3.2.2: A table shows a comparison of survival curves between RT-alone group and Control group. 23

Table 3.2.3: A table shows a comparison of survival curves between anti-PD-L1-alone group and Control group. 24

Table 3.2.4: A table shows a comparison of survival curves between RT + anti-PD-L1 group and Control group. 25

Table 3.3.1: A table shows the results from multiple comparisons using Two-way ANOVA. (For primary tumors) 32

Table 3.3.2: A table shows the results from multiple comparisons using Two-way ANOVA. (For lung metastases) 33

Table 4.2.1.1: A table shows the results from multiple comparisons using Two-way ANOVA. (For lung metastases, 4T1 model) 50

List of Figures:

Figure 2.3.1: A diagram (without cone) shows that the tumor is labeled with radio-markers (shown as black dots) on the dorsal region of an anesthetized mouse, irradiation takes place at 90 degree orientation..... 10

Figure 2.3.2: A diagram (with cone) shows the irradiation field which is confined to a square shape using a 8mmx12mm cone at 90 degree orientation..... 11

Figure 3.1.1: A plot shows primary tumor growth in control group over the treatment time..... 16

Figure 3.1.2: A plot shows primary tumor growth in RT-alone group over the treatment time..... 17

Figure 3.1.3: A plot shows primary tumor growth in anti-PD-L1-alone group over the treatment time. 17

Figure 3.1.4: A plot shows primary tumor growth in RT + anti-PD-L1 group over the treatment time. 18

Figure 3.1.5: A plot shows changes of median primary tumor volume over time.. 19

Figure 3.2.1: A plot shows percent survival for all 4 groups. 22

Figure 3.2.2: A plot shows percent survival for RT-alone group and Control group. 23

Figure 3.2.3: A plot shows percent survival for anti-PD-L1-alone group and Control group..... 24

Figure 3.2.4: A plot shows percent survival for RT + anti-PD-L1 group and Control group..... 25

Figure 3.3.1: A diagram shows the IVIS image with ROI data (total photon flux in photons/second) for primary tumor of mouse-3 in anti-PD-L1-alone group..... 28

Figure 3.3.2: A diagram shows the IVIS image with ROI data (total photon flux in photons/second) for lung tissue of mouse-3 in anti-PD-L1-alone group..... 28

Figure 3.3.3: A log-plot shows the total photon flux emitted from primary tumor cells for all individual mice. 30

Figure 3.3.4: A log-plot shows the total photon flux emitted from lung tissue for all individual mice.....31

Figure 3.3.5: A plot shows the variation of the median total photon flux emitted from primary tumors for each of four groups.....32

Figure 3.3.6: A plot shows the variation of the median total photon flux emitted from lung tissue for each of four groups.....33

Figure 3.5.1.1: A plot shows the changes in Hb-Sat(%) from the baseline values on the pre-treatment day over time for all individual mice. (Note that some mice are marked with "Suspected" data, such as those with pigment or scar on their skin surface and/or the data appear outside the range of the rest within the same group) 35

Figure 3.5.2.1: A plot shows the changes in total Hb(%) over time for all individual mice from all groups. (Note that some mice are marked with "Suspected" data, such as those with pigment or scar on their skin surface and/or the data appear outside the range of the rest within the same group).....36

Figure 4.1.1.1: A plot shows primary tumor growth over time from Weitzel's study.....43

Figure 4.1.1.2: A survival plot shows percent survival over time from Weitzel's study..44

Figure 4.1.1.3: A survival plot shows percent survival against days post treatment for the current study.....45

Figure 4.2.1: Two plots show tumor volume for primary tumor (left) and secondary tumor (right) changes over time from Weitzel's study. 47

Figure 4.2.1.1: A plot shows the average total photon flux emitted from lung tissue for each of the four groups using 4T1 model..50

Acknowledgements:

I would like to first express my deepest gratitude to both of my co- co-supervisors, Dr. Gregory Palmer and Dr. Mark Dewhirst, for their constructive opinions and patient guidance on my research. They not only offered opportunities for exposure to different research fields at the beginning, but also patiently provided their professional suggestions on my MS thesis. Their guidance helped me throughout research and writing of this thesis. I could not have imagined having better advisors and mentors for my MS research study. In addition to my advisors, I would like to seize this opportunity to thank Dr. James Bowsher (a director and professor for Medical Physics Program at Duke Kunshan University) and Dr. David Huang (my thesis committee) for their continuous monitoring, encouragement, insightful comments and hard questions. Sincere gratitude and appreciation are also given to Chen-Ting Lee (Kelly) for her constant support, patience and generosity in finding time from her busy schedule to help me solve my research problems. She always supported me and patiently offered instructions on my research, hands-on laboratory work, and the theories and concepts related to my MS thesis. Great thanks should also go to Yingchun Zhou, Yulin Zhao, and Heng Tao for their valuable suggestions and kind help during my MS study. I was very lucky and honored to work in their labs with such a harmonious working environment.

1. Introduction

1.1 Challenges of the Conventional Cancer Treatments and Some Konds of Immune Therapies:

Surgical removal, radiation therapy and chemotherapy have been at the forefront of conventional cancer treatments for the last several decades and remain the most commonly used treatment strategies. However, certain advanced cancers cannot be completely eliminated by these techniques and tumor recurrence and metastasis remain the leading cause of death among cancer patients. Few effective treatment options are available, thus, scientists have been investigating other options for cancer treatment. Immunotherapy is one such innovative treatment option. To date, different kinds of immune therapies have been available; cancer peptide vaccines, dendritic cell vaccines and adoptive transfer of cytotoxic T lymphocytes (CTLs) are currently being clinically applied[2]. Despite the therapeutic efficacies of these techniques in some certain types of cancers[3-5], clinical response and superior curative effects have not yet been guaranteed. This phenomenon could be explained by the emerging hallmark of cancer – the ability of cancer cells to evade immune destruction[6], which is associated with negative prognosis [7].

1.2 Emerging Hallmark of Cancer – Evading Immune Destruction and the Solution to Deal With It:

Cancer cells can escape host immunity by manipulating the tumor microenvironment and deriving immunosuppression[8]. For example, the cancer cells can

exploit the immune checkpoints to expand its ligands which combine with T-cell receptors (TCRs), resulting in dysfunction of immune response[6]. Therefore, patients may not have a sufficiently strong immune response that fully eliminates cancer cells; some of the cancer cells may just hide from being detected by the host immune system after conventional cancer treatments, such as radiation therapy.

To deal with this phenomenon, scientists have been making enormous efforts to investigate and alter the immunosuppressive conditions in the tumor microenvironment, such that the T cells can react against the cancer cells and hence eradicate the cancer cells[9].

1.3 Immune Checkpoints:

The immune system operates as a cycle within which there are many checkpoints. The immune checkpoints are molecules on certain immune cells that require to be activated or inactivated to start an immune response. Examples of the immune checkpoints are PD-1/PD-L1 and CTLA-4/B7-1/2. Importantly, an immunological homeostasis condition is mainly achieved by immune checkpoint molecules which transduce co-inhibitory signals to immune cells, such as T cells, so as to prevent the immune system from over-reacting and attacking the normal organs or tissue[10]. A number of immune checkpoint molecules have been identified and found to be highly expressed on the tumor cell surface and related to the generation of immunosuppressive conditions in the tumor microenvironment[10-15]. These findings implied that it would be

possible to eliminate the immunosuppressive conditions in the tumor microenvironment by applying specific antibodies to block the interaction between the immune checkpoint molecules and the corresponding ligands.

1.4 Immune Checkpoint Blockade (ICB):

Based on the above findings, Immune Checkpoint Blockade (ICB), a novel immunotherapy technique, has been developed. The concept of ICB is to modulate the host immune system so as to eliminate the immunosuppressive conditions of the tumor microenvironment[10-12]. Clinically available immune checkpoint molecules related to the tumor-associated immunosuppression include CTLA-4 (Cytotoxi T-Lymphocyte-Associated protein-4, CD152)[16-18] and PD-1 (Programmed Cell Death-1, CD279)[19-21]. The specific antibodies (abs) against each of those immune checkpoint molecules have been developed by several companies and approved by the FDA[10,11]. In 2011, ipilimumab (anti-CTLA-4 abs) became the first immune checkpoint inhibitor approved by the FDA for treating unresectable or metastatic melanoma[22]. Success targeting CTLA-4 has created enthusiasm for clinical approaches targeting other checkpoints, particularly PD-1/PD-L1. Various abs for PD-1/PDL1 differ in structure, but they can be largely categorized into two main groups: those that target PD-1 (nivolumab; pembrolizumab; pidilizumab) and those that target PD-L1 (MPDL3280A; MEDI4736; BMS-936559; MSB0010718C)[23]. Targeting PD-L1 is slightly different from targeting PD-1 in terms of their actions in relation to the immune system. For example, PD-L1 molecules not only

interact with PD-1, but also are believed to inactivate T cells by interacting with B7[24,25]; both interactions would results in negative signals exerted on T cells. Thus, to effectively prevent the immune system from being inactivated, targeting PD-L1 seems to be more preferable. The first anti-PD-L1 antibody applied to patients was a drug called BMS-956669, and it showed promising results with a variety of solid tumors[25-26]. Anti-PD-L1 abs have been also found to prevent either attenuation of T cell function or T cell exhaustion[27]. Other abs, such as MPDL3280A, MEDI4736, and MSB0010718C have had positive results in small patient populations of bladder cancer, and hence were used in early-phase clinical trials for several malignancies including bladder cancers, GI malignancies and head and neck cancers[28-31].

1.5 Combination of ICB and Radiation:

The promise of ICB is enhanced by radiation treatment. The objective of the immunotherapy is to partially reverse tolerance to weakly immunogenic tumor-associated antigens, which would subsequently activate an immune response to tumor cells[32]. Ionizing radiation (IR) was believed to be associated with the immunosuppressive effect [33]. However, with the increasing understanding about the underlying biological pathways triggered by IR, it has been found that radiation treatment would trigger the release of antigens from the tumor, which would subsequently activate host immune system[34]. Levy et al.[32] suggested that radiotherapy not only modulates tumor immunity, but also leads to a distant effect by recruiting

biological effectors. The complex relationship among the radiation, immune system and tumor response are currently being studied. A number of pre-clinical data and early phase clinical trials have suggested that radiation combined with ICB, a type of immunotherapy, has potential therapeutic advantages[27,35-37].

1.5.1 Pre-clinical Studies in Animal Models:

Several research studies have had success using animal models. Radiation combined with anti-PD-1 abs has shown prolonged survival of mice with intracranial gilomas[38]. In another study, the combination of radiation therapy and anti-CTLA-4 abs has shown promising effects on inhibiting primary tumor growth and lung metastases[39]. In addition, recently, an unpublished research paper conducted by our research team (Douglas H. Weitzel et al. 2015[1]) showed that radiation combined with anti-PD-L1 abs treatment has resulted in a complete removal of tumor burden with prolonged survival of mice and has shown abscopal effects with the presence of anti-tumor immunity. Therefore, these findings suggested that radiation itself not only eradicates tumor cells, but may also enhances the production of tumor specific antigens that can be acted on by fully functional T cells as a result of ICB.

1.5.2 Clinical Trials in Patients:

In clinical studies with humans, radiation combined with anti-CTLA-4 antibody (ipilimumab) has demonstrated abscopal effects in one metastatic melanoma patient[40]. Christina et.al (2015)[27] have also demonstrated tumor growth inhibition in patients with

metastatic melanoma through combined treatment of radiation and anti-CTLA-4 antibody. This inhibitory effect was reproducible in mouse models.

1.6 Rationales for Targeting PD-L1:

Therefore, the combination treatment of ICB and radiation therapy has a high potential to become one of the mainstream procedures for cancer treatment in the future, particularly because cancers express high levels of PD-L1 molecules, which positively correlate with the response of ICB [41,42]. PD-L1 molecules expressed on the surface of tumor cells when combined with the PD-1 molecules on the surface of T-cells will suppress the immune system. However, anti-PD-L1 antibody blocks the direct interaction between the PD-1 and PD-L1 molecules, therefore preventing the inactivation of host immune system. In other words, PD-L1 blockade prevents T-cell exhaustion in order to alleviate the depression in anti-tumor immunity and further encourage oligoclonal T-cell expansion[27]. On the other hand, radiation has been found to enhance the diversity of the T-cell receptor (TCR) repertoire of intratumoral T-cells and modulate the TCR repertoire of the expanded peripheral clones[27].

Important research is being done in these areas. By employing E0771 murine breast cancer cells in a syngeneic flank tumor model, Weitzel et al. (2015)[1] successfully demonstrated a complete removal of tumor burden with prolonged survivals after a combination treatment of a single radiation dose of 10 Gy and anti-PD-L1 immunotherapy. Subsequently, Weitzel et al. (2015)[1] employed a dual-flank tumor

model with both legs with the E0771 cancer cells being subcutaneously injected, but only the right leg (primary tumor) being irradiated, such that the tumors in the left leg were regarded as secondary tumors. With the same combination treatment, they demonstrated the presence of a distant effect, and an anti-tumor immunity on both primary and secondary tumors within the same animal. From the above results, it is pertinent to further investigate whether the radiation combined with anti-PD-L1 abs would inhibit tumor metastasis using a similar experimental setup.

Nevertheless, there were some limitations in the Weitzel et al. (2015)[1] experimental design. First of all, the tumors in the left leg regions were not real metastatic tumors, instead they were injected subcutaneously; that means the tumor microenvironment was not optimized. Because E0771 is a breast cancer cell line, it should have grown in fat tissue, instead of in leg muscle tissue. Therefore, in the current study, we kept using the same mouse models, cancer cell line, radiation dosage and antibody as Weitzel et al. (2015)[1] did. In addition, we attempted to develop an E0771 lung metastatic mode; we injected the E0771 breast cancer cells into the dorsal fat pad region of each mouse and increased the number of cancer cells for injection from half million (as Weitzel et al.[1] did) to one million.

With all these complex relations among the immune system, radiation, and immune checkpoints, it is pertinent to investigate the effects of radiation and anti-PD-L1 abs on the tumor metastasis, which is the main objective of the current study.

2. Methods and Materials

2.1 Cell culture:

The E0771 murine breast cancer cell line was engineered to obtain E0771-luc cells such that the E0771-luc cells express genes for coding luciferase and Green-Fluorescent Protein (GFP). This characteristic is essential for In-Vivo-Imaging-System (IVIS) imaging purpose. The E0771-luc cells were cultured in RPMI supplemented with 10% PBS (pH 7.4) and Anti-Anti, HIFBS as nutrient and maintained in an incubator with a humidified environment with 5% Carbon Dioxide and 37.1 Degree Celsius.

2.2 Luciferase Assay:

The luciferase activity of E0771-luc cells was tested by the Luciferase Assay. 0.25% Trypsin-EDTA was used for cell detachment. A 96-well plate was used, within which three non-consecutively separated wells were injected with 5x10^4 tumor cells/well. 200uL of RPMI was added into each of the three wells. The plate was then placed back into the incubator and maintained overnight. On the next day, 40uL of D-Luciferin was added into each of the three wells for the IVIS purpose.

2.3 Animals and Cell Implantation:

Twenty 6 week-old female C57/BL6 mice (purchased by Charles River Laboratories, Calco, Milano) were housed under pathogen free conditions. All procedures performed with animals were in accordance with the Duke University

Institutional Animal Care and Use Committee Guidelines at Duke University Medical Center.

For the dorsal fat pad injections, exponentially growing E0771-luc cancer cells were harvested, counted and re-suspended in PBS to a final concentration of 10^7 cells/ml. A Luciferase Assay was performed before the cells were injected into the dorsal fat pad region. During the cell implantation, the mice were anesthetized with ketamine (80mg/kg) and xylazine (8mg/kg). Animals were randomized into 4 groups on the treatment day, on which the tumor volume was targeted to be ~100-200mm^3.

2.4 Radiation Therapy for Orthotopically Transplanted Tumors:

To perform irradiation, mice were anesthetized with isoflurane gas mixed with oxygen and placed onto a platform inside an X-RAD 225Cx (Precision X-ray Inc) small animal micro-CT irradiator. A 8 x 12-mm collimator was employed to target the radiation beam to the dorsal mammary tumor. Two opposed radiation fields were applied in 90 degree with an intention to avoid excessive radiation damage to the spinal cord **(Figure 2.3.1, Figure 2.3.2)**. Fluoroscopy at 40 kVp and 2.5 mA with a 2-mm Al filter allowed proper alignment of the radiation field. Barium fiducial skin markers were used to mark the tumor location via visualization and palpation of the anesthetized mice. A single fraction of 10 Gy was administered as two exposures of 5 Gy from parallel-opposed fields. The dosimetry for the orthotpic tumor irradiation was similar to the

experiment conducted by a previous PhD student called Mary-Keara Boss[43]. The summary of the dosimetry measurement and calculation can be found in Appendix B.

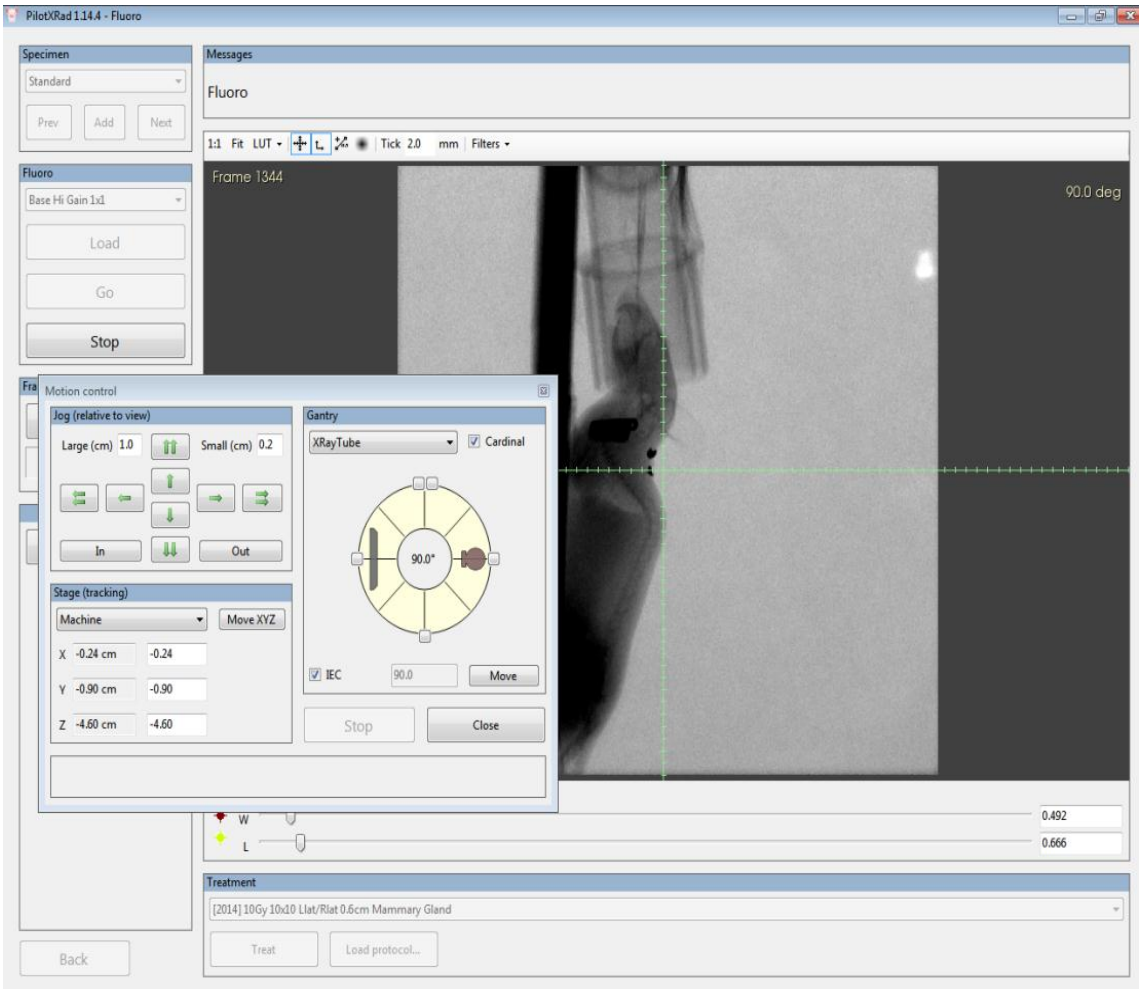

Figure 2.3.1: A diagram (without cone) shows that the tumor is labeled with radio-markers (shown as black dots) on the dorsal region of an anesthetized mouse, irradiation takes place at 90 degree orientation.

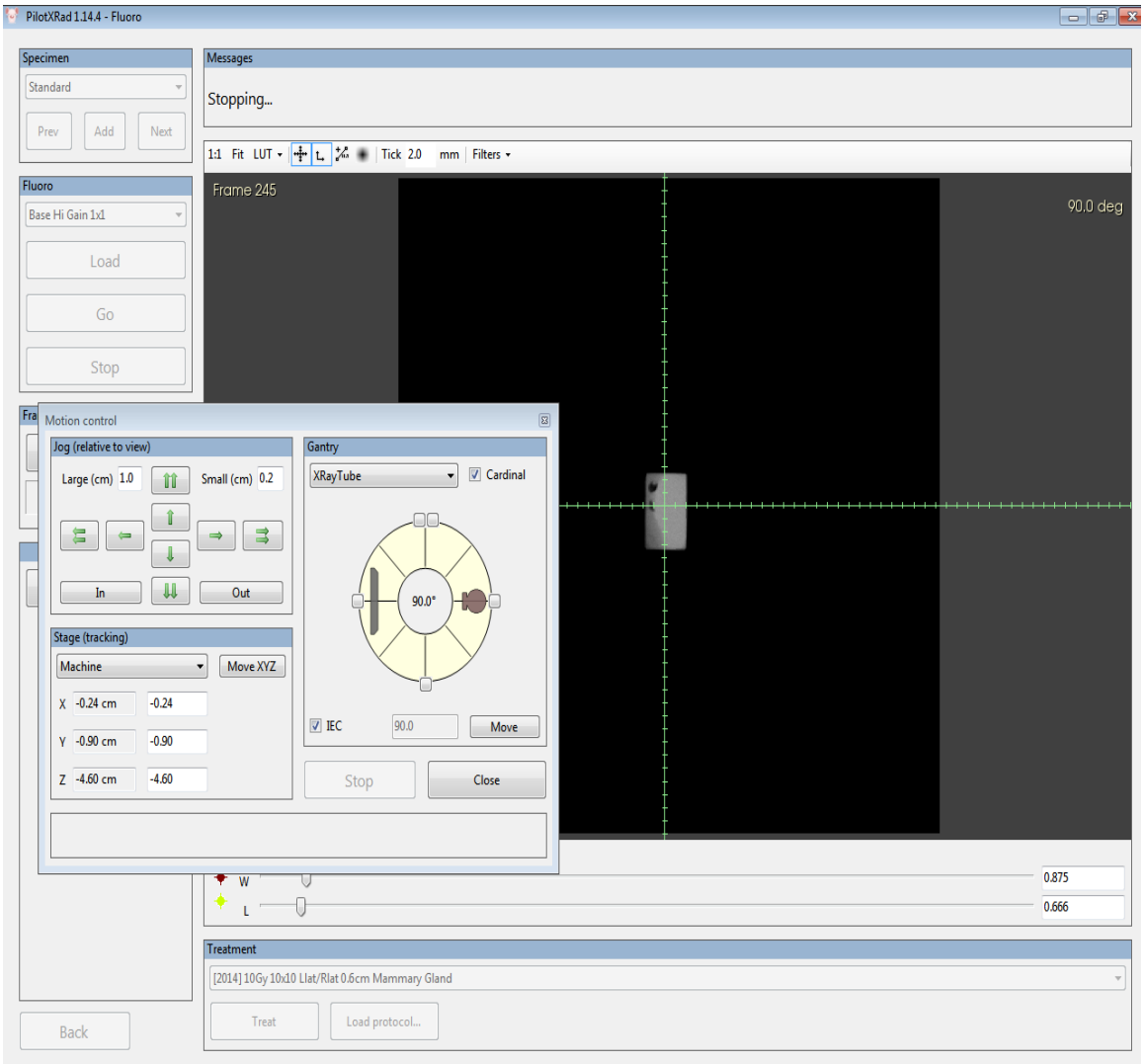

Figure 2.3.2: A diagram (with cone) shows the irradiation field which is confined to a square shape using an 8mmx12mm cone at 90 degree orientation.

2.5 Tumor Volume Measurement:

Tumor growth was monitored and quantified by caliper measurements every other day and the mouse weights were recorded regularly. Primary tumor volume was calculated as follows: $Tumor\ volume\ (in\ mm^3) = \frac{3.14 \times L \times W^2}{6}$, where L represents the largest dimension of the tumor, and W is the width of the tumor. Humane endpoints were observed for mice with tumors over 1500 up to 2000 mm^3 or with ulceration.

2.6 Zenalux Biomedical Zenascope:

In order to assess the treatment effects on the tumor oxygen status, Hemoglobin Saturation (Hb-Sat) levels and total hemoglobin levels were monitored using Zenascope before the treatment day, on the treatment day (day 0) and day 1, 2 and 3.

The Zenascope enables spectroscopic analysis of tissue. The system uses standard spectroscopic measurement hardware, proprietary software and patented algorithms to achieve rapid, quantitative and non-destructive analysis of biological tissue characteristics (biomarkers) that reflect the underlying function and composition of tissue. The Zenascope assesses different kinds of endpoints, which includes (1) wavelength-average reduced scattering, relating to cellular density and fibrous content; (2) wavelength-averaged absorption; (3) total hemoglobin content, relating to vascularity; and (4) hemoglobin saturation, relating to vascular oxygenation. In the current study, hemoglobin Saturation (Hb-Sat) and the total hemoglobin levels were measured.

The spectroscopy probe has a pressure sensing capability to monitor pressure during spectroscopic data capture or to enable repeated measurements at the same pressure. The probe includes a camera, a white light source for bright field imaging, and a UV light source with appropriate filters for fluorescence imaging.

2.7 In-Vivo Imaging System (IVIS) on the Day of Euthanasia:

IVIS includes a highly sensitive, charge-coupled digital camera with accompanying advanced computer software for image data acquisition and analysis. This system captures light photons that are emitted by reagents or cells that have been coupled or engineered to produce bioluminescence in the living animal.

For each time of operation, the IVIS program was first initialized, such that the stage temperature was 37^{o}C and the camera's temperature was -80^{o}C. The substrate D-luciferin (0.2ml/mouse) was then injected into the intra-peritoneal (i.p.) cavity, immediately followed by imaging under IVIS (Xenogen Corp., Alameda, CA). Mice were anesthetized with isoflurane and placed on the imaging stage, and dorsal images were collected using imaging sequencing with 1 minute exposure time until around 15 minutes after D-luc injection. Therefore, photons emitted from the primary tumor could be quantified using Living Image software (Xenogen Corp., Alameda, CA). After that, Euthasol (0.05ml/mouse) was injected through i.p. to euthanize the mice. The lungs with the entire trachea intact and/or the primary tumors in the dorsal region were dissected out for the whole-lung imaging purpose under IVIS. Similarly, photons emitted from the

lung region were also quantified. Finally, the lungs then were preserved for India-ink staining.

2.8 India-Ink Assay:

India ink assay was employed for visualization of lung metastases. A 1 mL syringe was used to inject the India ink (15% India Ink, 85% water, 3 drops of NH_4OH/100ml) into the lungs via the trachea. The lungs were completely inflated with ink until there was a strong resistance. Scissors were then used to cut the trachea and collect the lung with a high precaution to avoid damaging and contaminating the lung tissues. The lungs were then rinsed in a 1L beaker of water. In a chemical fume hood, the lungs were transferred to a glass scintillation vial containing 5mL of Fekete's solution (300ml 70% EtOH, 30ml 37% formaldehyde, 5ml glacial acetic acid). The tumor tissue emerged as white nodules on the black lungs after a few minutes. The tumor nodules could subsequently be counted and stored in Fekete's solution indefinitely.

2.9 Drugs:

Control IgG (LTF-2) and anti-PD-L1 antibody (10F .9G2) (BioXCell, West Lebanon, NH) were injected through intra-peritoneal injection (i.p.) with 200µg on Day 0, and every 3 days after the treatment day for a total of 4 doses. D-luciferin (Goldbio.com) was injected i.p. 200µg for each mouse before imaging the mouse using the IVIS.

2.10 Statistical Analysis:

Statistical analyses were performed with the GraphPad Prism-7 software, and Microsoft Excel software. Survival curves were created using the method of Kaplan and Meier with the 95% confidence interval for fractional survival at any particular time.

Log-rank and Gehan-Wilcoxon tests generated the p-value, which tests the null hypothesis that the survival curves are identical in the overall populations. The null hypothesis is that the treatment(s) did not change the survival.

The Log-rank test and Gehan-Wilcoxon test were employed to compare two or more survival curves. Two-way ANOVA was employed for the data analysis. Dunn's multiple comparisons test was used to analyze the data and used to generate the p value. The results were considered statistically significant for $p < 0.05$.

3. Results

3.1 Primary Tumor Growth:

To monitor the primary tumor growth among all four groups, calipers' measurements were taken every other day. Day 0 refers to the treatment day on which the tumor volume was targeted to be 100-200mm^3. The measurement data, in terms of tumor volume, were plotted against post- treatment days. These plots are shown in **figure 3.1.1** for control group, **figure 3.1.2** for RT-alone group, **figure 3.1.3** for anti-PD-L1-alone group and **figure 3.1.4** for RT + anti-PD-L1 group.

3.1.1 Control Group:

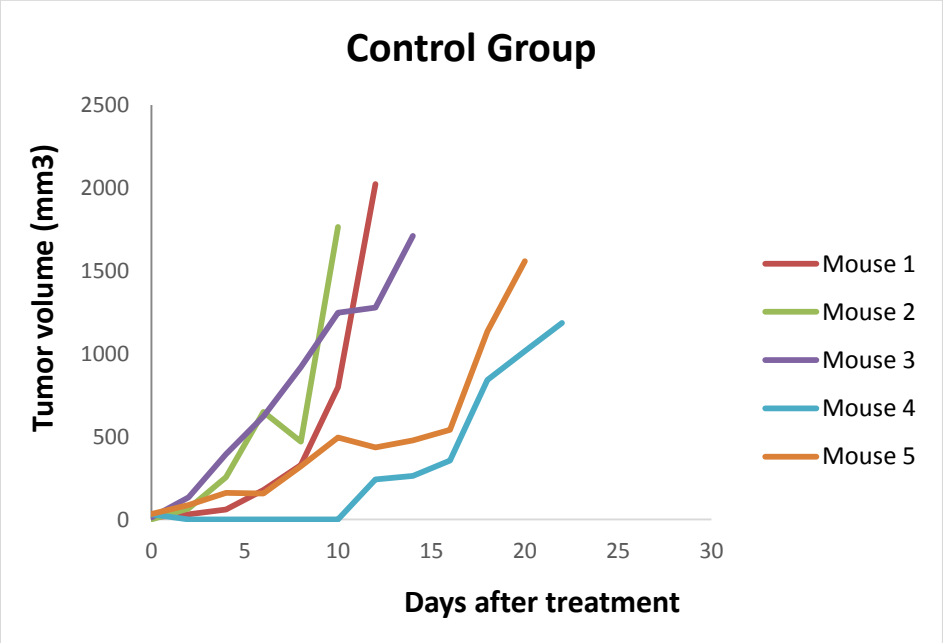

Figure 3.1.1: A plot shows primary tumor growth in control group over the treatment time.

3.1.2 Radiation-alone Group:

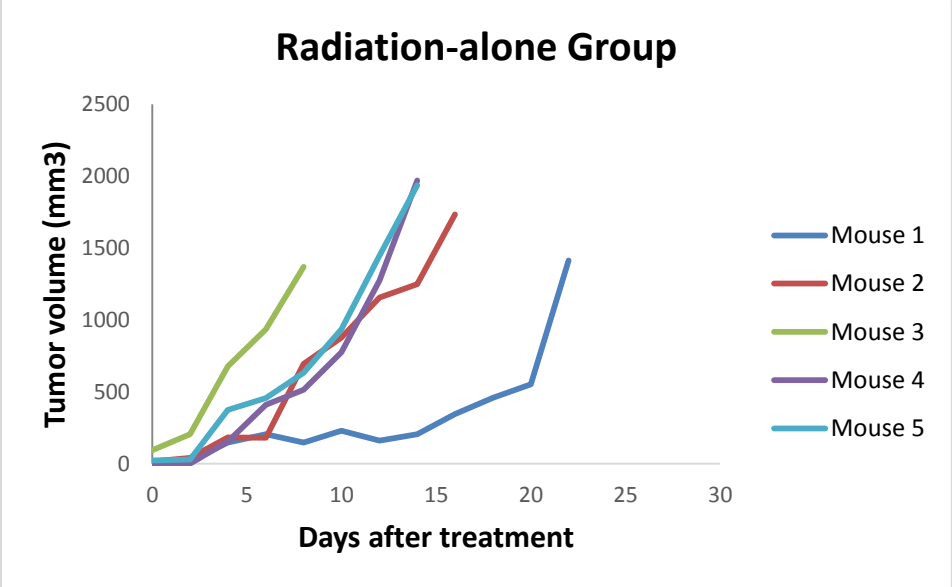

Figure 3.1.2: A plot shows primary tumor growth in RT-alone group over the treatment time.

3.1.3 Anti-PD-L1-alone Group:

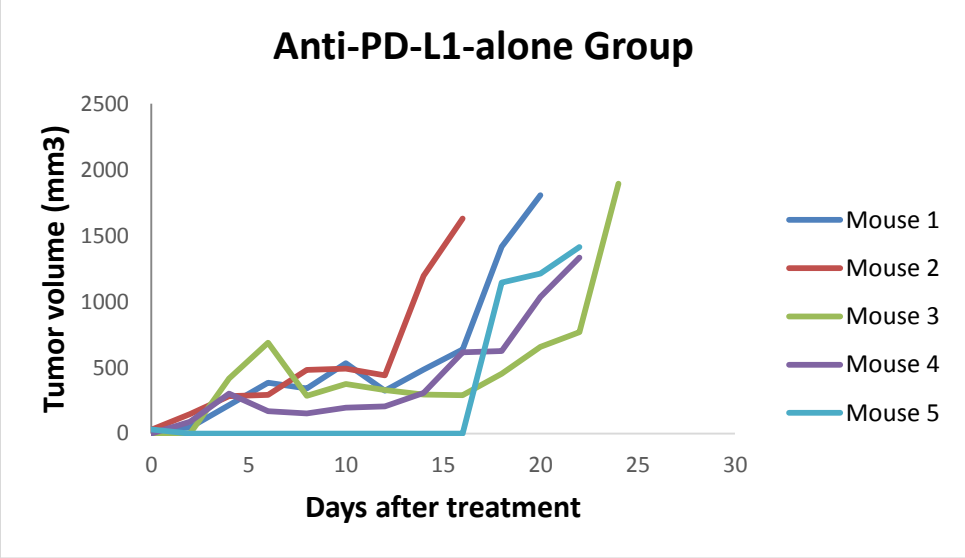

Figure 3.1.3: A plot shows primary tumor growth in anti-PD-L1-alone group over the treatment time.

3.1.4 Radiation and Anti-PD-L1 Group:

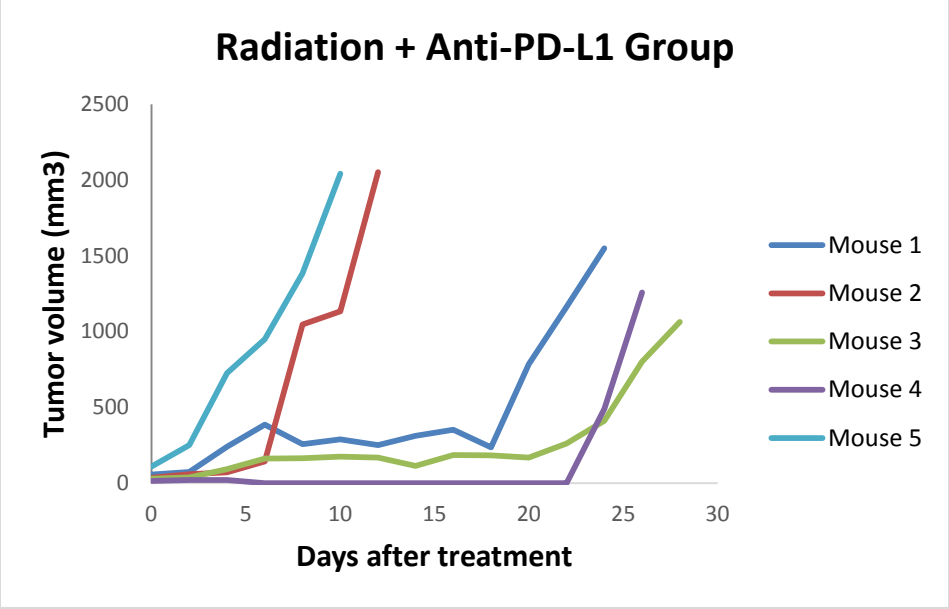

Figure 3.1.4: A plot shows primary tumor growth in RT + anti-PD-L1 group over the treatment time.

3.1.5 Comparison among Different Groups:

In addition to the individual plots shown in **figure 3.1.1, figure 3.1.2, figure 3.1.3 and figure 3.1.4, figure 3.1.5** shows a comparison among all groups. To do this, a median value for each group was calculated for each measurement day. Subsequently, the median values were plotted against days post treatment for all groups.

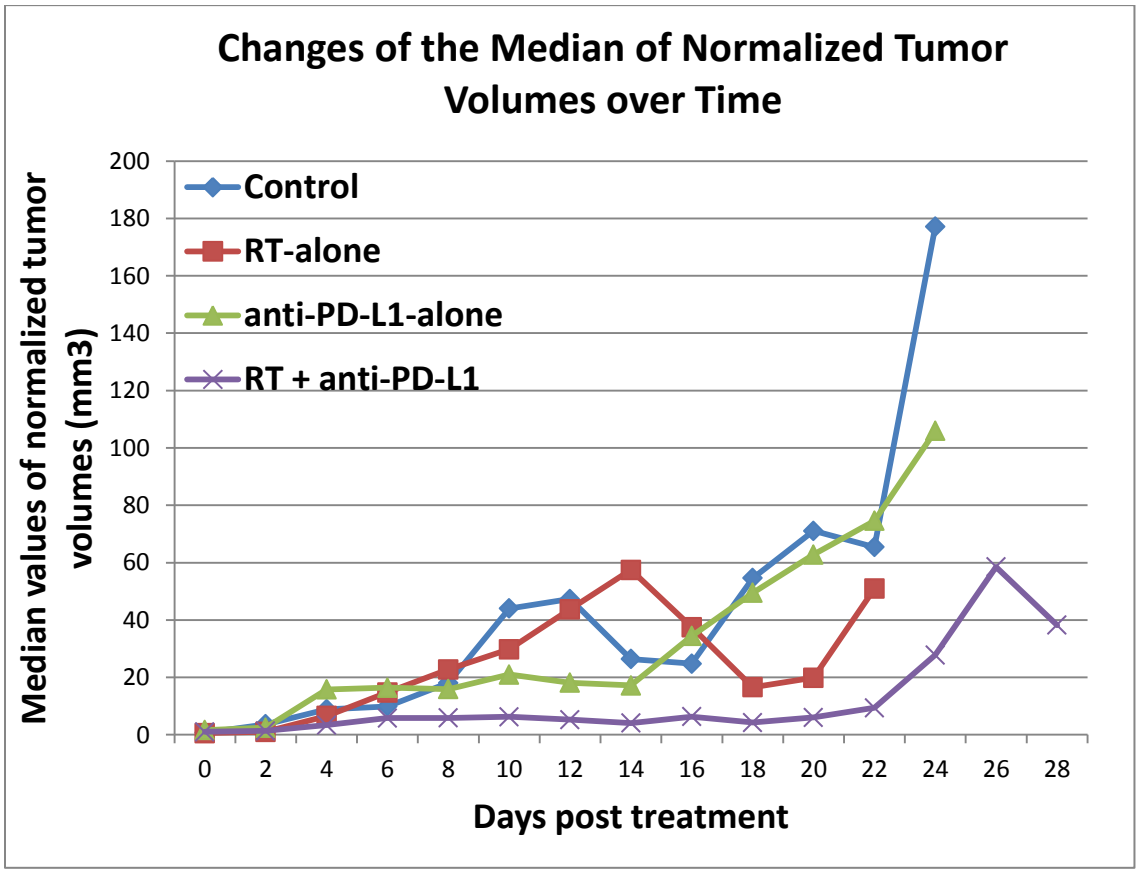

Figure 3.1.5: A plot shows changes of median primary tumor volume over time.

From **figure 3.1.1 to figure 3.1.5**, compared to the control group, it can be seen that radiation treatment alone did not have any effects on primary tumor growth, while anti-PD-L1 antibody treatment alone slightly delayed the primary tumor growth. The combination treatment of radiation and anti-PD-L1 antibody treatment showed a non-durable delay growth, as 3 out of 5 mice indicated primary tumor growth delay, but the primary tumor regrew after 20 days post treatment.

Furthermore, the amount of days required for each tumor to reach the limit of volume≥1500mm^3 is tabulated in **table 3.1.1**.

Table 3.1.1: A table shows the amount of days required for each tumor to exceed the volume limit of 1500mm^3.

	Amount of days required for tumor to reach ≥1500mm^3
Control-1	12
Control-2	10
Control-3	14
Control-4	24
Control-5	20
Median-Control	**14**
RT-1	22
RT-2	16
RT-3	8
RT-4	14
RT-5	14
Median-RT	**14**
Anti-PD-L1-1	20
Anti-PD-L1-2	16
Anti-PD-L1-3	24
Anti-PD-L1-4	22
Anti-PD-L1-5	22
Median-PD-L1	**22**
RT + Anti-PD-L1-1	24
RT + Anti-PD-L1-2	12
RT + Anti-PD-L1-3	28
RT + Anti-PD-L1-4	26
RT + Anti-PD-L1-5	10
Median-RT+PD-Ll	**24**

3.2 Survival Curves:

Survival plots were generated using Kaplan-Meier estimate, which is one of the best choices to measure the fraction of experimental subjects living for a certain amount of time after the treatment. **Figure 3.2.1** shows the percent survival for all 4 groups, and **figure 3.2.2, figure 3.2.3** and **figure 3.2.4** for RT-alone group vs Control group, anti-PD-L1-alone group vs Control group and RT + anti-PD-L1 group vs Control group, respectively.

It should be noted that in this current study, mice were euthanized when the tumor volume reached the endpoint of 1500 mm^3 for the sake of lung harvests. Therefore, the survival curves here do not actually chart survival. Instead, they chart related endpoints. The plots for all four groups were compared using both the log-rank test and the Gehan-Wilcoxon test. The comparisons were tabulated and shown in **table 3.2.1, table 3.2.2, table 3.2.3 and table 3.2.4**.

Percent Survival for All 4 Groups:

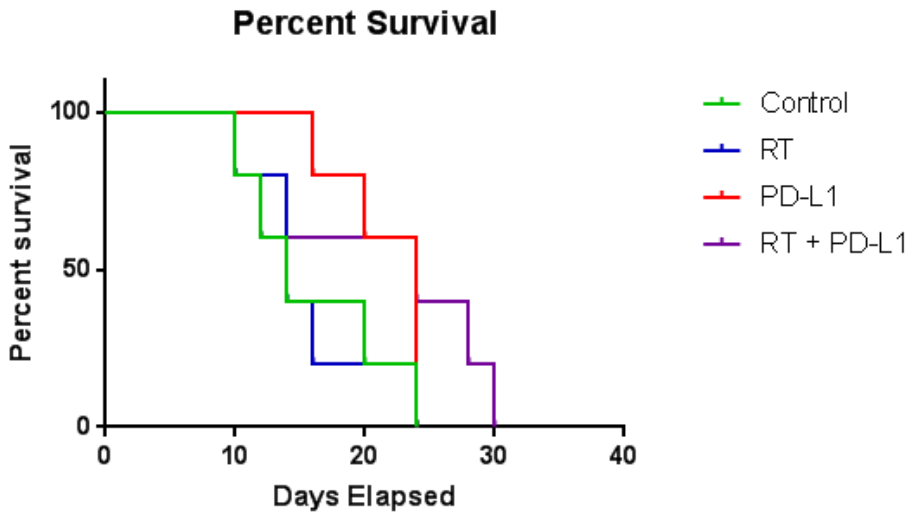

Figure 3.2.1: A plot shows percent survival for all 4 groups.

Table 3.2.1: A table shows a comparison of survival curves among all 4 groups.

Comparison of All Four Survival Curves	
Log-rank (Mantel-Cox) test (recommended)	
P value	0.2345
P value summary	ns
Are the survival curves sig different?	No
Gehan-Breslow-Wilcoxon test	
P value	0.3374
P value summary	ns
Are the survival curves sig different?	No

Percent Survival for RT-alone Group and Control Group:

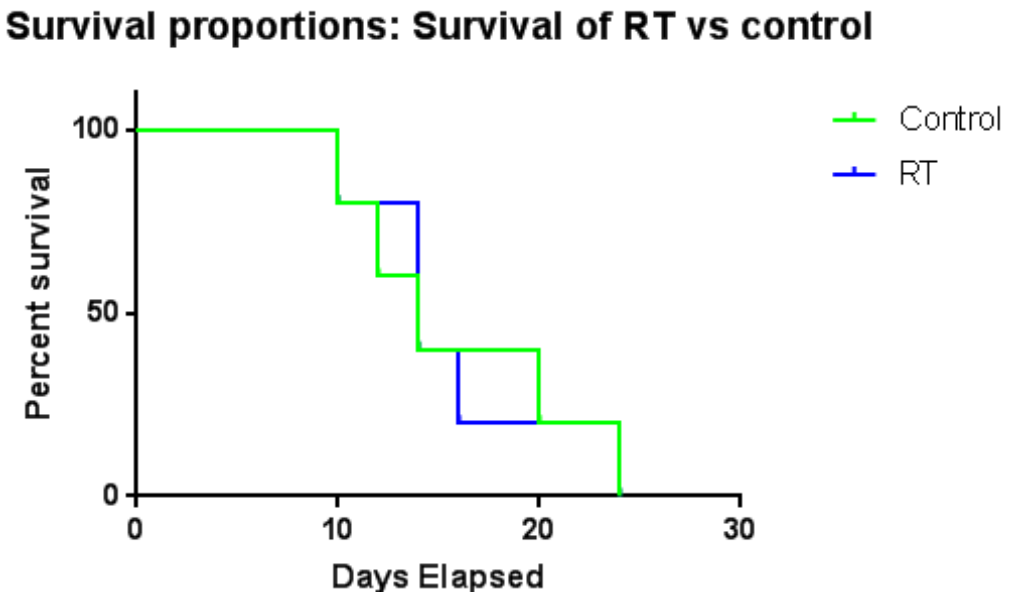

Figure 3.2.2: A plot shows percent survival for RT-alone group and Control group.

Table 3.2.2: A table shows a comparison of survival curves between RT-alone group and Control group.

Comparison of Survival Curves between RT-alone group and Control group	
Log-rank (Mantel-Cox) test	
P value	0.9705
P value summary	ns
Are the survival curves sig different?	No
Gehan-Breslow-Wilcoxon test	
P value	0.9163
P value summary	ns
Are the survival curves sig different?	No

Percent Survival for anti-PD-L1-alone Group and Control Group:

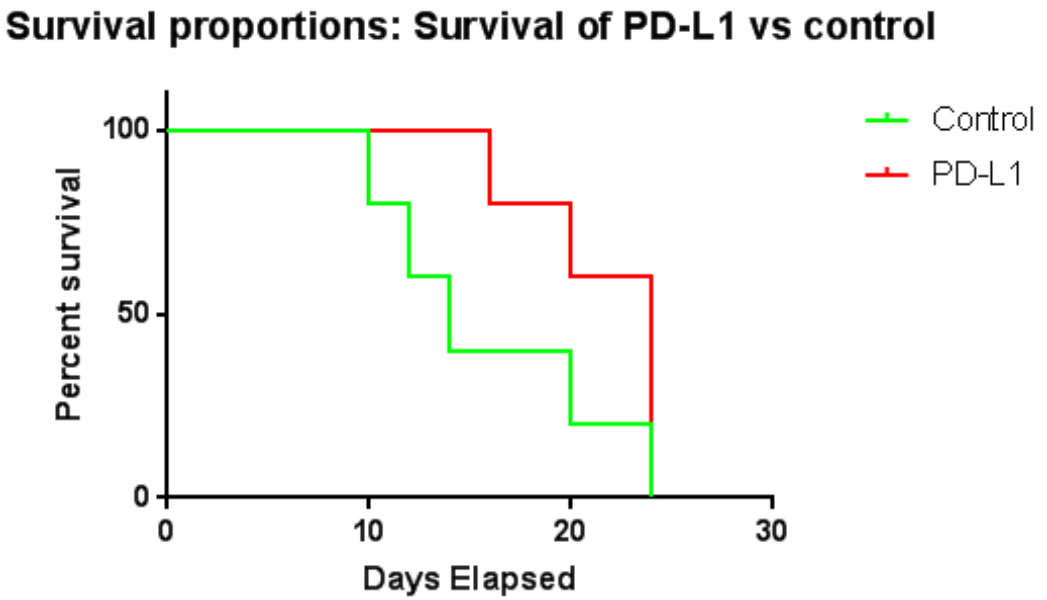

Figure 3.2.3: A plot shows percent survival for anti-PD-L1-alone group and Control group.

Table 3.2.3: A table shows a comparison of survival curves between anti-PD-L1-alone group and Control group.

Comparison of Survival Curves between anti-PD-L1 group and Control group	
Log-rank (Mantel-Cox) test	
P value	0.1283
P value summary	ns
Are the survival curves sig different?	No
Gehan-Breslow-Wilcoxon test	
P value	0.0993
P value summary	ns
Are the survival curves sig different?	No

Percent Survival for RT + anti-PD-L1 Group and Control Group:

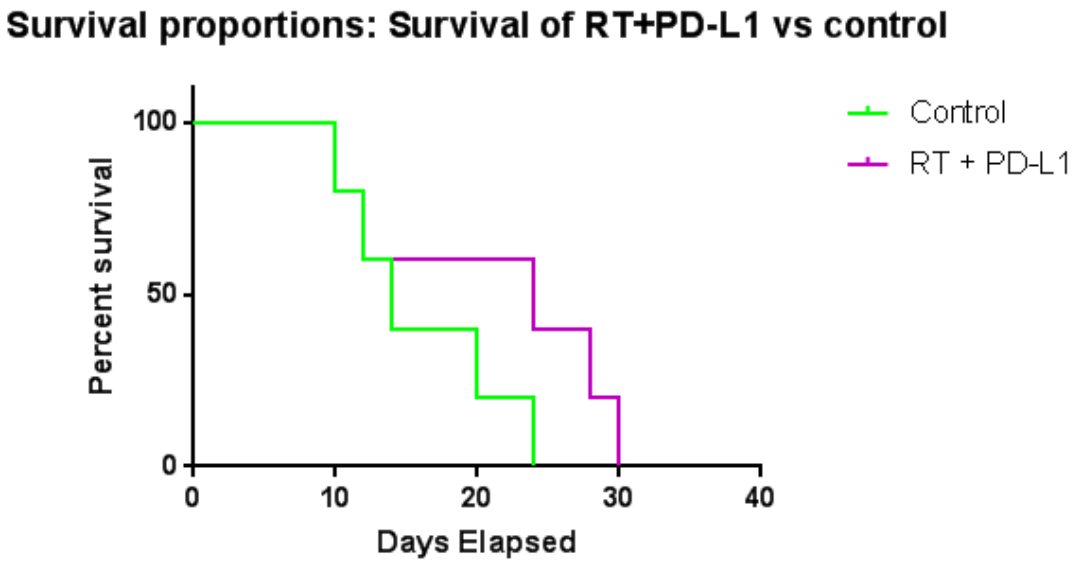

Figure 3.2.4: A plot shows percent survival for RT + anti-PD-L1 group and Control group.

Table 3.2.4: A table shows a comparison of survival curves between RT + anti-PD-L1 group and Control group.

Comparison of Survival Curves between RT+PD-L1 group and Control group	
Log-rank (Mantel-Cox) test	
P value	0.2077
P value summary	ns
Are the survival curves sig different?	No
Gehan-Breslow-Wilcoxon test	
P value	0.4013
P value summary	ns
Are the survival curves sig different?	No

Based on **figure 3.2.1 to figure 3.2.4** and **table 3.2.1 to table 3.2.4,** there are no significant differences for the survival curves for all the treatment groups, either among themselves or when they were compared with the control group. In other words, overall, the treatment (RT-alone or anti-PD-L1-alone or RT + anti-PD-L1) did not affect the time at which the mice reach their endpoints (tumor volume ≥ 1500mm^3).

3.3 IVIS Data - Primary tumors and Lung Metastases:

IVIS captures light photons that are emitted by E0771 luc- cancer cells that have been genetically engineered to express firefly luciferase. D-luciferin is the substrate for firefly luciferase's bioluminescence reaction. When exposed to D-luciferin, which is administered to mice prior to imaging, the tumor cells that express the luciferase will breakdown D-luciferin to produce light. This reaction requires the presence of ATP and Oxygen, enabling the firefly luciferase to catalyze the chemical reaction to convert the substrate – D-luciferin to a chemical called Oxyluciferin. The Oxyluciferin with an electronically excited state releases its excessive energy by giving a photon of light in order to return to the ground state. This photon will then be captured by the IVIS.

In the current study, mice were first injected i.p. with D-luciferin, and then anesthetized with isoflurane and placed on the imaging stage in a ventral recumbent position. IVIS imaging was carried out either immediately after the D-luciferin injection and the anesthesia by using imaging sequencing for approximately 15 minutes with 1

minute exposure time per each sequence. The bioluminescent data are acquired by the instrument and reported as total flux (photons/second). Quantification was performed using Living Image software (Xenogen Corp., Alameda, CA). After completion of imaging, Euthasol (0.05ml/mouse) was injected i.p. to euthanize the mice.

The lungs with the entire trachea intact and/or the primary tumors in the dorsal region were dissected out for the whole-lung imaging purpose under IVIS. The imaging methods depended on many factors and varied in this current study. It was either imaged by one single shot at a specific time point or by imaging sequencing (automatically 15mins-long or manually at different time points). Photons emitted from the lung region were also quantified, and expressed in terms of photons emitted per second. ROI analysis using the Living Image software was performed to obtain the total photon flux, shown in a text box (in red words) next to the ROI. Examples are shown in **figure 3.3.1** for primary tumors and **figure 3.3.2** for lungs. All those images for both primary tumors and the lungs obtained from IVIS can be found in Appendix A.

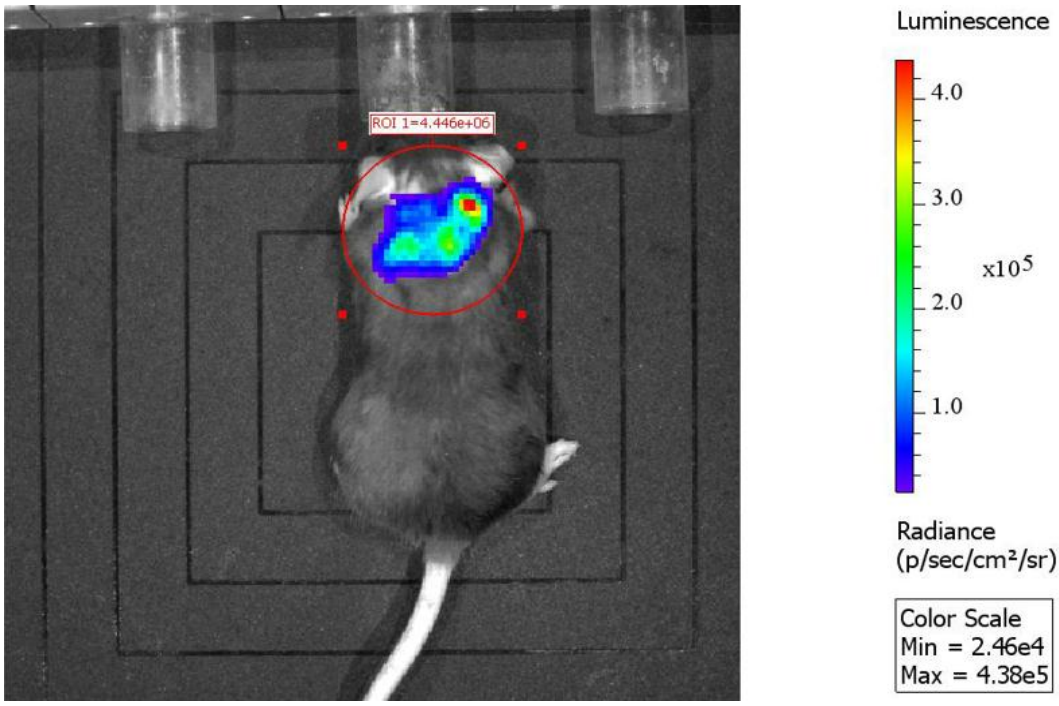

Figure 3.3.1: A diagram shows the IVIS image with ROI data (total photon flux in photons/second) for primary tumor of mouse-3 in anti-PD-L1-alone group.

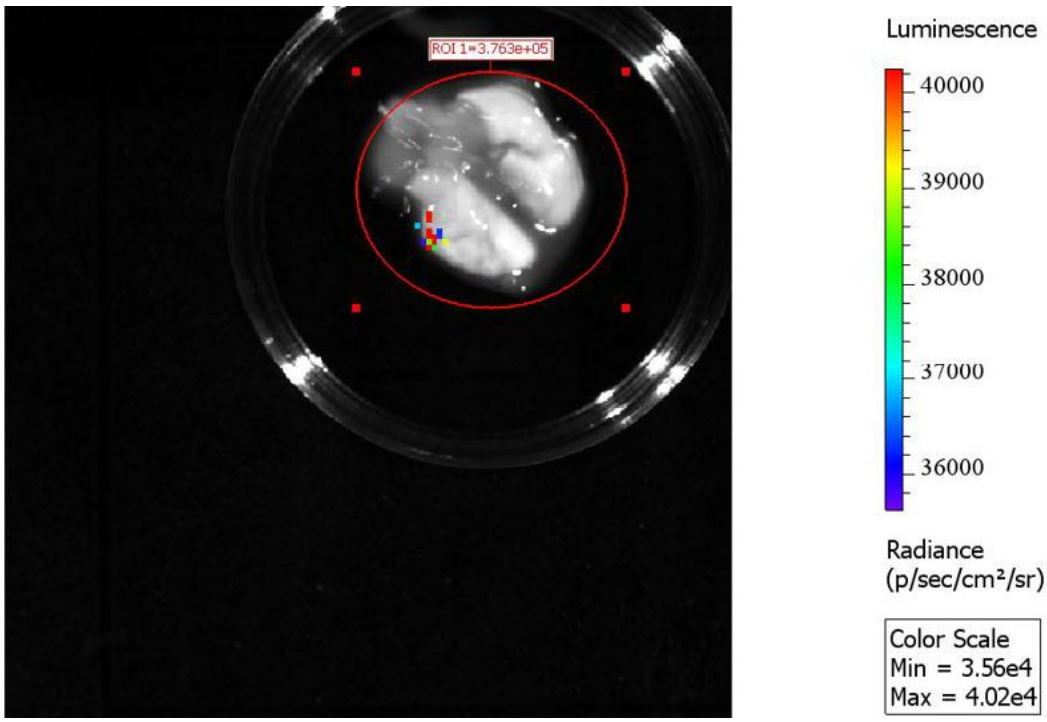

Figure 3.3.2: A diagram shows the IVIS image with ROI data (total photon flux in photons/second) for lung tissue of mouse-3 in anti-PD-L1-alone group.

With the ROI analysis, total photon flux for each individual mouse was obtained and shown as in **figure 3.3.3** and **figure 3.3.4** for primary tumors and lungs, respectively. Due to several reasons, such as machine breakdown, technical problems and/or the poor mouse conditions at the day of euthanasia, ROI analyses for some mice were not able to be performed or images were not saved successfully. Therefore, total photon flux values were not recorded for some of the mice (anti-PD-L1-4, RT-3, RT-5 in **figure 3.3.3** and Control-4, anti-PD-L1-1, anti-PD-L1-2, anti-PD-L1-4, RT-1 and RT-3 in **figure 3.3.4)**. On the other hand, due to the superior huge difference among some subjects in different groups, data bars representing some of the mice (Control-1, Control-2, Control 4, RT + anti-PD-L1-5 in **figure 3.3.3**) are not observable in **figure 3.3.3**. All such incidents that cause failure to perform the ROI analyses are described in **Appendix A**.

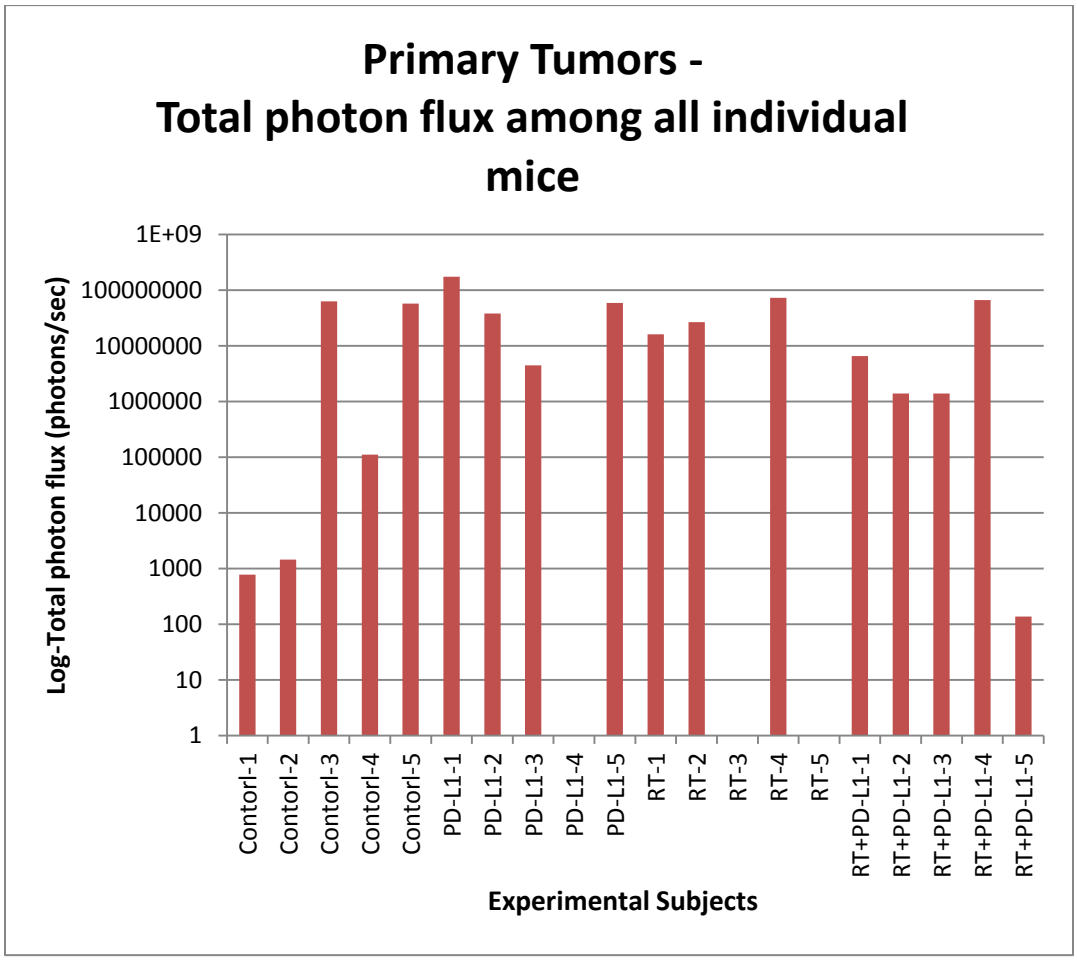

Figure 3.3.3: A log-plot shows the total photon flux emitted from primary tumor cells for all individual mice.

From **figure 3.3.3**, it can be seen that the total photon flux values among the mice within the SAME group varied dramatically, especially for anti-PD-L1-alone group and RT + anti-PD-L1 group. For example, the anti-PD-L1-1(173900 x 10^3 photons/sec) has the total photon flux value 39 times higher than that of the anti-PD-L1-3 (4446 x 10^3 photons/sec). The RT + anti-PD-L1-4 (66660 x 10^3 photons/sec) has the total photon flux value 48 times higher than that of RT + anti-PD-L1-3 (1392x10^3 photons/sec) and RT + anti-PD-L1-2 (1392x10^3 photons/sec).

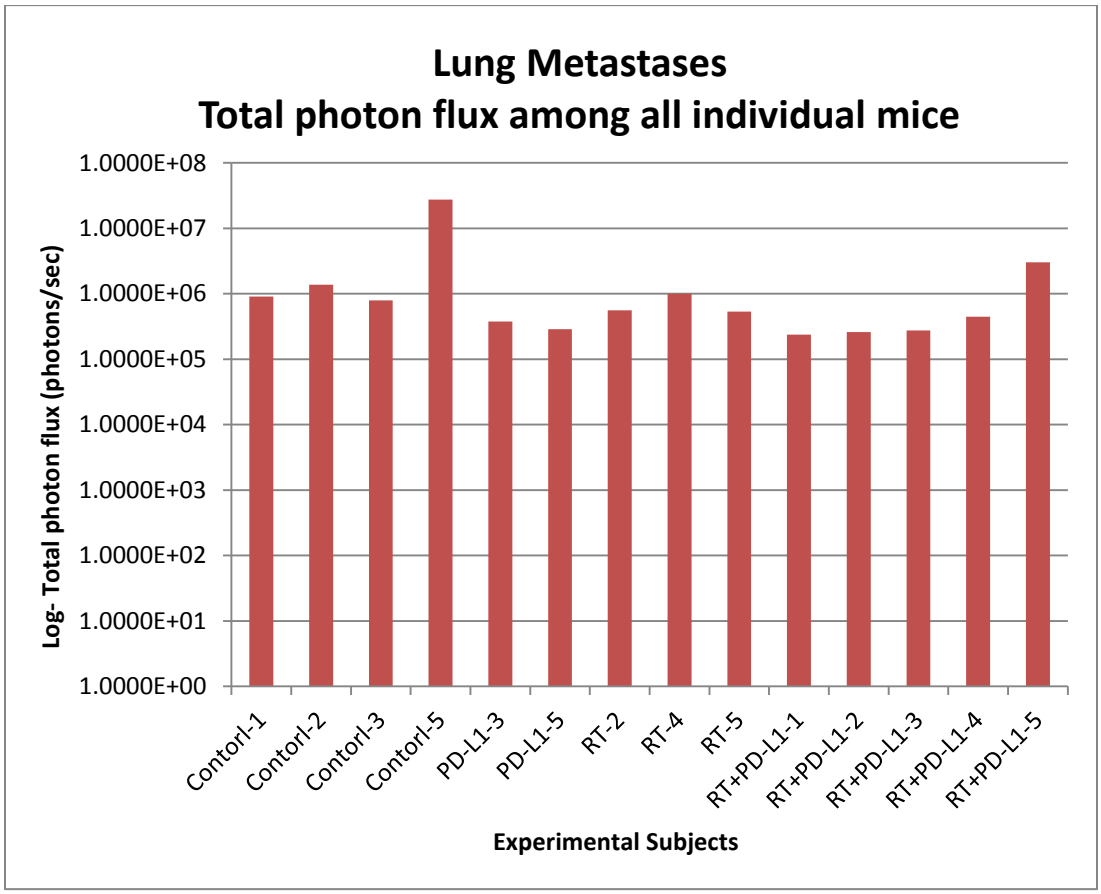

Figure 3.3.4: A log- plot shows the total photon flux emitted from lung tissue for all individual mice.

In comparison, from **figure 3.3.4**, the total photon flux values for the lung tissue among almost all subjects are relatively similar to each other. In other words, they are much less fluctuated, except for one subject in control group (control-5), which has a flux value of 274.2 $x10^5$ photons/sec that is 35 times higher than that of control-3 ($7.886x10^5$ photons/sec).

Apart from this, a median value of the total photon flux was calculated for each group. A variation of the median total flux among all groups was plotted as **figure 3.3.5** and **figure 3.3.6** for primary tumors and lung metastases, respectively.

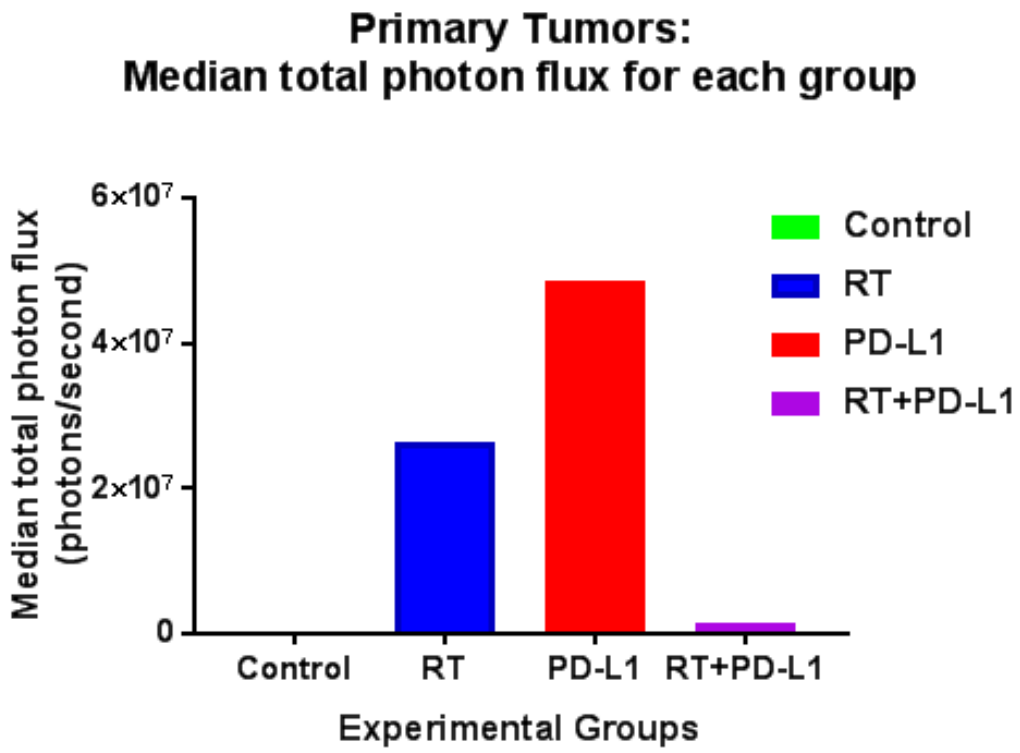

Figure 3.3.5: A plot shows the variation of the median total photon flux emitted from primary tumors for each of four groups.

Table 3.3.1: A table shows the results for multiple comparisons using Two-way ANOVA. (For primary tumors)

Dunn's multiple comparisons test	Significant?	Summary	Adjusted P Value
Control vs. RT-alone	No	ns	0.9999
Control vs. anti-PD-L1-alone	No	ns	0.6676
Control vs. RT + anti-PD-L1	No	ns	0.9871

From **figure 3.3.5** and **table 3.3.1**, it can also be seen that there is no significant difference between RT-alone or anti-PD-L1-alone or RT + anti-PD-L1 group and the control group. These findings suggested that all the treatments did not help in eliminating the primary tumor cells.

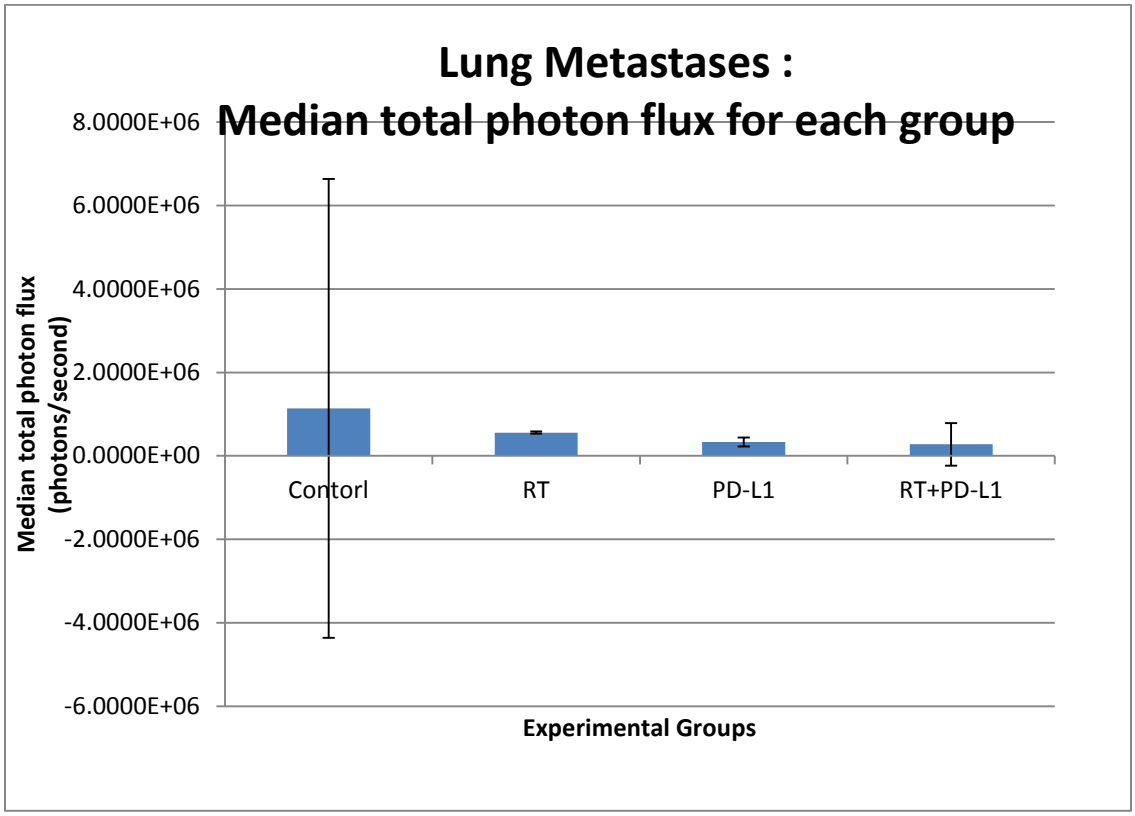

Figure 3.3.6: A plot shows the variation of median total photon flux emitted from lungs for each of four groups.

Table 3.3.2: A table shows the results for multiple comparisons using Two-way ANOVA. (For lung metastases)

Dunn's multiple comparisons test	Significant?	Summary	Adjusted P Value
Control vs. RT-alone	No	ns	0.3433
Control vs. anti-PD-L1-alone	No	ns	0.3058
Control vs. RT + anti-PD-L1	No	ns	0.4053

From **figure 3.3.6** and **table 3.3.2**, it can be interpreted that there is no significant difference between RT-alone or anti-PD-L1-alone or RT + anti-PD-L1 group and the control group. These findings suggested that none of the treatments reduced the burden of metastatic cancer cells in lungs, compared to the control group.

3.4 India-ink Assay:

India-ink Assay was performed as a secondary method to verify the lung mass formation. Unfortunately, grossly observable lung nodules were not observed. In other words, the results from the India-ink Assay suggested that the primary tumors in the dorsal fat pad region did not result in grossly visible metastases in any groups.

3.5 Zenascope Measurement:

Hemoglobin saturation (Hb-Sat) and the total hemoglobin levels were measured in order to assess the endpoints of vascular oxygenation and vascularity information, respectively.

3.5.1 Changes in Hemoglobin Saturation (Hb-Sat) Levels:

Changes in Hb-Sat (%) from baseline values on the pre-treatment day over time for each mouse are plotted separately, and then combined to a single plot with a fixed range of y-axis values as shown in **figure 3.5.1.1**:

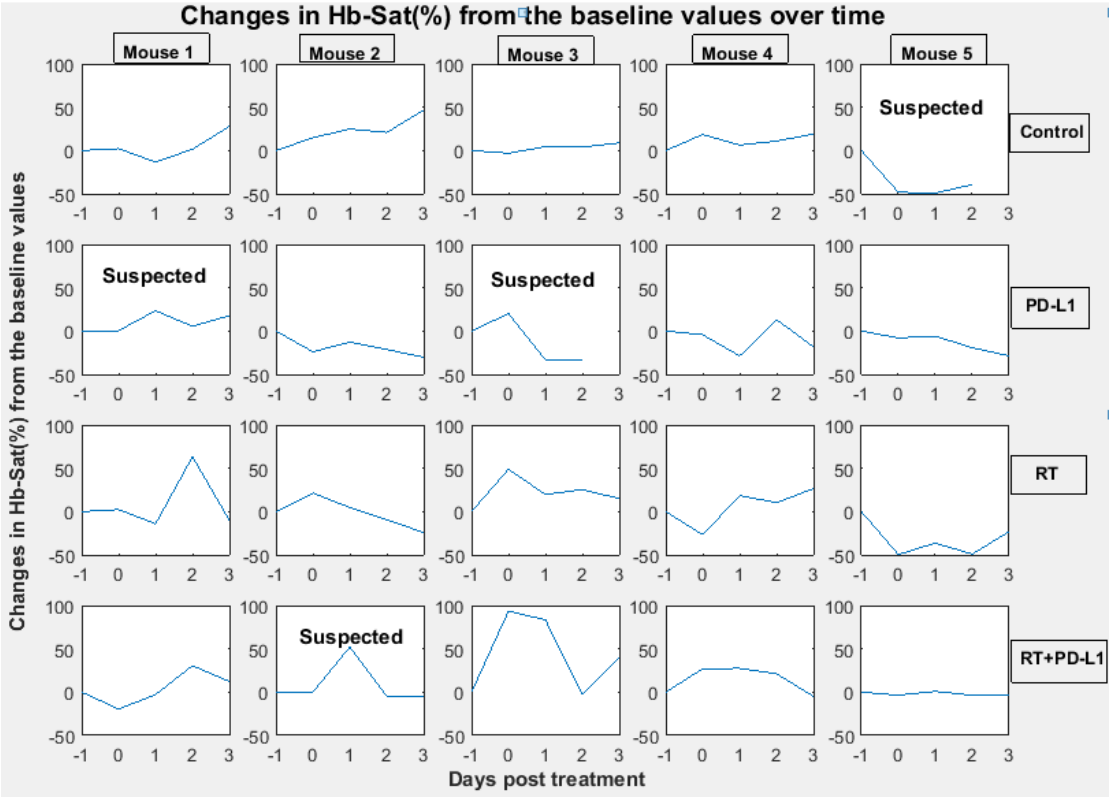

Figure 3.5.1.1: A plot shows the changes in Hb-Sat(%) from the baseline values on the pre-treatment day over time for all individual mice. (Note that some mice are marked with "Suspected" data, such as those with pigment or scar on their skin surface and/or the data appear outside the range of the rest within the same group)

From **figure 3.5.1.1**, excluding the suspected data, it can be seen that there is a gradual increase in Hb-Sat for mice in the control group, which may correlate to the blood vessels growth in these primary tumors in the control group. In contrast, there is a gradual decrease in Hb-Sat for mice in the anti-PD-L1-alone group, which may correlate to the inhibition of blood vessels growth by anti-PD-L1 antibody. In RT-alone group, the response is not clearly shown from **figure 3.5.1.1**, suggesting that a single radiation fraction of 10 Gy may not have significant effects on blood vessels growth in tumors and

hence the tumor oxygenation status. From **figure 3.5.1.1**, when RT combined with anti-PD-L1 antibody treatment, 3 out of 4 mice demonstrated a relatively flat response against the combination treatment. (Further discussion can be found in section 4.3)

3.5.2 Changes in Total Hb Levels:

Changes in Total Hb (%) from baseline values on the pre-treatment day over time for each mouse are plotted separately, and then combined to a single plot with the fixed range of y-axis values as shown in **figure 3.5.2.1**:

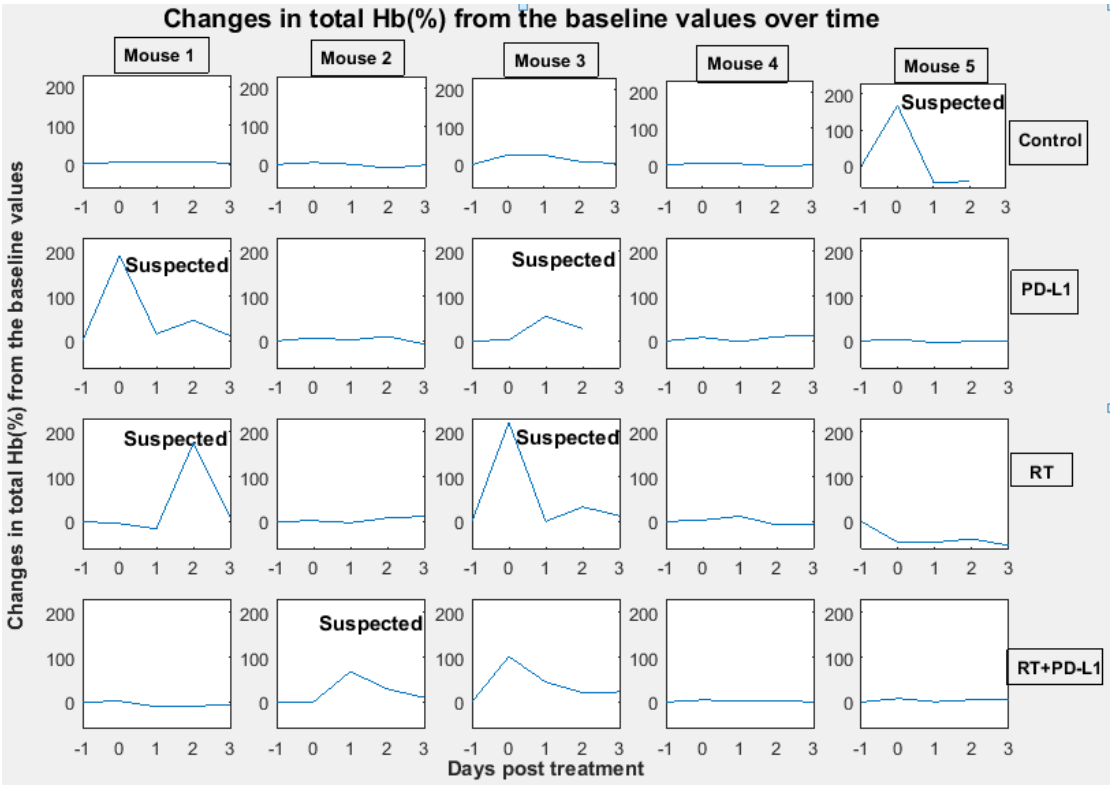

Figure 3.5.2.1: A plot shows the changes in total Hb(%) over time for all individual mice from all groups. (Note that some mice are marked with "Suspected" data, such as those with pigment or scar on their skin surface and/or the data appear outside the range of the rest within the same group)

From **figure 3.5.2.1**, excluding the suspected data, there is not much change in the normalized total Hb levels within tumors for all individual mice. This finding, overall, suggested that all kinds of treatment methods used in this current study did not affect the total hemoglobin levels in primary tumors, and hence the vascularity in tumor microenvironment. (Further discussion can be found in section 4.3)

4. Discussions:

Two previous studies performed by Weitzel et al. (2015)[1] are compared to our experimental results. In his first study, a half million E0771 breast cancer cells were subcutaneously injected into each mouse's leg muscle (only one side). When tumor volumes in the right leg reached 100-200mm^3, mice were randomized into 4 different groups (Control, RT-alone, anti-PD-L1-alone and RT + anti-PD-L1); 10Gy of single radiation dose was given to tumors. The treatment endpoint was defined as when tumor volume exceeds 1500mm^3.

In his second study, most of the treatment designs were similar, except that he employed a dual-tumor flank model, the same amount of the same breast cancer cell was subcutaneously injected into each mouse's leg muscle (both sides). When tumor volumes in the right leg reached 100-200mm^3, mice were randomized into 3 different groups (Control, RT-alone and RT + anti-PD-L1); the same dose of radiation was given to tumors of the right leg for the RT-alone group and the RT+ anti-PD-L1 group. With such a treatment design, the tumors in the right leg were regarded as primary tumors, while tumors in the left leg were considered as secondary tumors.

Nevertheless, there were some limitations in Weitzel et al. (2015)'s [1] second experimental design. First of all, the tumor microenvironment was not optimized, because E0771 is a breast cancer cell line, which should grow in fat tissue but not in muscle tissue. Therefore, E0771 cancer cells should be injected into the dorsal mammary

fat pad region of the mouse, instead of subcutaneous injection into muscle tissue. In fact, studies have shown that tumors grown orthotopically reflect the clinical effects of drugs more closely than the tumors grown subcutaneously; this is most likely because the tumor microenvironment would affect tumor growth, survival, metastasis and response to treatment. Therefore, such an orthotopic model reproduces the microenvironment at the primary site of human breast cancers, with a hope to provide efficacious evaluation in a preclinical tumor model. This allows for a more representative tactic of primary tumor growth, metastatic activity and response to treatments to be more accurately quantified.

Secondly, the tumors in the left leg regions were not real metastatic tumors, but were instead injected subcutaneously. In other words, we did not know whether the E0771 cancer cells in their primary site (right leg muscles) did metastasize to the left leg muscles. Therefore, before the current treatment study, two additional preliminary studies were performed using similar methodologies and the same endpoints, but neither radiation nor drug treatment was given. The preliminary studies were conducted with a hope to obtain a better treatment design for the current study.

The procedures and results from the two preliminary studies are described and discussed as follows:

1. The first preliminary study aimed to establish an E0771 metastatic model, so as to confirm that the tumor cells in the primary site of

the dorsal mammary fat pad region would spontaneously metastasize to the lungs. We injected half million E0771 cells (same as in Weitzel et al. 's study[1]) orthotopically; primary tumor growth was then monitored by caliper measurement. Results suggested that it took 14-18 days for the primary tumors to grow, and 22-25 days to exceed the limit of 1500mm^3. Lung metastasis was evaluated by IVIS and India-ink Assay. When the tumor volume exceeded the limit, we sacrificed the mice and dissected the lungs out for IVIS. To perform IVIS, D-luciferin was first injected into mouse body through i.p. injection, followed by 20 minutes waiting time for the luciferin to react before the image was taken. Results from the IVIS showed that lungs from both mice indicated lung metastatic tumors, though no nodule was observed in both lungs using India-ink Assay.

2. The second preliminary study aimed to confirm the E0771 metastatic model by using orthotopic injection, and to optimize the time for primary tumor by injecting more cancer cells. Half million E0771 cancer cells were orthotopically injected into two mice, and one million were injected in the other two mice. Results from the caliper measurement showed that the tumor grew very

slowly for the half-million-cell injection, which was consistent with the first preliminary study; while 10 days would be sufficient for the primary tumor volume to reach 100-200mm^3 for the one-million-cell injection, which allowed us to identify the location of tumors and hence define the irradiation site. Besides, 20 days would be enough for the tumor volume to exceed the limit of 1500mm^3. To perform IVIS, we found that the luc-signals decayed much faster than the first preliminary study, implying that 20-minute waiting-time was too long and not necessary to obtain the IVIS image. Therefore, we imaged the mice almost immediately after the D-luciferin injection; a sequence of images was then obtained to monitor the change of signal expression over time. For the one-million-cell injection, results from IVIS showed that only 1 out of 2 mice showed luciferase signals from lungs through lung IVIS imaging. (Probability or Fast decay). No nodule was found from both lungs. After that, we decided to speed up the procedures of dissecting the lungs out, and imaged the mice 15 minutes after luc-injection for the other two mice with the half-million-cell-injection. At the same time, we performed a time point study for luciferase expression to see how long it took for

the signal to reach its maximum value, which was crucial for data analyses. For the half-million-cell-injection, results from IVIS showed that only 1 out of 2 mice showed signals from primary tumors under whole-mouse imaging, although there was a palpable tumor seen on the dorsal region. Later on, when we took out the lung, we also dissected the primary tumors out, and performed the primary tumor IVIS imaging. Results showed that both primary tumors from two mice had luciferase signals. For the lung IVIS imaging, luciferase signals from the lungs were only seen in one mouse, with much less signal intensity compared to the primary tumors. Again, no nodule was found from the lungs of the two mice using India-ink Assay.

Based on results from the two preliminary studies and the aforementioned rationales, we shifted from the dual-flank model to the orthotopic model, with doubled amount of cancer cells injected, and we defined 10 days after the cancer-cell implantation as the treatment day (day 0). With these modifications, we would like to determine whether we could replicate Weitzel et al. (2015)'s results[1]. Comparisons between our experiment results and Weitzel et al. (2015)'s results[1] are made and are divided into two categories for discussion: Primary tumor, and lung metastases, respectively.

4.1 Primary Tumors:

4.1.1 Caliper Measurement and Survival Plots

Caliper measurement results from Weitzel's studies[1] showed that RT-alone led to primary tumor growth delay; anti-PD-L1-alone had no significant effect on primary tumor growth; while RT combined with anti-PD-L1 antibody treatment inhibited primary tumor growth, as shown in **figure 4.1.1.1**.

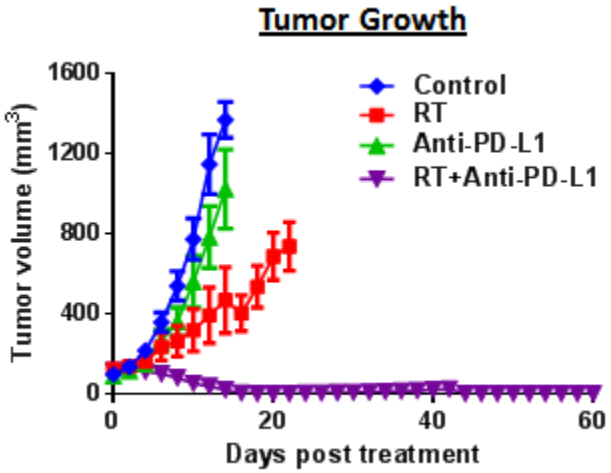

Figure 4.1.1.1 A Plot shows primary tumor growth over time from Weitzel's study[1].

However, caliper measurement from the current study showed a different result. As shown in the Result section, RT-alone showed no effects on the primary tumor growth; anti-PD-L1-alone slightly delayed the primary tumor growth; and combined RT with anti-PD-L1 antibody treatment showed non-durable delayed primary tumor growth.

On the other hand, survival curves from Weitzel's study[1] are shown in **figure 4.1.1.2**. It showed that RT combined with anti-PD-L1 antibody treatment caused prolonged survival of the mice, and 7 (out of 8) mice were still alive for 2 months after the treatment.

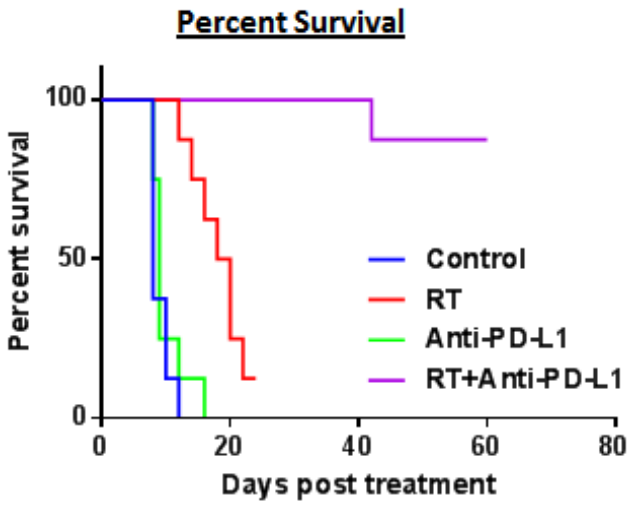

Figure 4.1.1.2: A survival plot shows percent survival over time from Weitzel's study[1].

However, in our experiment, we did not see any prolonged survival for all groups, as shown in **figure 4.1.1.3**. All mice died eventually, meaning that all the mice reached their endpoints (tumor volume≥ 1500mm^3).

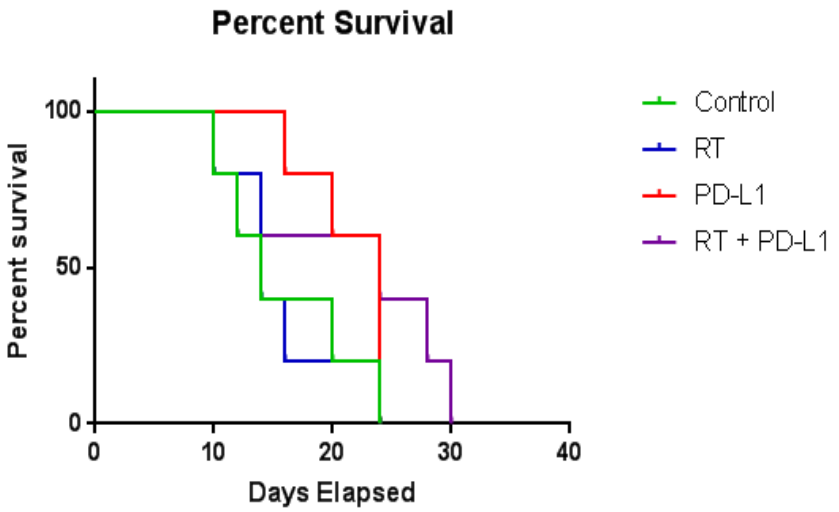

Figure 4.1.1.3: A survival plot shows percent survival against days post treatment for the current study.

There are several possible explanations to account for those differences between our results and Weitzel's results[1]:

i. A single radiation dose of 10Gy was enough for mouse models with subcutaneous injection, but that may not be enough for mouse models with orthotopic injection. Because of the difference between the two models, the tumor microenvironment was not identical, which affects tumor growth and their responses to treatment.

ii. The timeline was not optimized. In Weitzel's study[1], they claimed that the tumor volumes reached 100-200mm^3 on the treatment day, allowing them to identify the tumor locations, and hence the irradiation sites. However, in our experiment, we estimated that the orthotopic tumors need 10 days after cell implantation to reach a volume of 100-200mm^3, based on the preliminary

studies. Unfortunately, in the current treatment study, we found that the tumor grew surprisingly slowly, even when we doubled the amount of cells for injection. In other words, 10 days was not enough for the orthotopic tumors to reach 100-200mm^3, implying that the tumor location was not well defined; the irradiation site was just assumed to be the injection site for most of the mice. This may cause uncertainties to the treatment response for the current study.

4.1.2 In-Vivo Imaging System (IVIS):

It should be noted that there was no IVIS experiment performed from Weitzel's study[1], because the mouse model that they employed was not genetically engineered. Here, data of primary tumors obtained from IVIS for the current study are shown in **figure 3.3.5** and are discussed.

None of the treatment groups showed significant difference, when they were compared with the control group (RT-alone vs control: p=0.9999; anti-PD-L1-alone vs control: p=0.6676; RT + anti-PD-L1 vs control: p=0.9871). These findings suggested that the combination treatment of RT and anti-PD-L1 antibody treatment did not kill the primary tumor cells effectively. However, interestingly, neither RT-alone nor anti-PD-L1-alone reduced the signal intensity (in terms of median total photon flux), compared with the control group. These findings provoked us to question the validation of the relationship between the luciferase-signal expression and the tumor response. On the

other hand, when we looked at the luciferase-expression for each individual mouse, we found that the luciferase-expression dramatically varied among each other, even within the same treatment group, as shown in **figure 3.3.3**. Some of the mice were excluded when performing the data analysis, resulting in a reduction in the sample size. Also, two subjects were excluded from data analysis because of the technical problems, which further decreased the sample size. Therefore, the validation from the IVIS data analysis for the primary tumor was doubted.

4.2 Lung Metastases:

In Weitzel's second study[1] using the dual-flank tumor model, E0771 cancer cells were injected subcutaneously into both leg muscles, while radiation was only given to the right leg. The results are shown in **figure 4.2.1**.

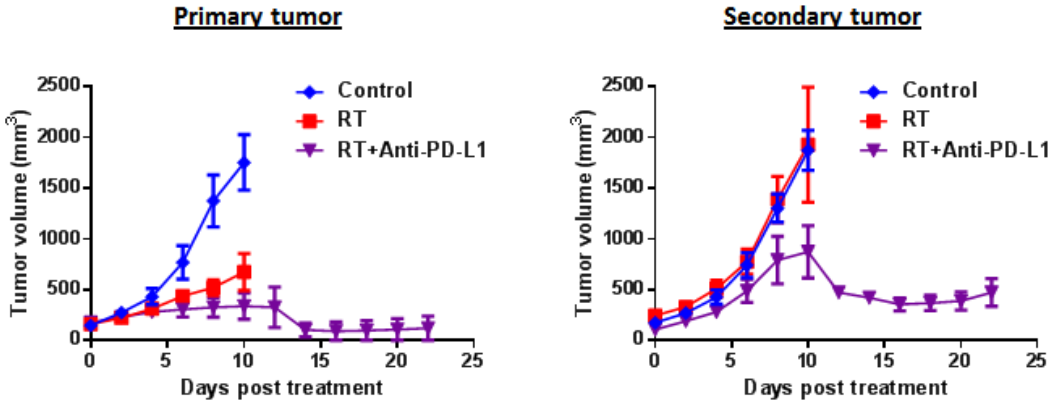

Figure 4.2.1: Two plots show tumor volume for primary tumor (left) and secondary tumor (right) changes over time from Weitzel's study[1].

Results of his study showed that the primary tumors responded consistently with his previous study; RT-alone delayed the primary tumor growth and combination treatment inhibited the primary tumor growth. Furthermore, from the right figure of **figure 4.2.1**, it can be seen that RT combined with anti-PD-L1 antibody treatment showed a distant effect in eliminating the tumors that are un-irradiated and distant from the primary tumors; while RT-alone had no difference, compared to the control group.

Due to the fact that the tumors in left legs in his study were not real metastatic tumors, several modifications were made in the current study with a hope to develop a metastatic model. We injected the E0771 cancer cells into their dorsal fat pad region (primary tumors) to see whether the cancer cells would grow in the lungs (metastatic lung masses). After that, we used IVIS and India-ink Assay to evaluate and validate the lung mass formation.

4.2.1 In-Vivo Imaging System (IVIS):

Results of the preliminary studies using IVIS showed that lung mass formation was confirmed in some of the mice with orthotopic injection, but not all. In the current treatment study, statistical analysis of p-values for IVIS data **(figure 3.3.6)** showed that RT-alone ($p=0.3433$), anti-PD-L1-alone ($p=0.3058$) and RT + anti-PD-L1 ($p=0.4053$) did not show significant difference when they were compared to the control group. This finding suggested that all the treatment methods used in the current study did not help reducing the burdens of the lung metastases. Nevertheless, there were some limitations

when using the IVIS. First of all, the luciferase expression was not stable for E0771 cancer cell line; this expression dramatically varied among the mice, even within the same group. The luciferase expression relies on the ATP storage of the subjects, which may be markedly different among the mice and hence may account for the instability of the signal expression. Secondly, the decay rate of the luciferase signal expression decayed unstably, meaning that the expression reached their peaks at very different times post-luciferin-injection, ranging approximately from 5 minutes to 30 minutes. In some occasions, there was no luciferase signal expression for some mice, even though a large palpable tumor was observed. Therefore, we concluded that luciferase expression may not correlate well to the metastatic lung mass formation. This has raised a question as to whether the results would be different if a better metastatic model was selected.

To have a better idea to answer this question, results from another previous study using another mouse model (4T1 model) may help. The 4T1 model, which also involves a breast cancer cell line – 4T1, is a well-established metastatic model with stable luciferase expression. The experimental procedures to evaluate the lung mass formations were basically the same as the current study using IVIS. The results of IVIS data are shown in **figure 4.2.1.1**.

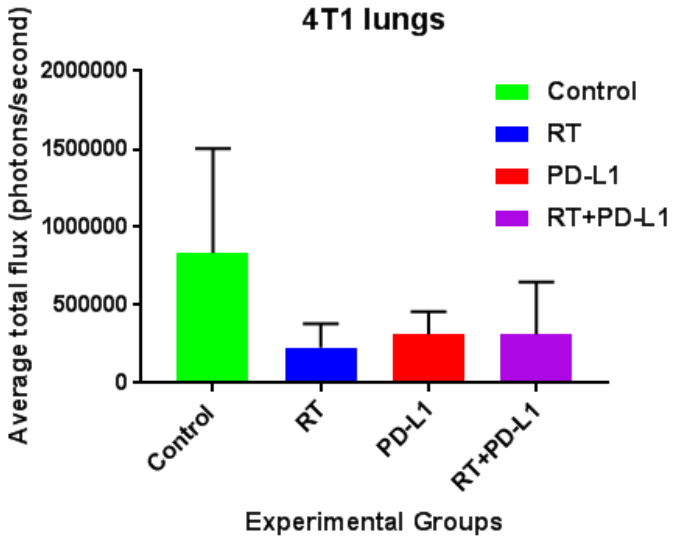

Figure 4.2.1.1: A Plot shows the average total photon flux emitted from lung tissue for each of the four groups using 4T1 model.

Table 4.2.1.1: A table shows the results from multiple comparisons using Two-way ANOVA (For lung metastases, 4T1 model)

Dunnett's multiple comparisons test	Significant?	Adjusted P Values
Control vs. RT-alone	No	0.2571
Control vs. anti-PD-L1-alone	No	0.2841
Control vs. RT + anti-PD-L1	No	0.3747

Data analysis with p-values, shown in **table 4.2.1.1**, suggested that with a good metastatic model, the combination treatment did not significantly reduce the burdens of lung metastases, also neither did the RT-alone nor the anti-PD-L1-alone treatment. This finding implies that the combination treatment may not be able to produce a statistically significant distant effect, when orthotopic injection is used.

4.2.2 India-ink Assay:

The India-ink Assay is a histological method, which makes use of the color contrast by injecting the dark ink into the air pipes. The nodules (if existent) would appear as white spots. In this current study, there were limitations when performing this technique. Ideally, whole intact lungs with tracheas should be dissected out, and then the ink should be injected via the tracheas. However, there might be damage to the lungs or tracheas during the lung harvest, such that the ink would not go through the whole lungs. Despite that, we assumed such human errors should not greatly affect the results because the main objective of this assay is to make a strong contrast to facilitate the nodules counting process.

Most importantly, we found that all of the lung samples from all of the groups did not show any grossly observable nodules using India-ink Assay, though invisible micro-metastases might exsit. This would probably explain why some of the lung samples did show the luciferase signal using IVIS, but did not develop observable nodules using India-Ink Assay.

4.3 Zenascope Measurement:

There are a number of limitations of zenascope measurement with the use of an optical probe. The first limitation is the pigmentation with the black mice, which hinders

the light passing through the skin tissue to reach the deep seated tumors. Several mice were marked as "suspected" data, due to the pigmentation or scars on skin, etc.

Secondly, the fur also affects the performance of optical measurement. It should be noted that a shave was used to remove the fur. The use of "Nair", a branch product for hair removal, was avoided in the current study, so as to avoid any skin effects which would affect the performance of optical measurement.

In addition, from the results shown in section 3.5.1 and 3.5.2 (excluding those with "suspected data"), it can be seen that there was a gradual increase in Hb-sat levels in the control group, possibly relating to the blood vessel growths within those tumors. Also, there was a gradual decrease in Hb-sat levels in anti-PD-L1-alone group. However, when radiation was involved (RT-alone and RT + anti-PD-L1 group), the relationship between the changes in Hb-sat levels and the tumor growth becomes unclear. On the other hand, the total-Hb levels remained almost unchanged in both the control group and anti-PD-L1-alone group. However, when radiation was involved, the change becomes unclear again. One possible explanation may be that this is due to the non-optimized timeline to start the treatment. Due to the fact that most of the tumors grew very slowly and did not reach a palpable volume, and that the optical measurement was performed in the early days after the treatment (day-1, day0, day1, day2, day3), there may be uncertainties in defining the tumor locations and also the sites for placing the optical probe for the measurement.

Other possible limitations for this measurement include the motion of the mouse and/or hands of operators. Apart from this, it would also be interesting to determine whether 10 Gy of radiation dose in a single fraction causes any local vascular damage, which in turn would affect the results of the zenascope measurement.

4.4 Future Study:

Results from the current study appeared to be inconsistent with the previous findings from Weitzel's study[1]. In addition, IVIS used in the current study displayed a large variation in the data. Here, a number of possible explanations and suggestions are provided for improvements for future study.

First of all, the ability to know the tumor size before beginning the treatment is crucial. However, the selection of the optimal starting point of the treatment day is complex because of the variation in the tumor growth rate among individual mice. To address the irregular growth rate of the cancer cells, one possible solution is to increase the amount of cancer cells for injection. This might help the cells multiply more quickly and hence the tumors would reach the optimal starting point in a more consistent manner.

Secondly, although a single fraction of 10 Gy was sufficient to almost completely eliminate the subcutaneously implanted tumors, 10 Gy appeared to be inadequate to affect the growth of the orthotopically implanted tumors. The failure to affect the orthotopic tumors' growth may have been due to other confounding factors, such as the

unoptimized starting point of the treatment previously mentioned. Nevertheless, in future study, a higher radiation dose, for example 15 Gy or 20 Gy, could be used to test the effectiveness of the radiation.

Thirdly, regarding the IVIS, it was found that there was no signal from the primary tumors even though there was a palpable tumor on the dorsal mammary fat pad. It could possibly be ascribed to the following four scenarios.

a) The heterogeneity in the level of expression of the reporter gene (the luciferase) within the tumor cell population may account for the absence of the signal in the images. If a tumor started from a group of cells that had low to no expression of the reporter gene, then it would not be possible to get any signal in that particular animal.

b) The pigmentation of the mice might block the light photons reaching the built-in camera of IVIS. Therefore, performing in-vitro primary tumor imaging using IVIS may eliminate the influence of the pigmentation.

c) The fast decay of the luciferase signal might also result in the absence of the signal in the images. In general, the luciferase signal diminishes dramatically within 20 minutes post D-luciferin injection, though the signal decay rate varies. Therefore, the time required for lung harvesting becomes crucial and expertise in lung dissection becomes a factor. In addition, performing an imaging sequencing immediately after the injection of D-luciferin could

guarantee the imaging process would take place within the appropriate time frame.

d) The insufficient amount of infiltrating-D-Luciferin interacting with the E0771-luciferase cancer cells in the tumor microenvironment could also account for the absence of the signal. This infiltration problem could be solved by increasing the injection rate of the D-Luciferin.

e) Finally, the current experiments were rather small; there were only five animals per group. Thus, a rigorous statistical testing was not possible. Future studies could increase the sample size to increase the amount of data for analysis.

5. Conclusions:

The untapped potential of this combination treatment of radiation and ICB for improving the outcome of the cancer treatment is yet to be fully realized. In the current study, radiation combined with anti-PD-L1 immunotherapy using E0771 model did not significantly eliminate the primary tumors and reduce the burden of lung metastases. However, the treatment response and the E0771 model were affected by a number of technical problems that render the evaluation inconclusive. Solutions to some of these technical problems have been provided, enabling future reseachers to replicate and improve on this study and futher determine the treatment response and the usefulness of the E0771 model. Further research is needed to uncover the promise of this combined therapy.

6. Appendix A (The IVIS Images with the E0771-luc Model):

Control- Mouse 1:

Day of euthanasia: 12 days post treatment;

ROI data used: 7.713×10^2 photons per second;

The segment used for data analysis: The third segment, which was obtained at 9 minutes 36 seconds after the D-luc injection.

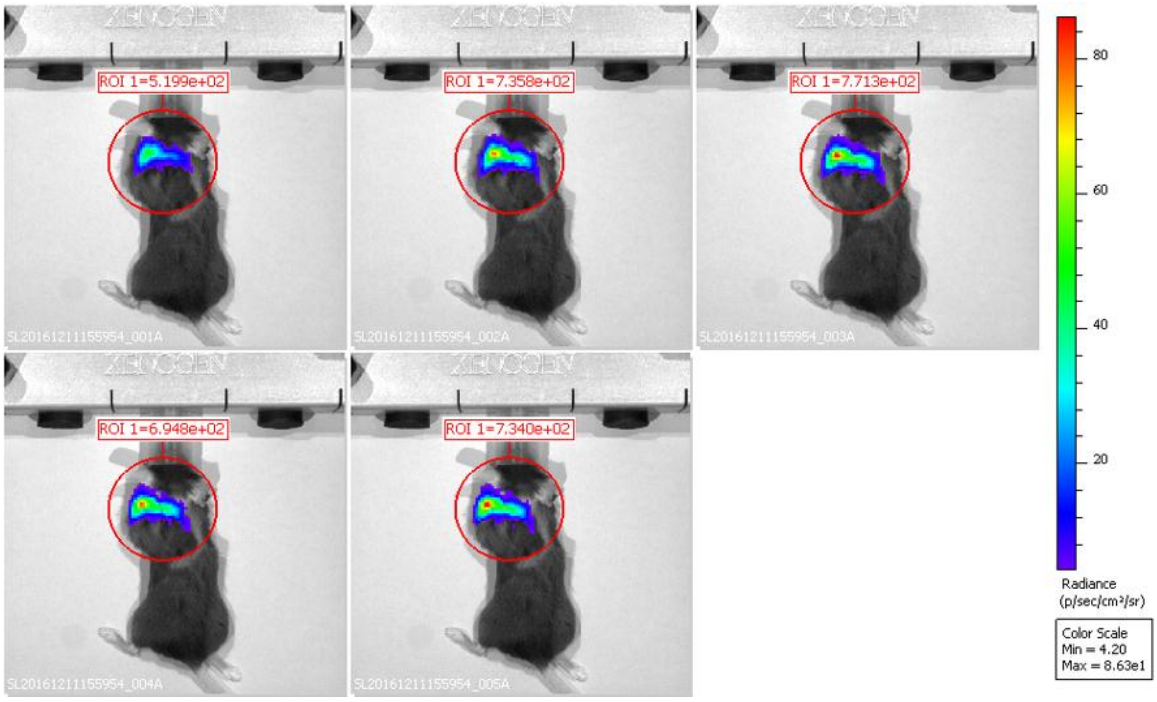

Control- Mouse 2:

Day of euthanasia: 10 days post treatment;

ROI data used: 1.436×10^3 photons per second;

The segment used for data analysis: The first segment, which was obtained at 9 minutes after the D-luc injection.

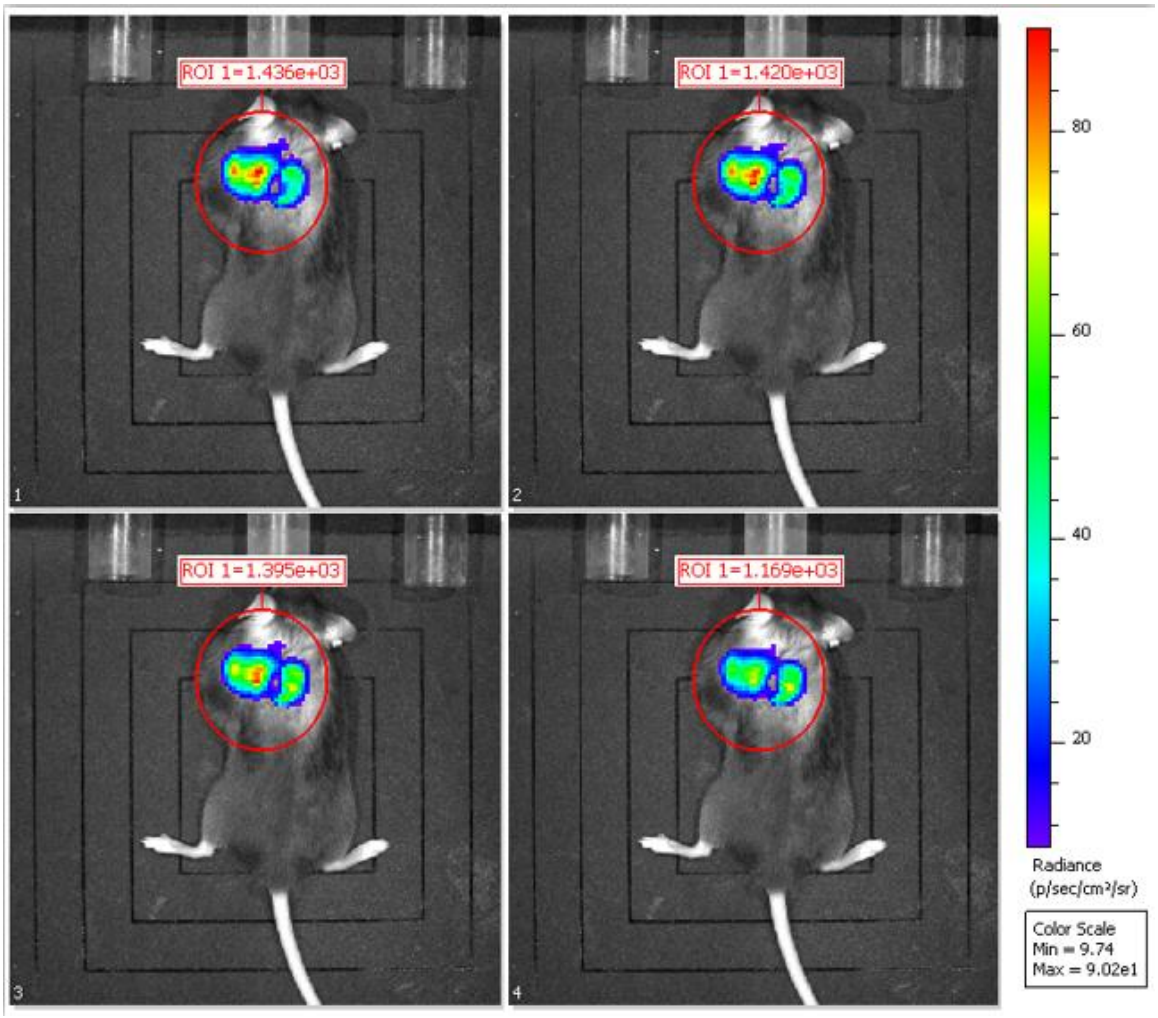

Control- Mouse 3:

Day of euthanasia: 14 days post treatment;

ROI data used: 6.263 x 10^7 photons per second;

The segment used for data analysis: The second segment, which was obtained at 9 minutes 43 seconds after the D-luc injection.

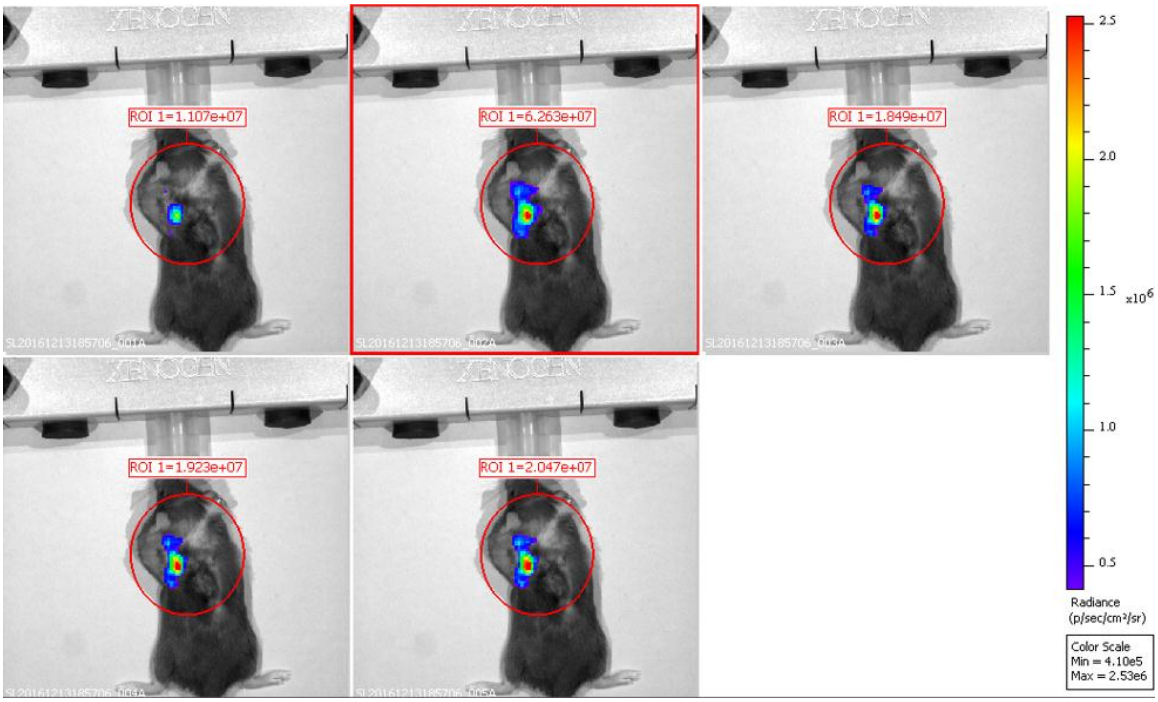

Control- Mouse 4:

Day of euthanasia: 24 days post treatment;

ROI data used: 1.104×10^5 photons per second;

The image used for data analysis: The image below was taken at 15 minutes 50 seconds after the D-luc injection.

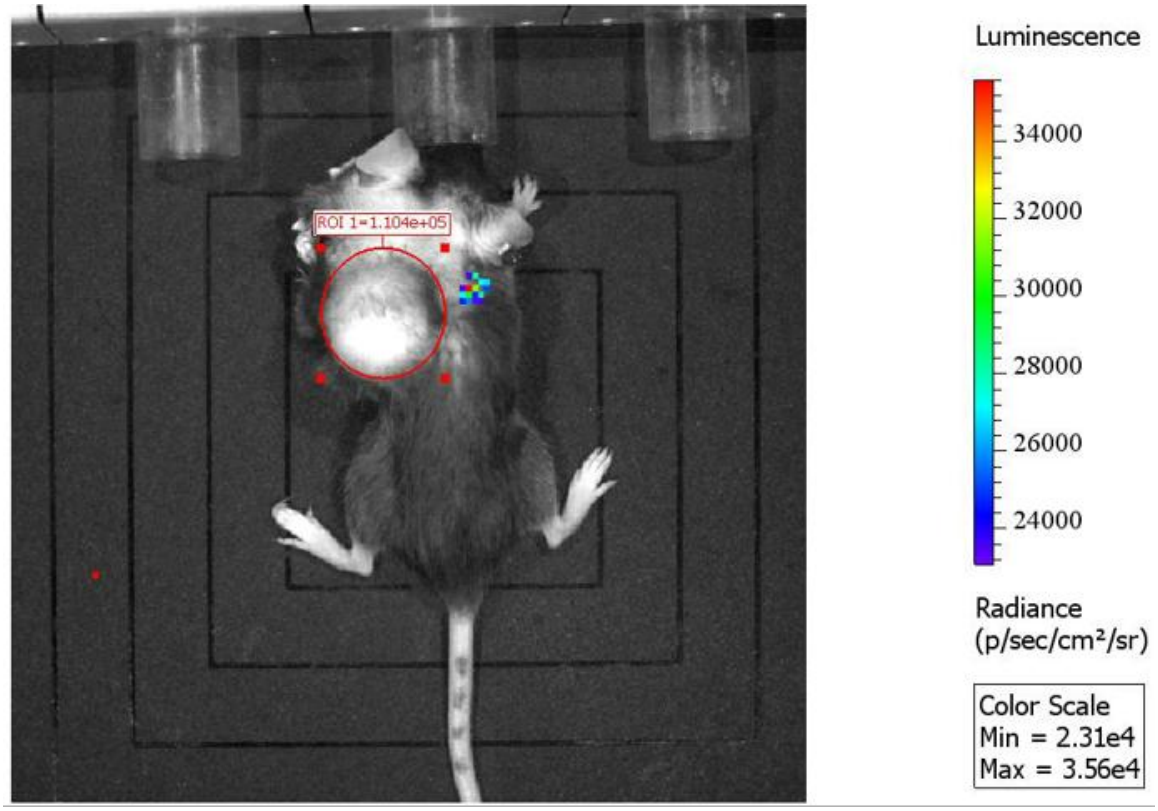

Control- Mouse 5:

Day of euthanasia: 20 days post treatment;

ROI data used: 5.699×10^7 photons per second;

The segment used for data analysis: The fourth segment, which was obtained at 13 minutes 20 seconds after the D-luc injection.

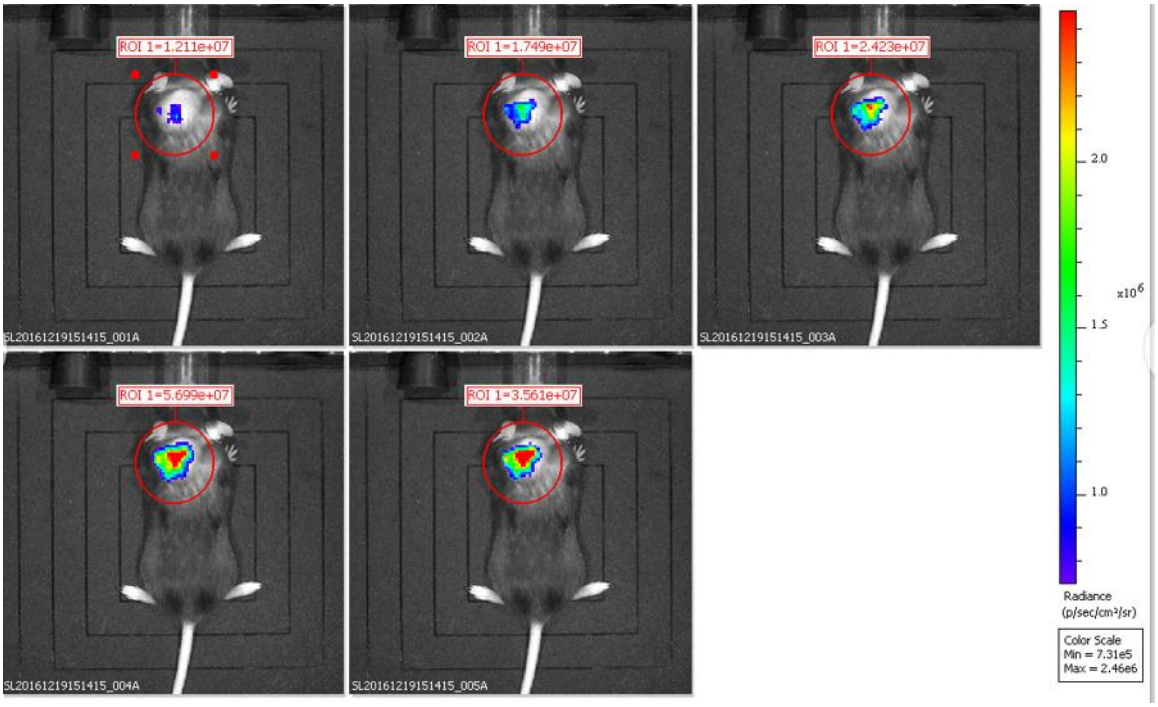

RT-alone- Mouse 1:

Day of euthanasia: 22 days post treatment;

ROI data used: 1.600 x 10^7 photons per second;

The image used for data analysis: The image below was taken at 18 minutes after the D-luc injection.

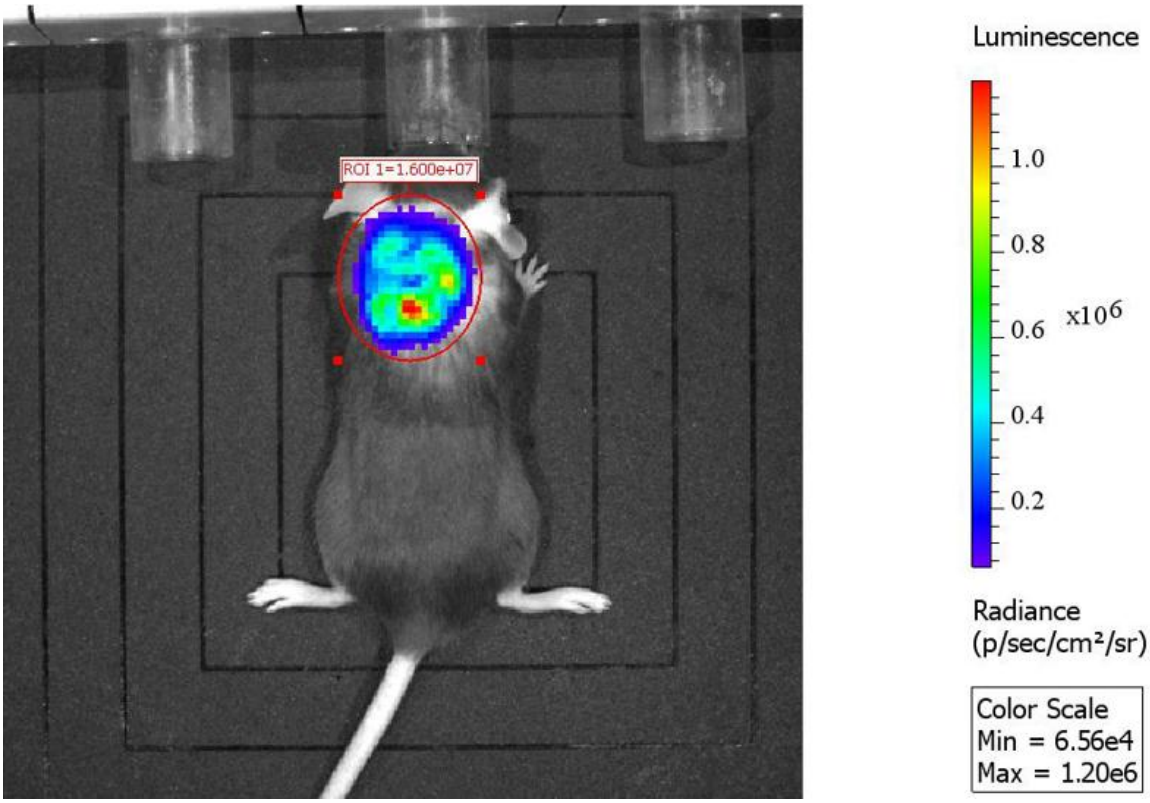

RT-alone - Mouse 2:

Day of euthanasia: 16 days post treatment;

ROI data used: 2.652×10^7 photons per second;

The segment used for data analysis: The sixth segment, which was obtained at 15 minutes 42 seconds after the D-luc injection.

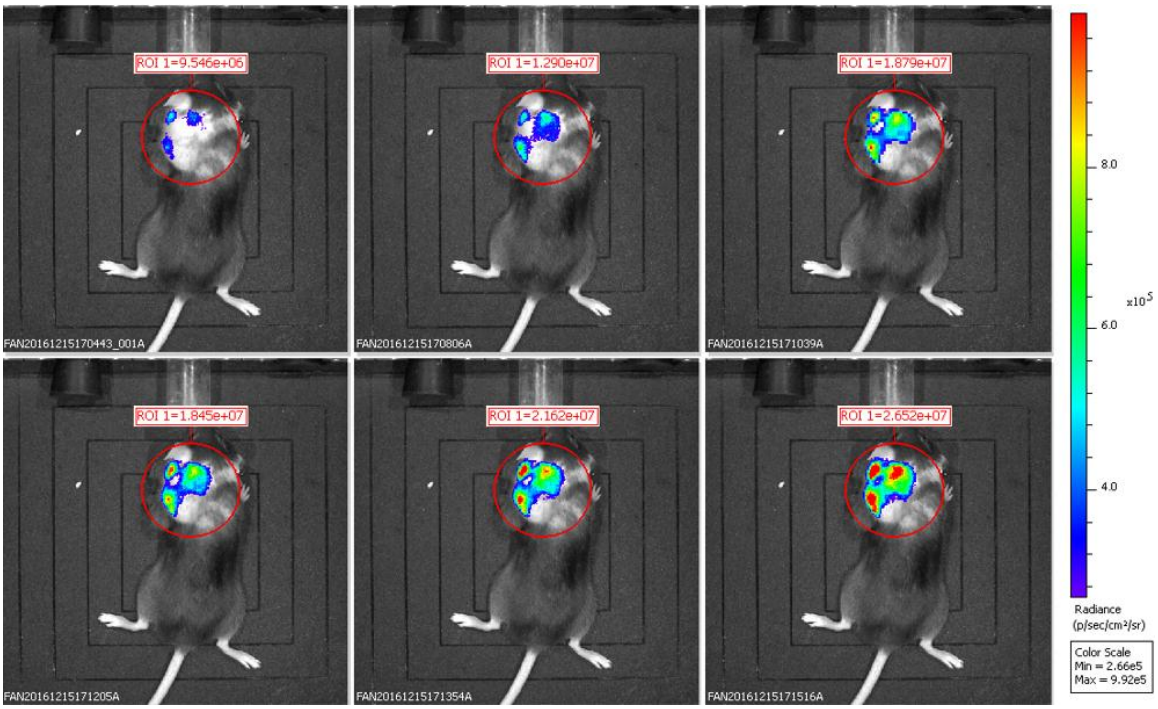

RT-alone - Mouse 3:

Day of euthanasia: 8 days post treatment;

ROI data used: Not recorded;

Remarks: Data lost.

RT-alone - Mouse 4:

Day of euthanasia: 14 days post treatment;

ROI data used: 7.300×10^7 photons per second;

The segment used for data analysis: The first segment, which was obtained at 4 minutes 30 seconds after the D-luc injection.

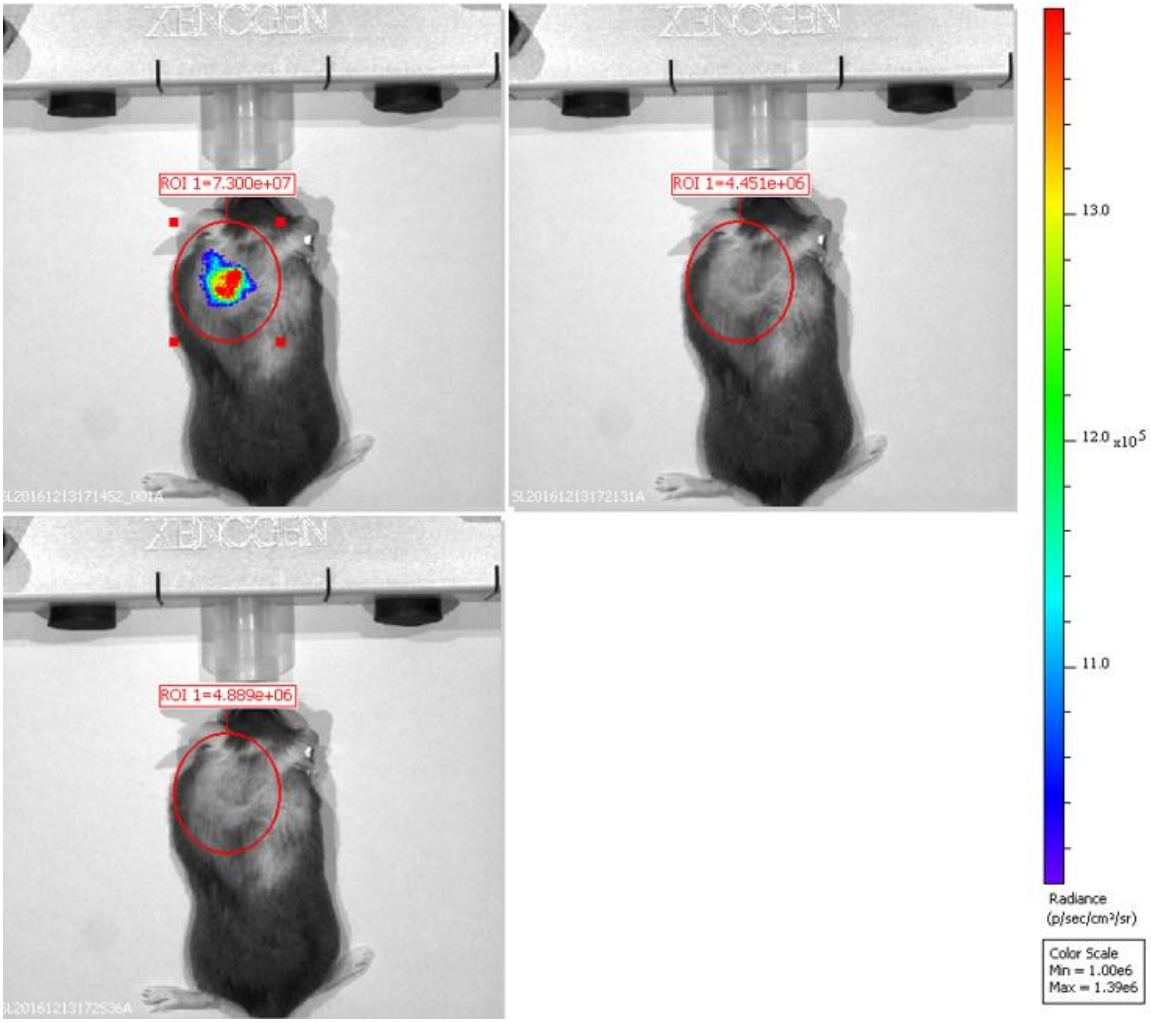

RT-alone - Mouse 5:

Day of euthanasia: 14 days post treatment;

ROI data used: Not recorded.

Remarks: The IVIS suddenly shut off without automatically saving the images.

Anti-PD-L1-alone - Mouse 1:

Day of euthanasia: 20 days post treatment;

ROI data used: 1.739 x 10^8 photons per second;

The segment used for data analysis: The fifth segment, which was obtained at 17 minutes 50 seconds after the D-luc injection.

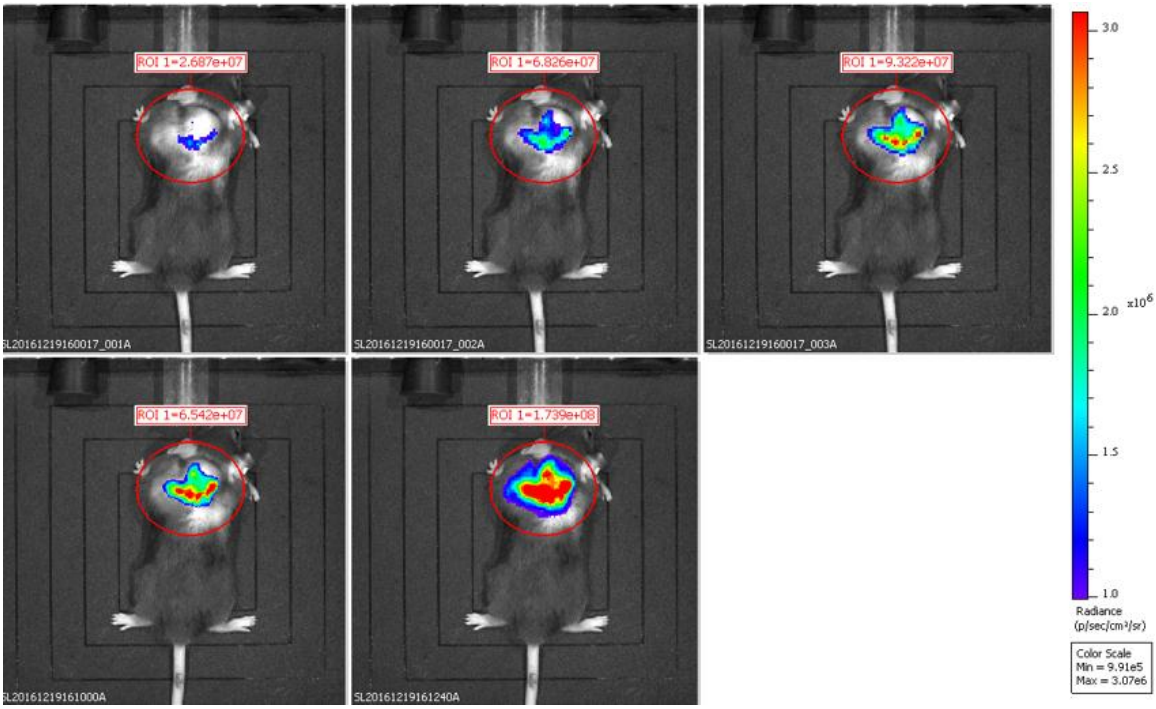

Anti-PD-L1-alone - Mouse 2:

Day of euthanasia: 16 days post treatment;

ROI data used: 3.811×10^7 photons per second;

The segment used for data analysis: The third segment, which was obtained at 11 minutes 19 seconds after the D-luc injection.

Remarks: Due to machine breakdown, it was not possible to image more than three segments.

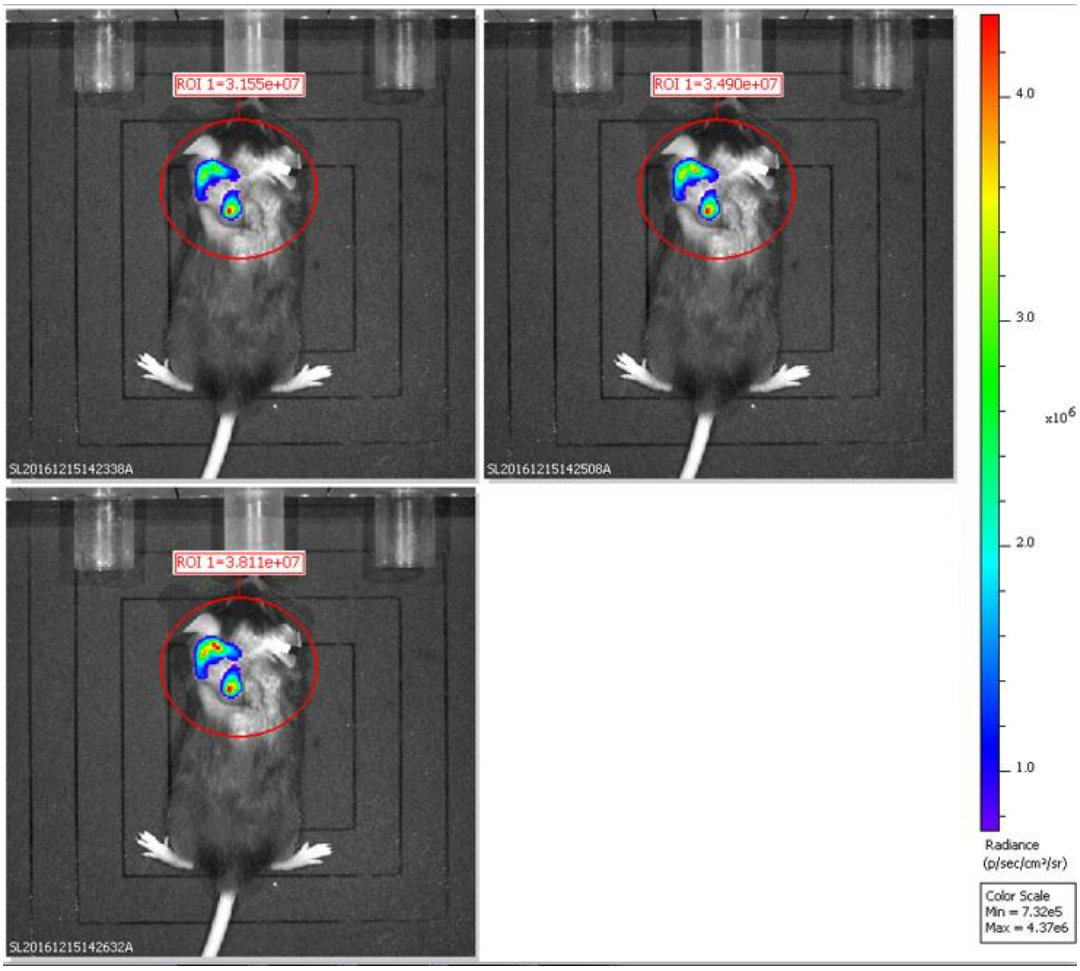

Anti-PD-L1-alone - Mouse 3:

Day of euthanasia: 24 days post treatment;

ROI data used: 4.446 x 10^6 photons per second;

The image used for data analysis: The image below was taken at 13 minutes 30 seconds after the D-luc injection.

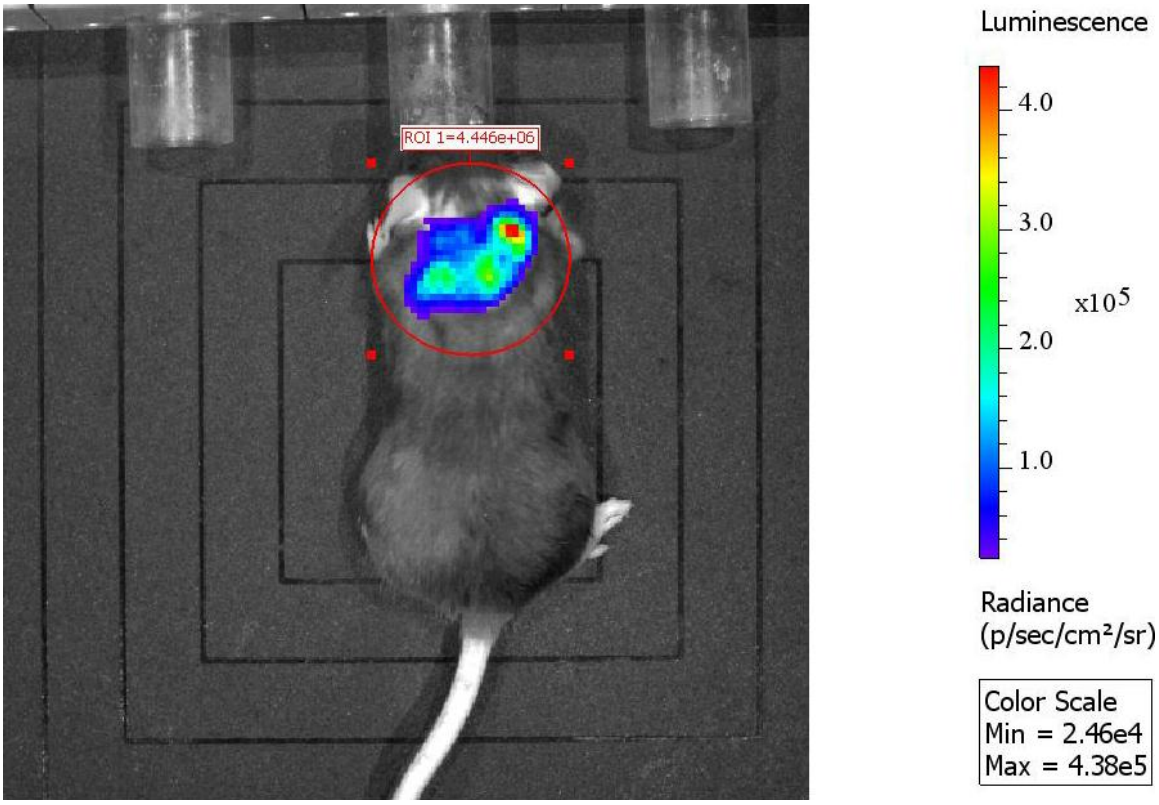

Anti-PD-L1-alone - Mouse 4:

Day of euthanasia: 22 days post treatment;

ROI data used: Not recorded;

Remarks: Data lost.

Anti-PD-L1-alone - Mouse 5:

Day of euthanasia: 22 days post treatment;

ROI data used: 5.887 x 10^7 photons per second;

The image used for data analysis: The image below was taken at 16 minutes after the D-luc injection.

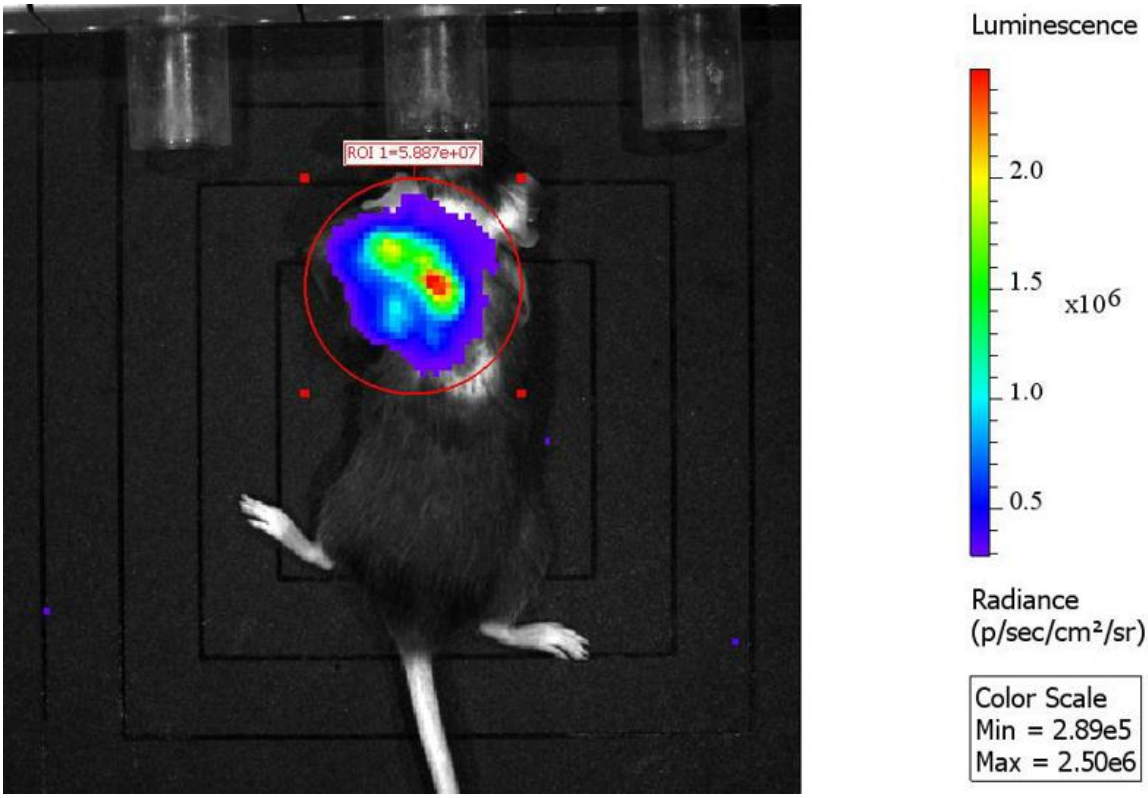

RT + Anti-PD-L1 – Mouse 1:

Day of euthanasia: 24 days post treatment;

ROI data used: 6.497 x 10^6 photons per second;

The image used for data analysis: The image below was taken at 16 minutes after the D-luc injection.

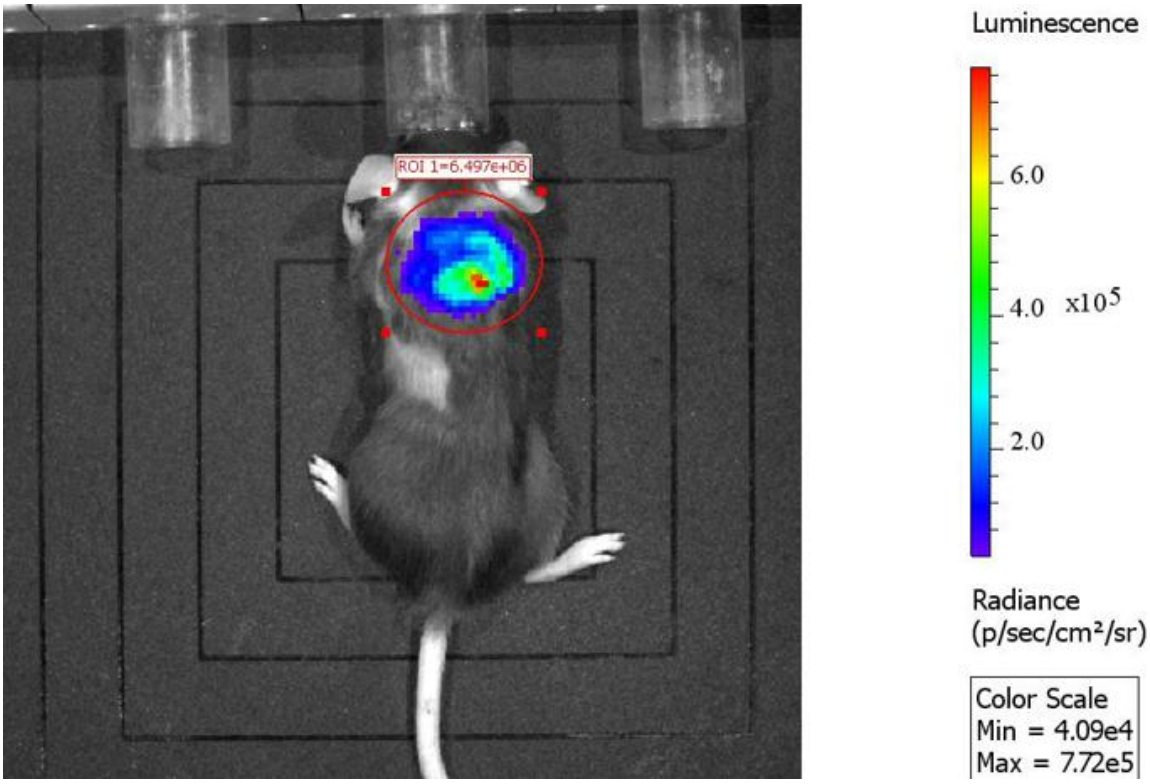

RT + Anti-PD-L1 – Mouse 2:

Day of euthanasia: 13 days post treatment;

ROI data used: 7.627×10^2 photons per second;

The segment used for data analysis: The third segment, which was taken at 11 minutes 02 seconds after the D-luc injection.

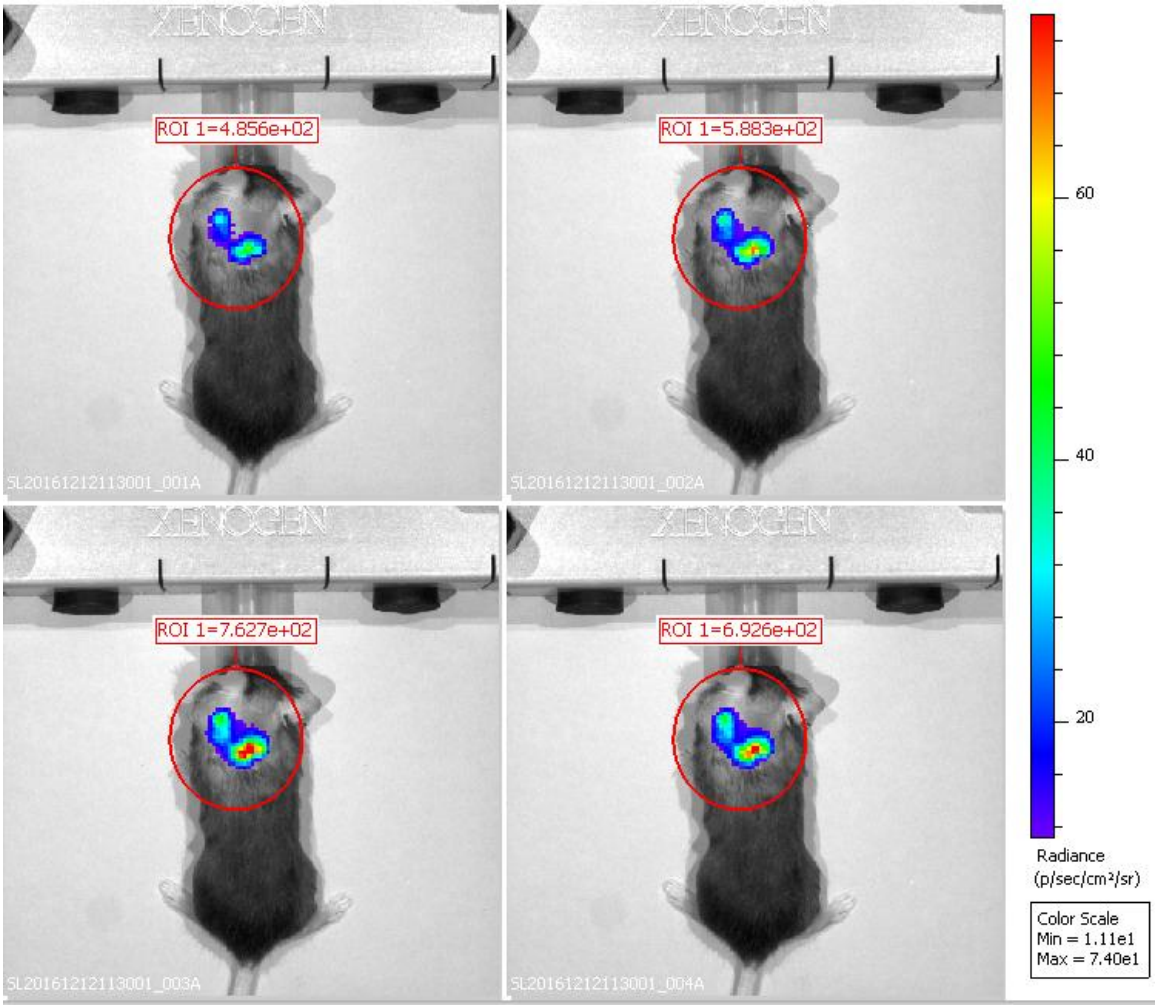

RT + Anti-PD-L1 – Mouse 3:

Day of euthanasia: 28 days post treatment;

ROI data used: 1.392 x 10^6 photons per second;

The image used for data analysis: The image below was taken at 06 minutes 30 seconds after the D-luc injection.

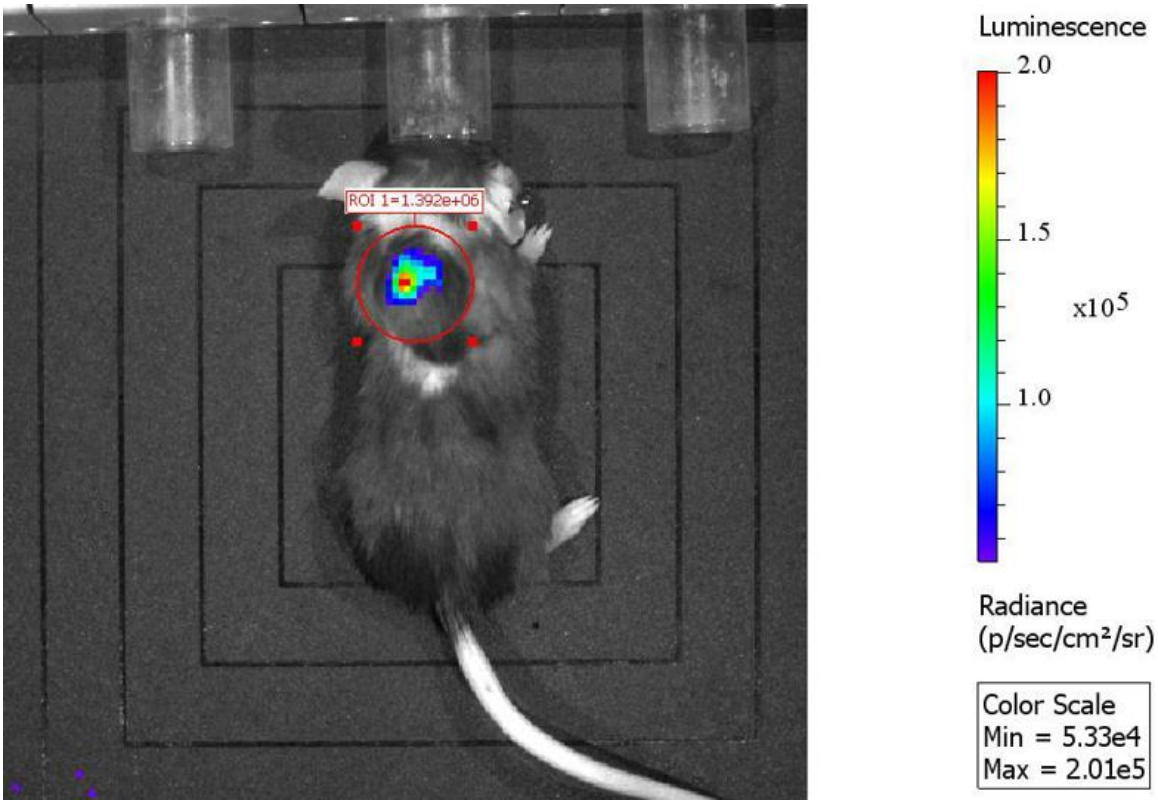

RT + Anti-PD-L1 – Mouse 4:

Day of euthanasia: 28 days post treatment;

ROI data used: 6.666 x 10^7 photons per second;

The image used for data analysis: The image below was taken at 16 minutes after the D-luc injection.

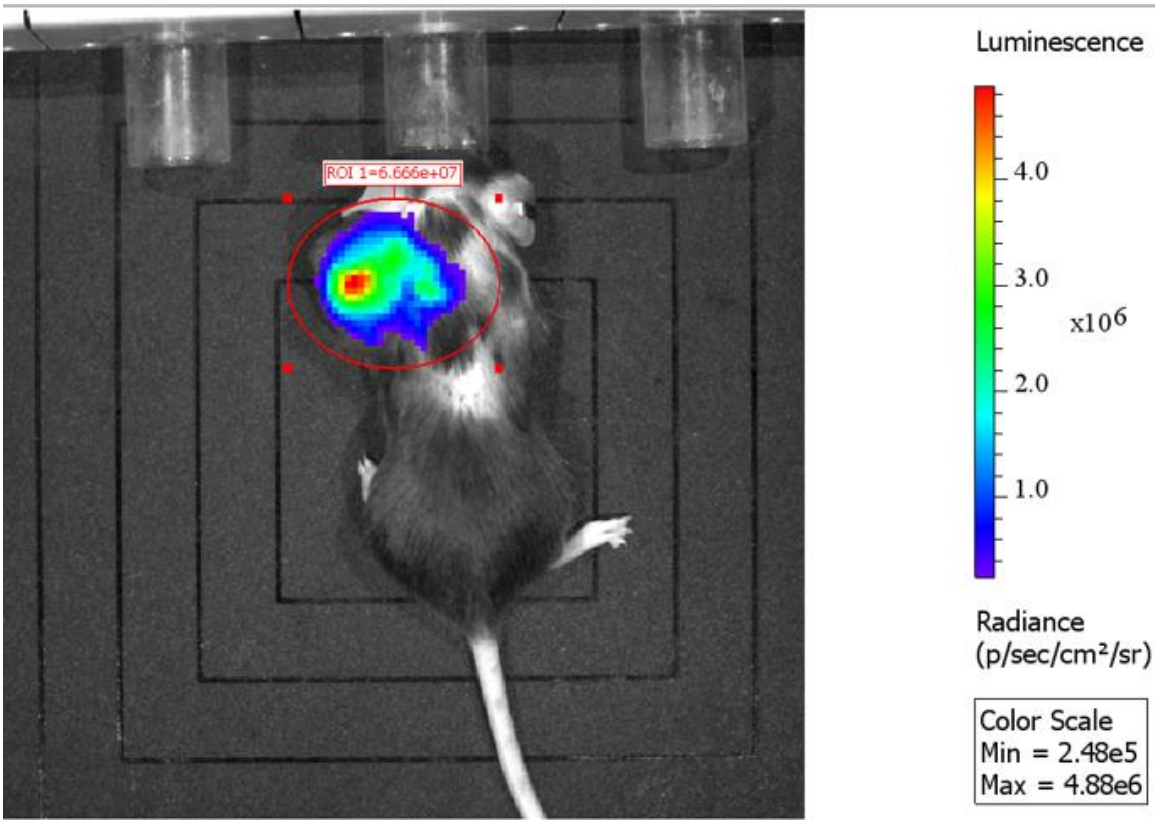

RT + Anti-PD-L1 – Mouse 5:

Day of euthanasia: 10 days post treatment;

ROI data used: 1.369 x 10^2 photons per second;

The segment used for data analysis: The fifth segment, which was obtained at 17 minutes 32 seconds after the D-luc injection.

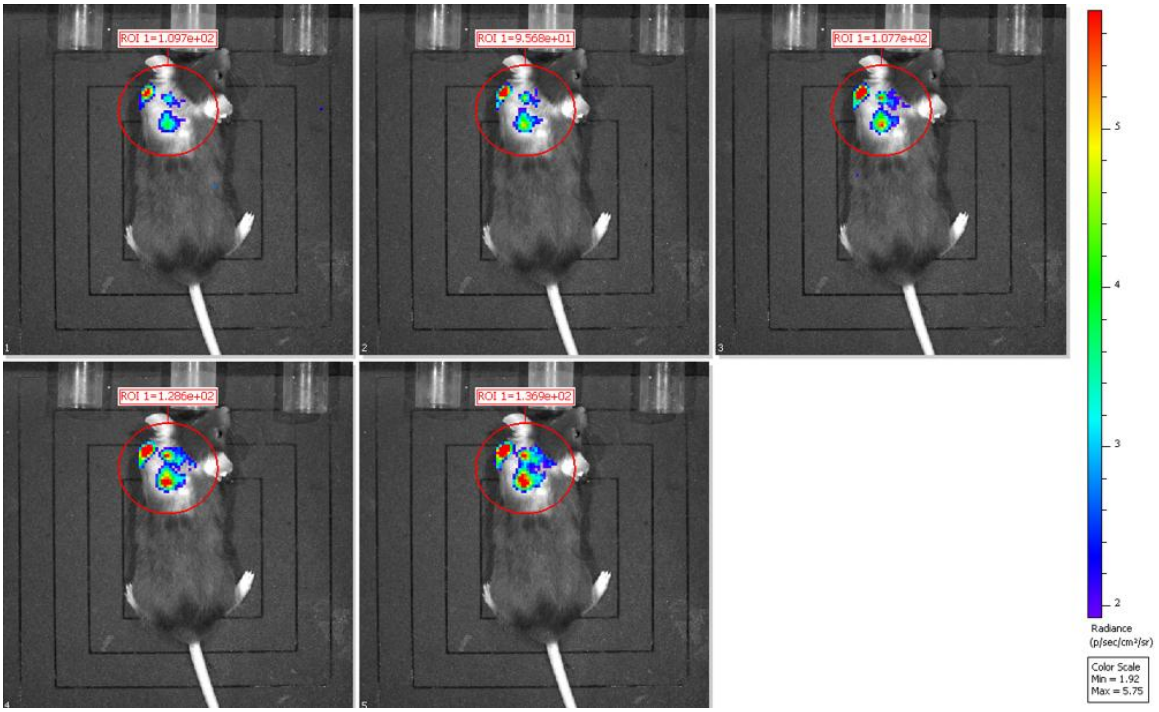

Control - Lung 1:

Day of euthanasia: 12 days post treatment;

ROI data used: 9.021×10^5 photons per second;

The image used for data analysis: The image below was taken at 17 minutes 32 seconds after the D-luc injection.

Remarks: These seem very close to background levels, further study should pay attention to subtract the background levels in order to improve the image quality.

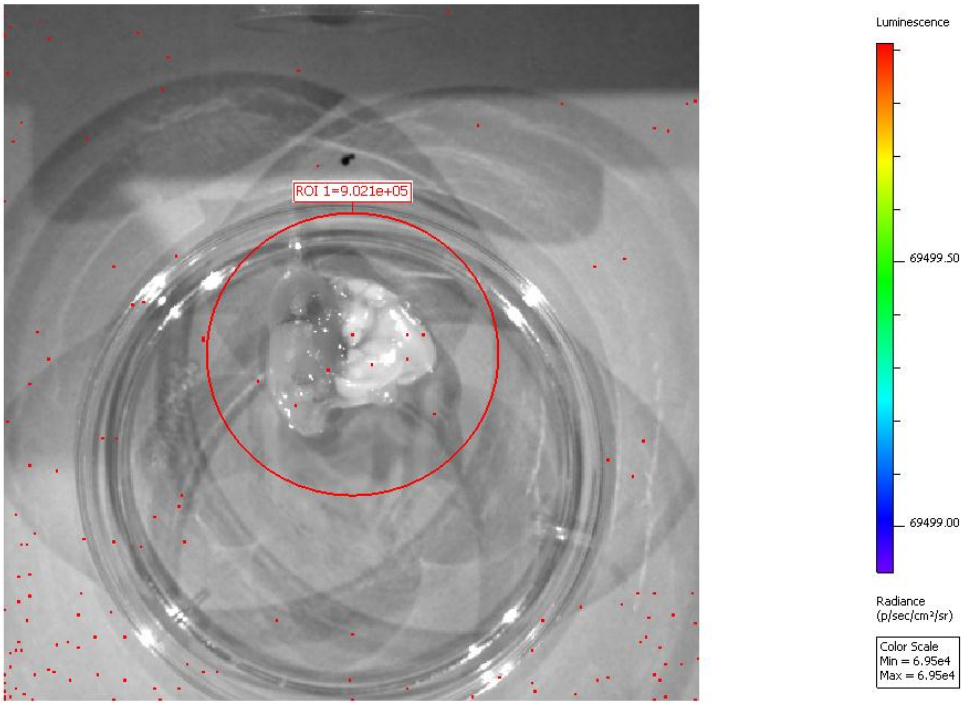

Control - Lung 2:

Day of euthanasia: 10 days post treatment;

ROI data used: 1.370 x 10^6 photons per second;

The segment used for data analysis: The first segment, which was obtained at 19 minutes 20 seconds after the D-luc injection.

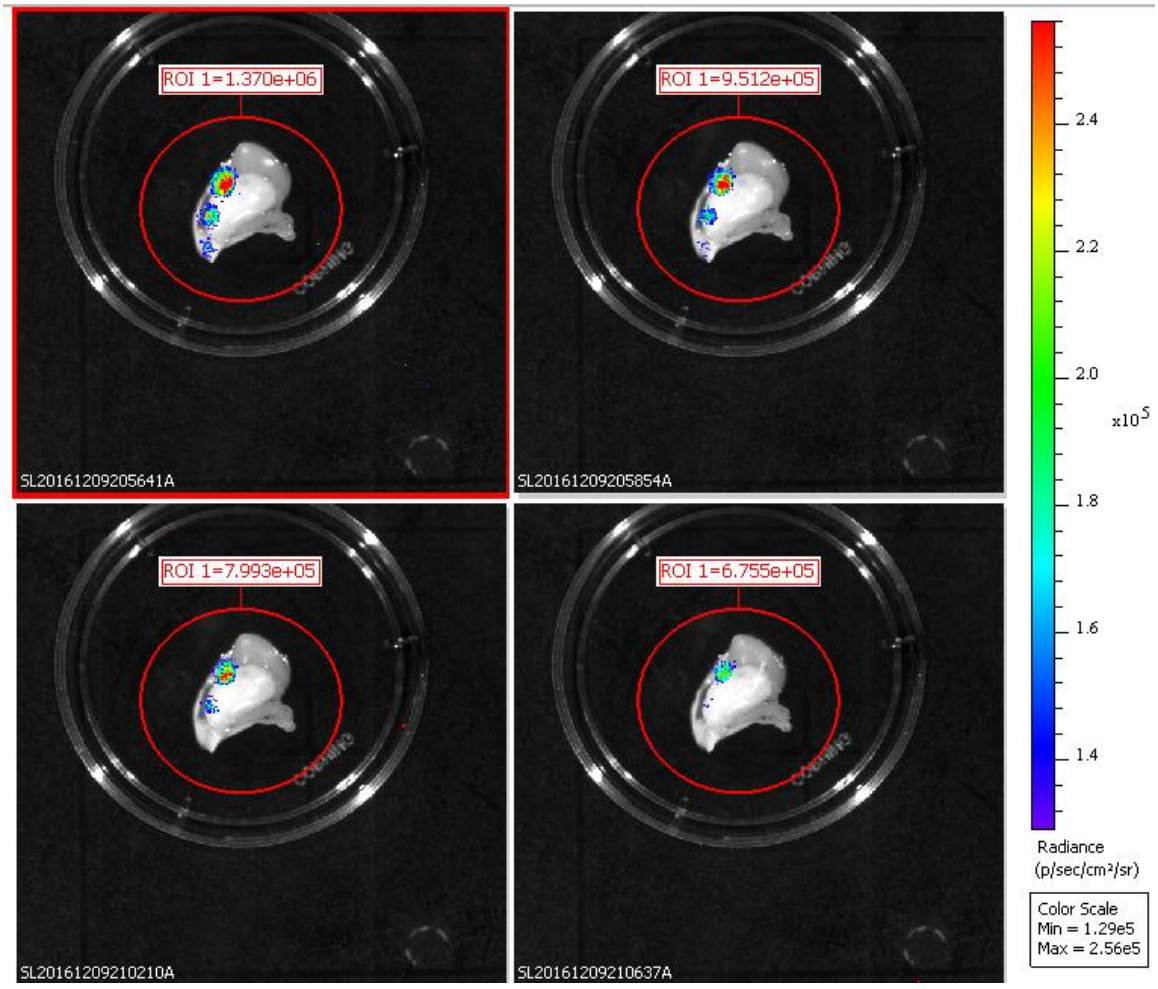

Control - Lung 3:

Day of euthanasia: 14 days post treatment;

ROI data used: 7.886 x 10^5 photons per second;

The segment used for data analysis: The first segment, which was obtained at 8 minutes 41 seconds after the **second** D-luc injection.

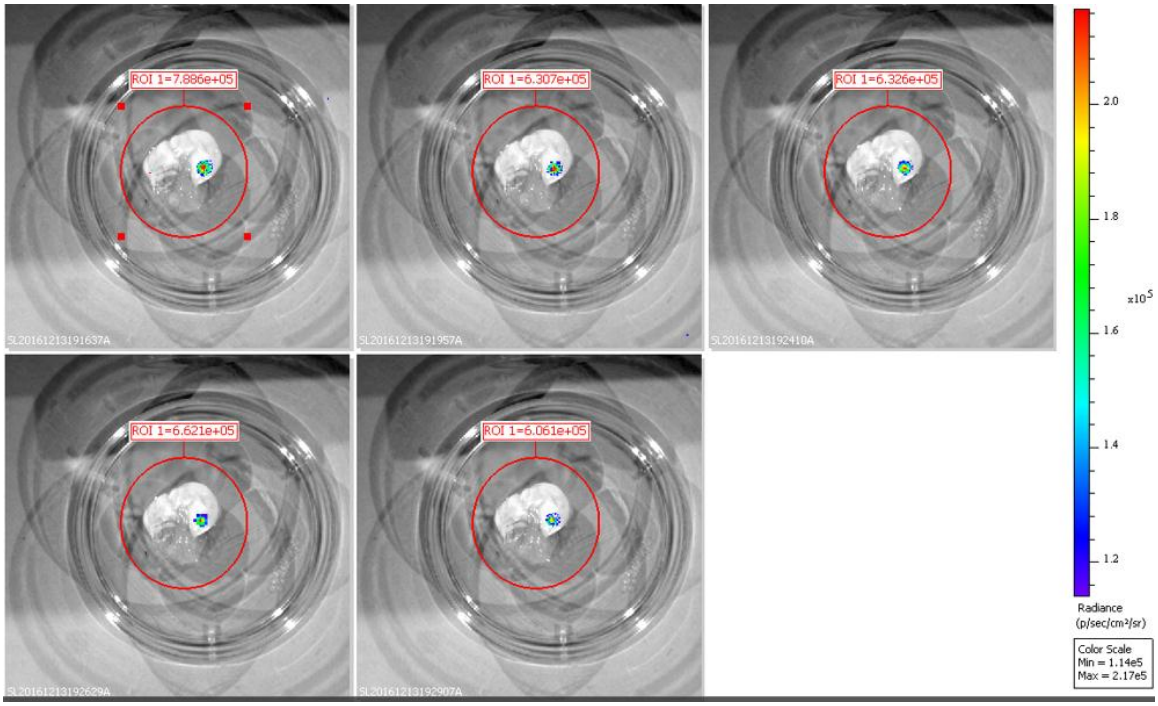

Control - Lung 4:

Day of euthanasia: 24 days post treatment;

ROI data used: Not recorded;

Remarks: The mouse was very weak, it died after the ketamine injection.

Control - Lung 5:

Day of euthanasia: 20 days post treatment;

ROI data used: 2.742×10^7 photons per second;

The segment used for data analysis: The second segment, which was obtained at 27 minutes 10 seconds after the D-luc injection.

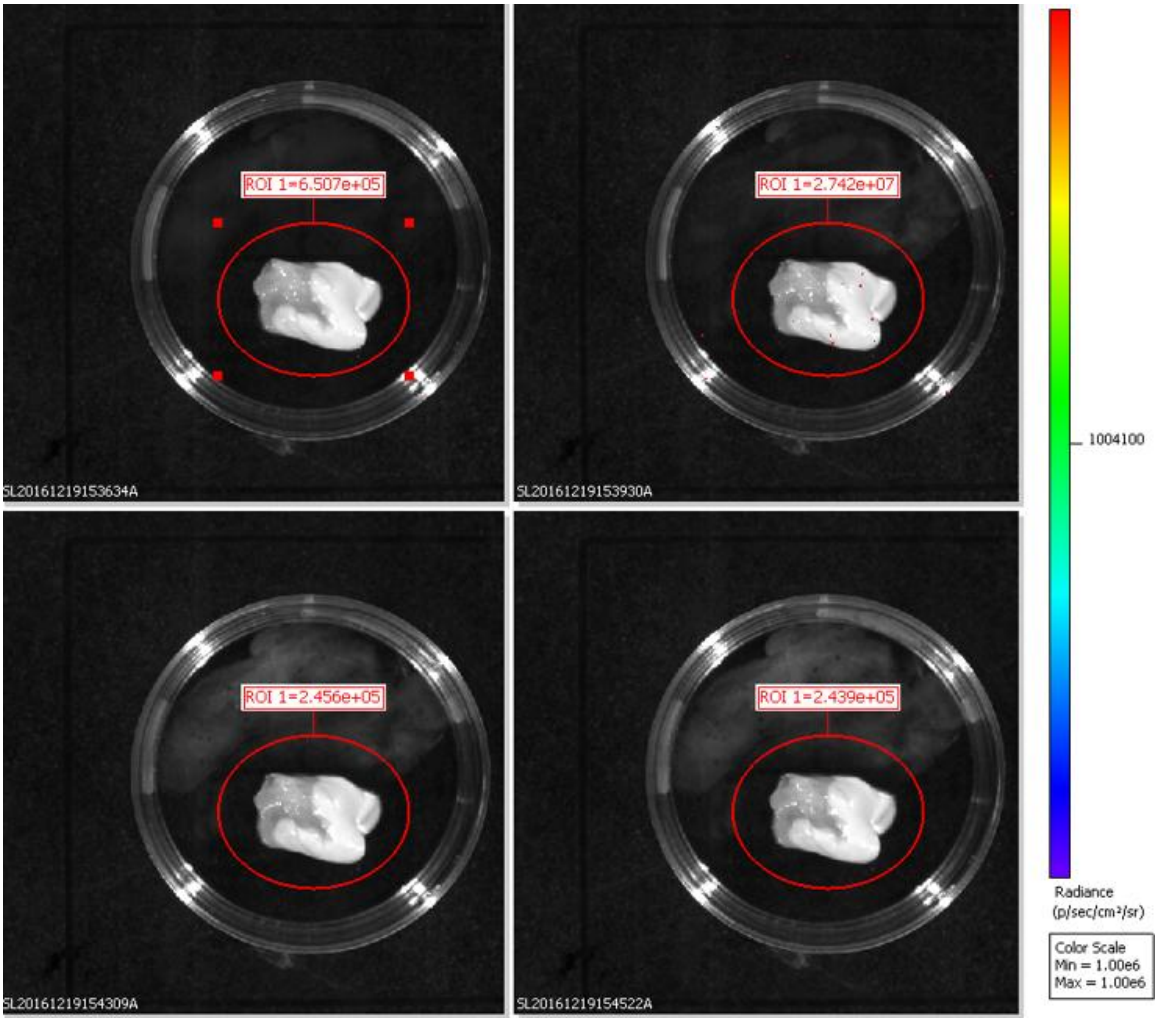

RT-alone - Lung 1:

Day of euthanasia: 22 days post treatment;

ROI data used: Not recorded;

The image used for data analysis: The image below was taken at 28 minutes after the D-luc injection.

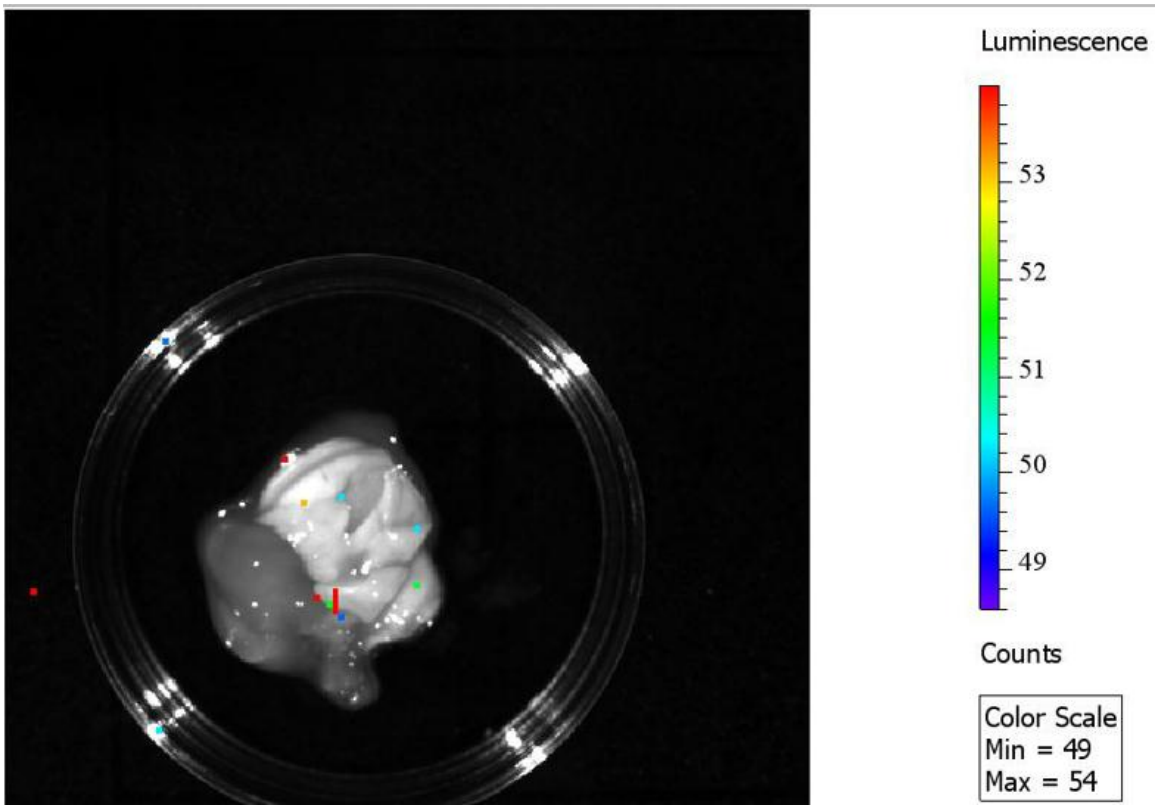

RT-alone - Lung 2:

Day of euthanasia: 16 days post treatment;

ROI data used: 5.556 x 10^5 photons per second;

The segment used for data analysis: The first segment, which was obtained at 25 minutes after the D-luc injection.

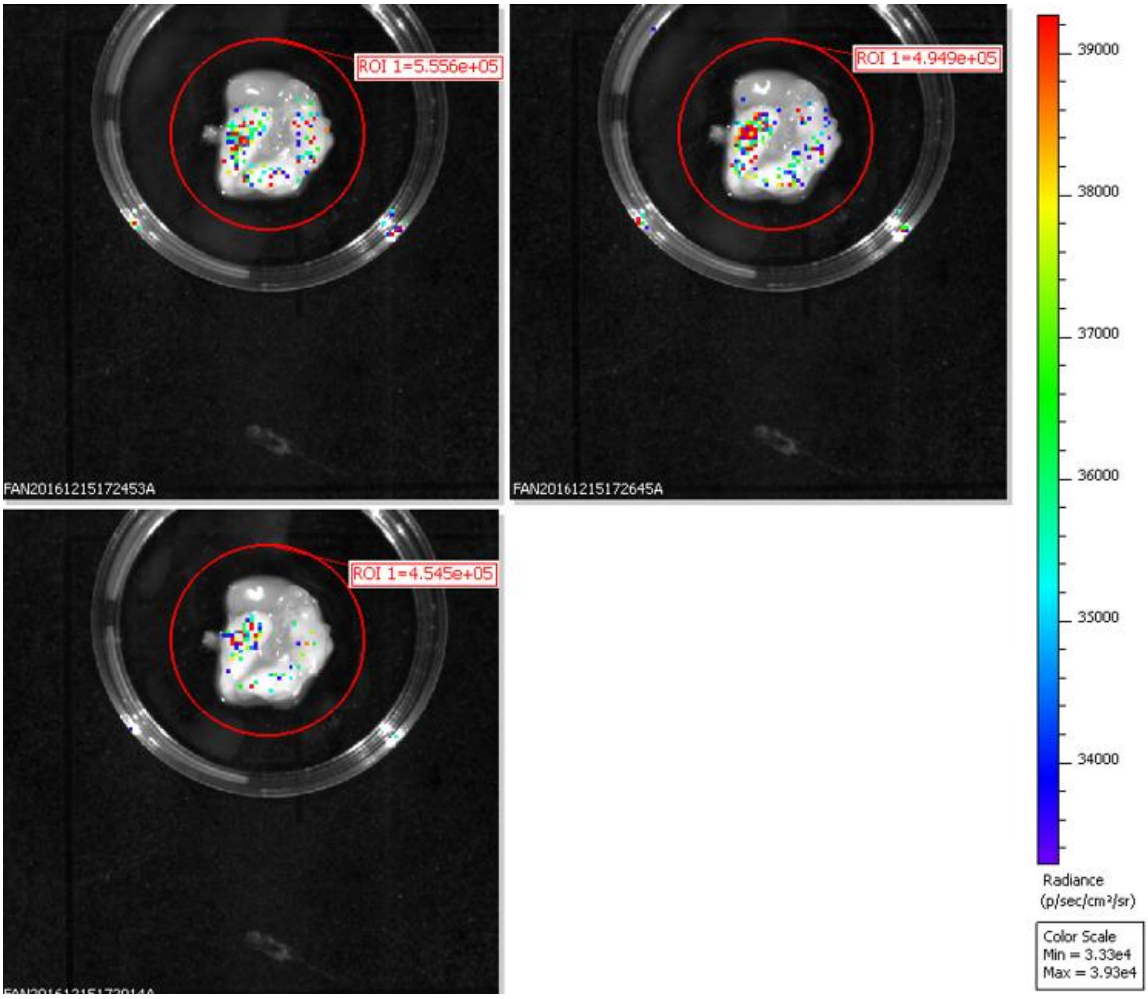

RT-alone - Lung 3:

Day of euthanasia: 8 days post treatment;

ROI data used: Not recorded;

Remarks: Data was missed.

RT-alone - Lung 4:

Day of euthanasia: 14 days post treatment;

ROI data used: 1.001×10^6 photons per second;

The segment used for data analysis: The first segment, which was obtained at 8 minutes after the **second** D-luc injection.

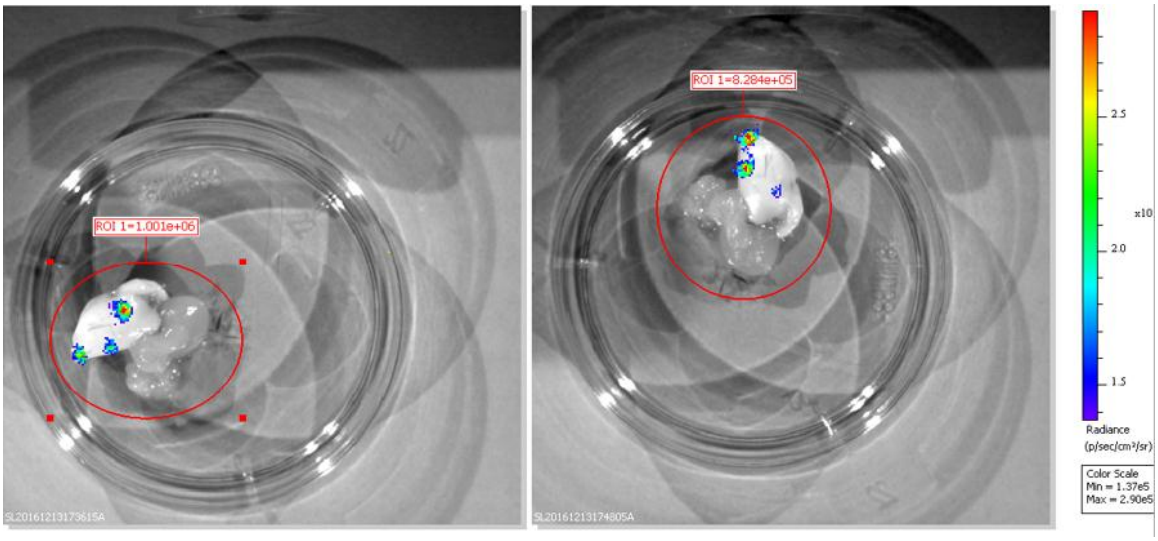

RT-alone - Lung 5:

Day of euthanasia: 14 days post treatment;

ROI data used: 5.321×10^5 photons per second;

The segment used for data analysis: The fifth segment, which was obtained at 23 minutes 45 seconds after the **second** D-luc injection.

Remarks: The IVIS suddenly shut off without automatically saving the images.

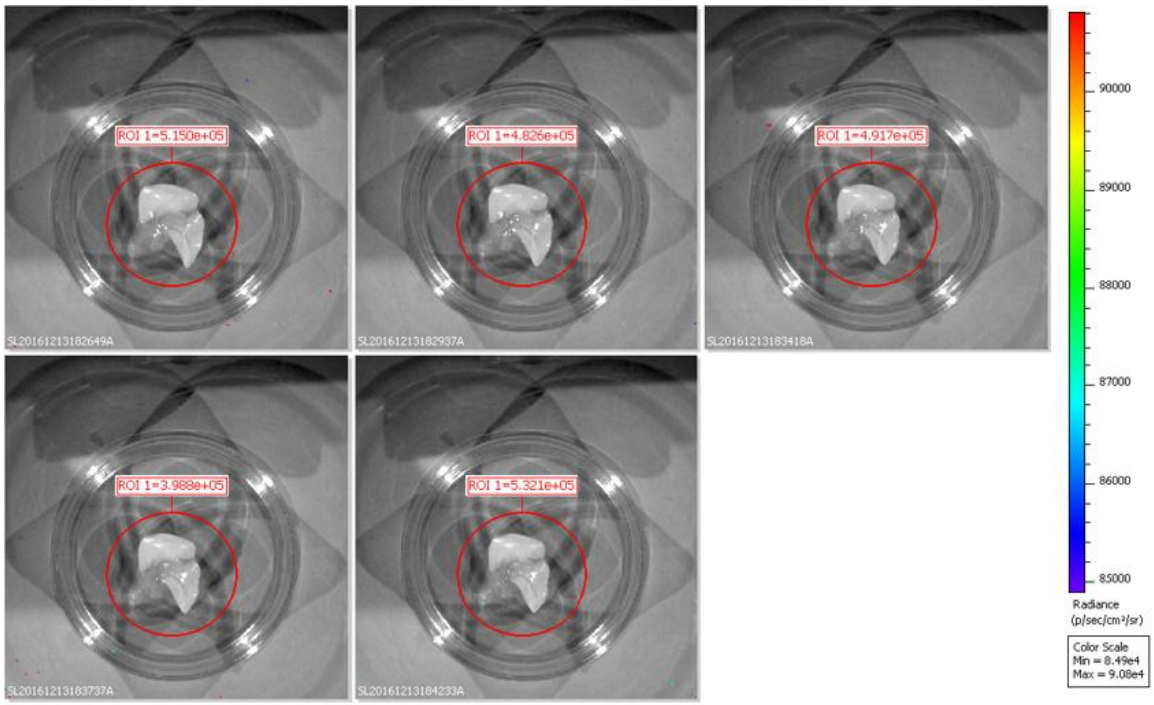

Anti-PD-L1-alone - Lung 1:

Day of euthanasia: 20 days post treatment;

ROI data used: Not recorded;

Remarks: Machine breakdown occurred during the lung imaging process, therefore no ROI analysis was performed.

Anti-PD-L1-alone - Lung 2:

Day of euthanasia: 16 days post treatment;

ROI data used: Not recorded;

Remarks: Due to the machine breakdown, it was not possible to perform lung imaging and ROI analysis. However, I was lucky to have one image before the machine breakdown (as shown below), but no ROI analysis was performed.

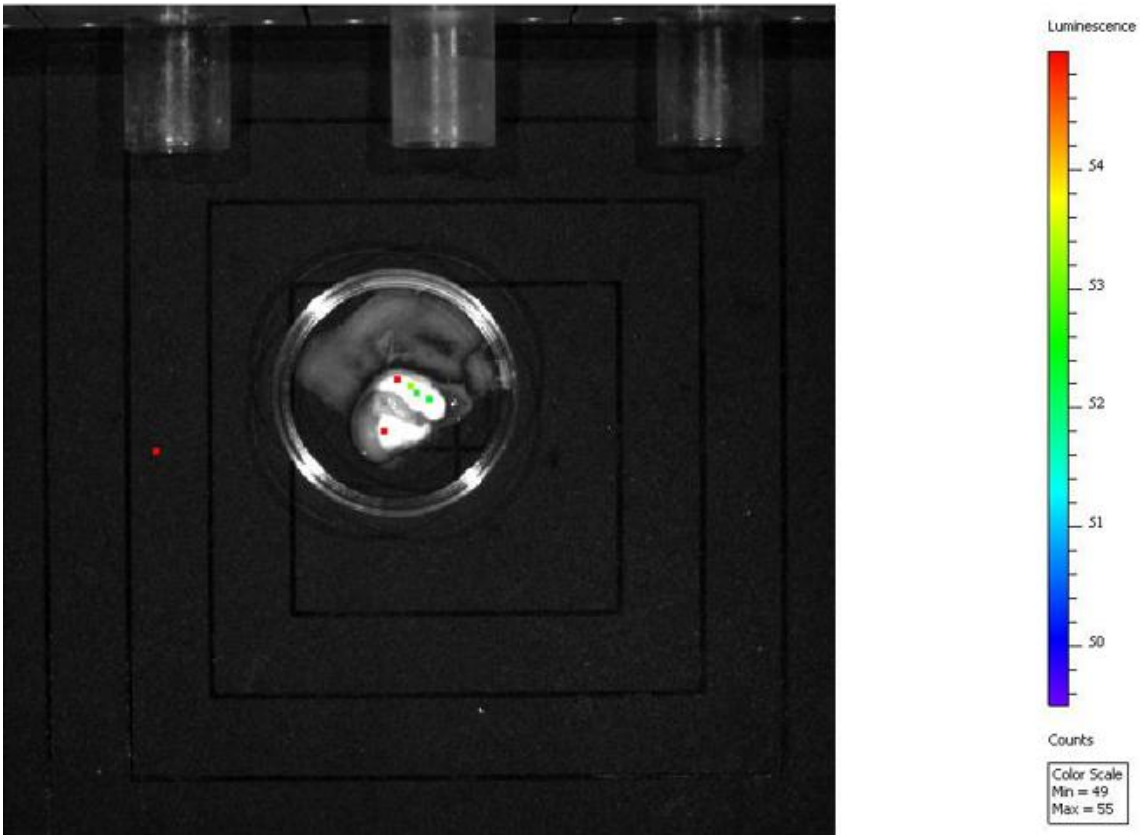

Anti-PD-L1-alone - Lung 3:

Day of euthanasia: 24 days post treatment;

ROI data used: 3.763 x 10^5 photons per second;

The image used for data analysis: The image below was taken at 24 minutes after the D-luc injection.

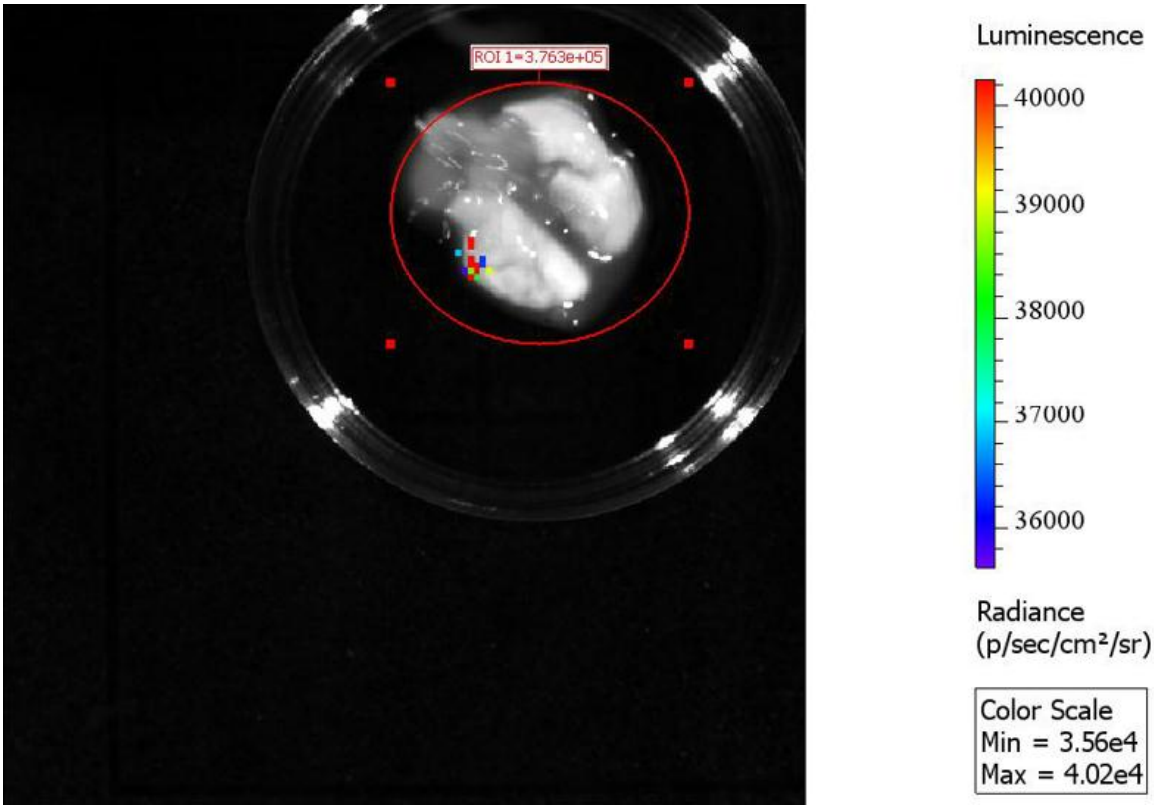

Anti-PD-L1-alone - Lung 4:

Day of euthanasia: 22 days post treatment;

ROI data used: Not recorded;

Remarks: Data lost.

Anti-PD-L1-alone - Lung 5:

Day of euthanasia: 22 days post treatment;

ROI data used: 2.877×10^5 photons per second;

The image used for data analysis: The image below was taken at 26 minutes after the D-luc injection.

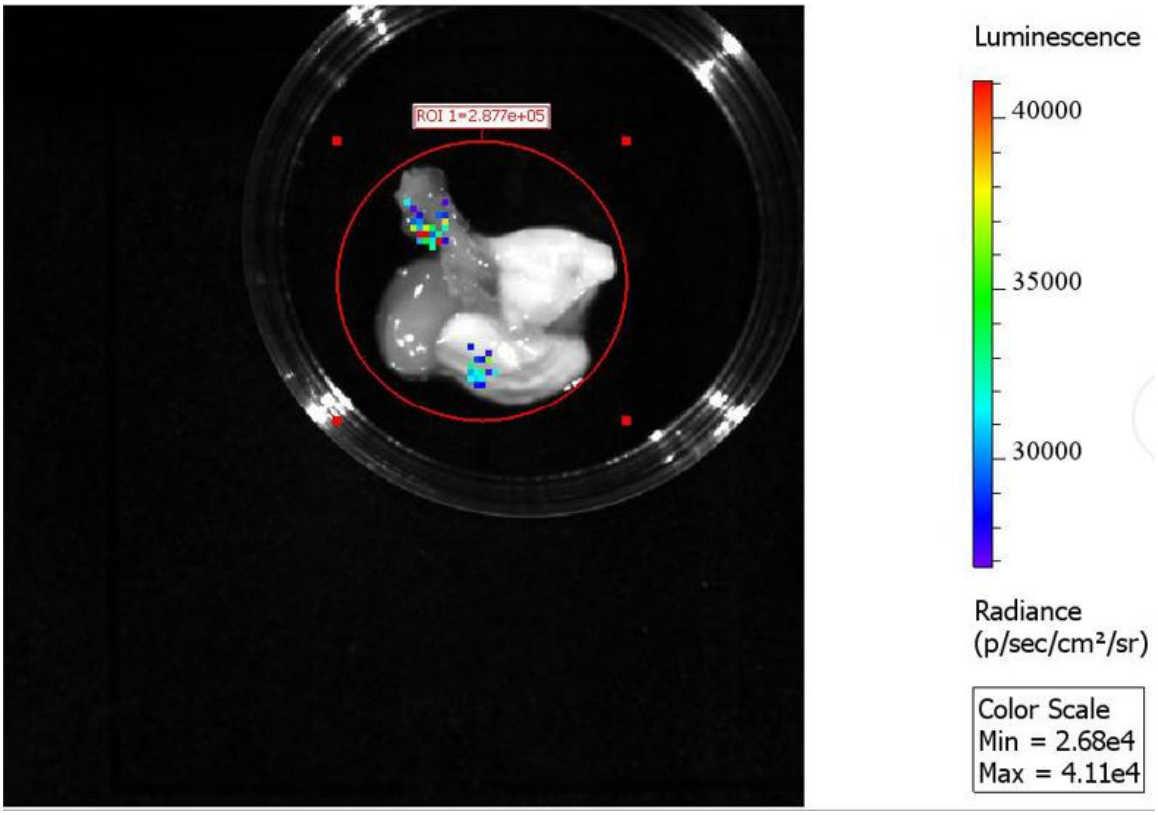

RT + Anti-PD-L1 –Lung 1:

Day of euthanasia: 24 days post treatment;

ROI data used: 2.363 x 10^5 photons per second;

The image used for data analysis: The image below was taken at 23 minutes after the D-luc injection.

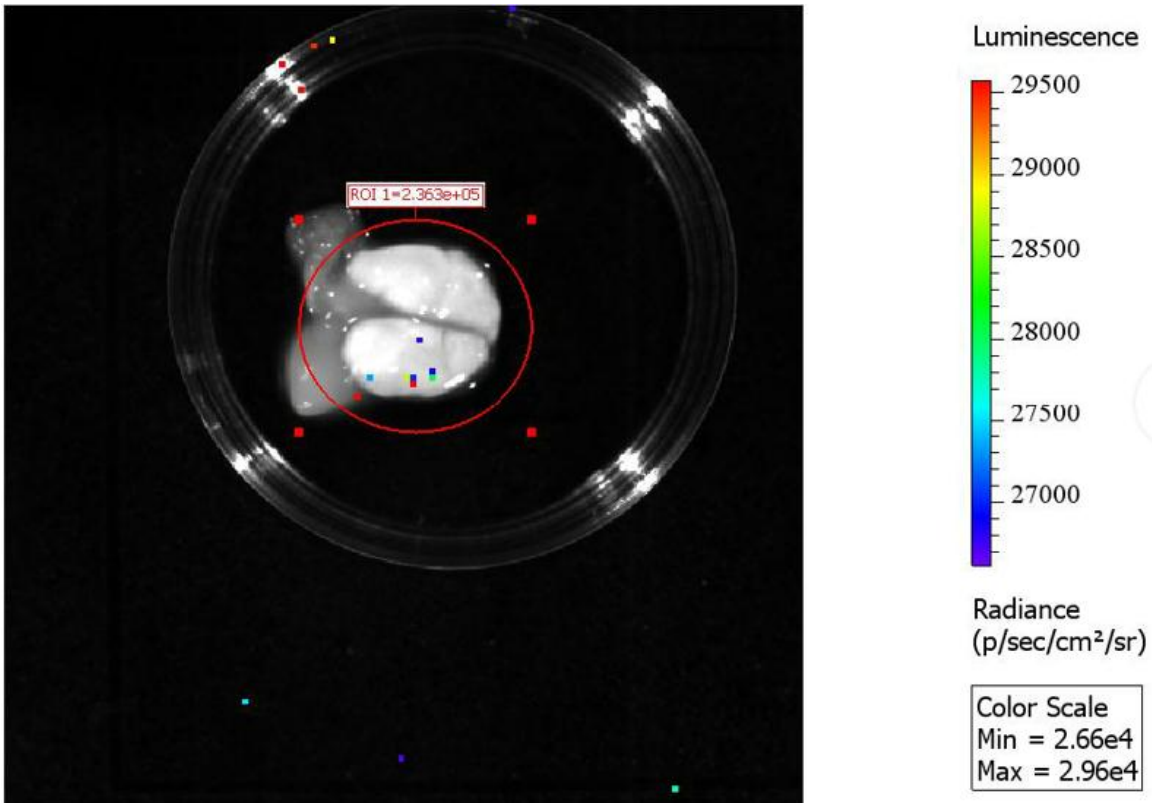

RT + Anti-PD-L1 –Lung 2:

Day of euthanasia: 13 days post treatment;

ROI data used: 2.609×10^5 photons per second;

The image used for data analysis: The image below was taken at 12 minutes after the **second** D-luc injection.

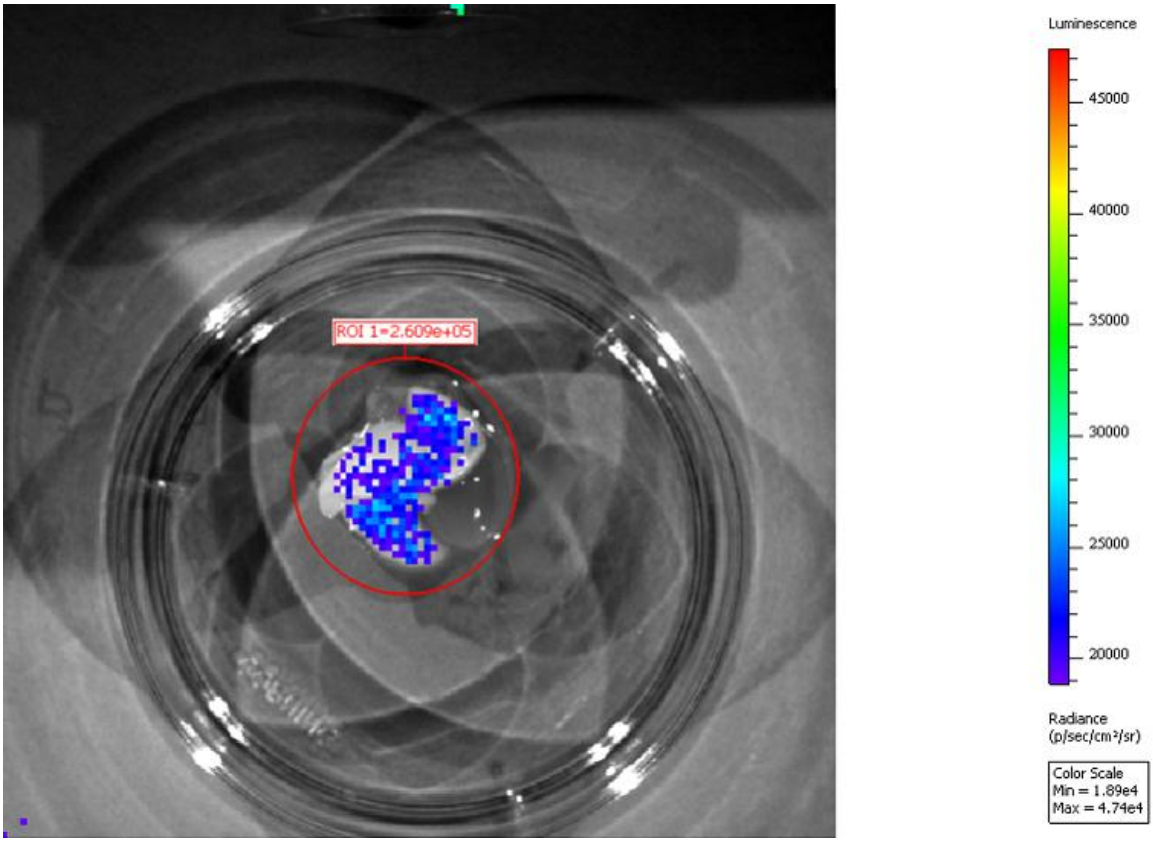

RT + Anti-PD-L1 –Lung 3:

Day of euthanasia: 28 days post treatment;

ROI data used: 2.749 x 10^5 photons per second;

The image used for data analysis: The image below was taken at 5 minutes 40 seconds after the **second** D-luc injection.

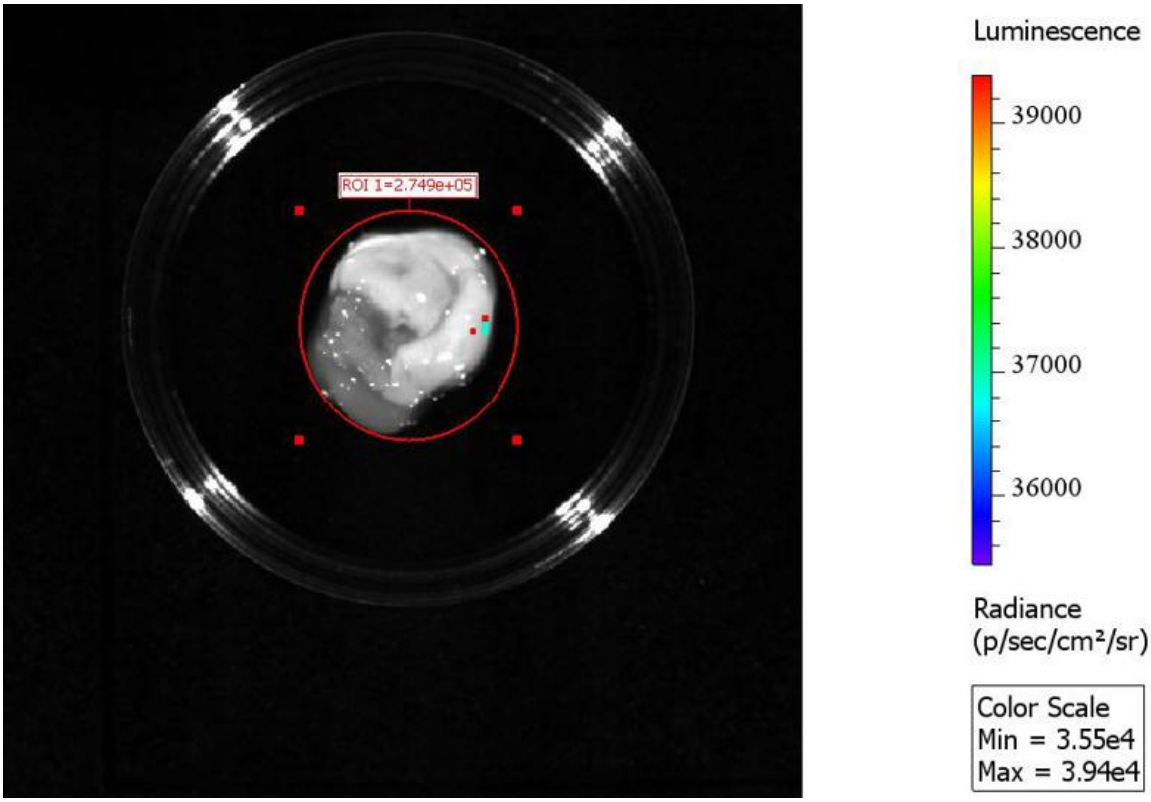

RT + Anti-PD-L1 –Lung 4:

Day of euthanasia: 28 days post treatment;

ROI data used: 4.468 x 10^5 photons per second;

The image used for data analysis: The image below was taken at 23 minutes after the D-luc injection.

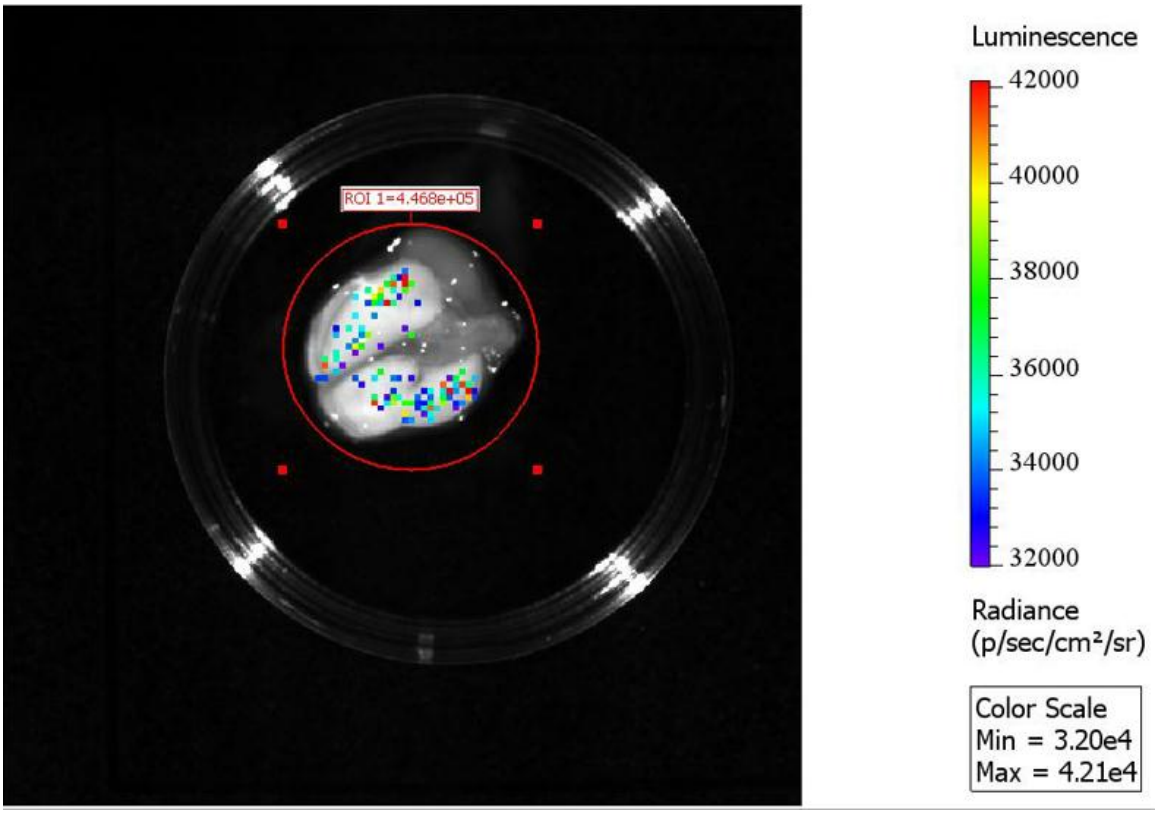

RT + Anti-PD-L1 –Lung 5:

Day of euthanasia: 10 days post treatment;

ROI data used: 3.022 x 10^6 photons per second;

The segment used for data analysis: The second segment, which was obtained at 35 minutes after the D-luc injection.

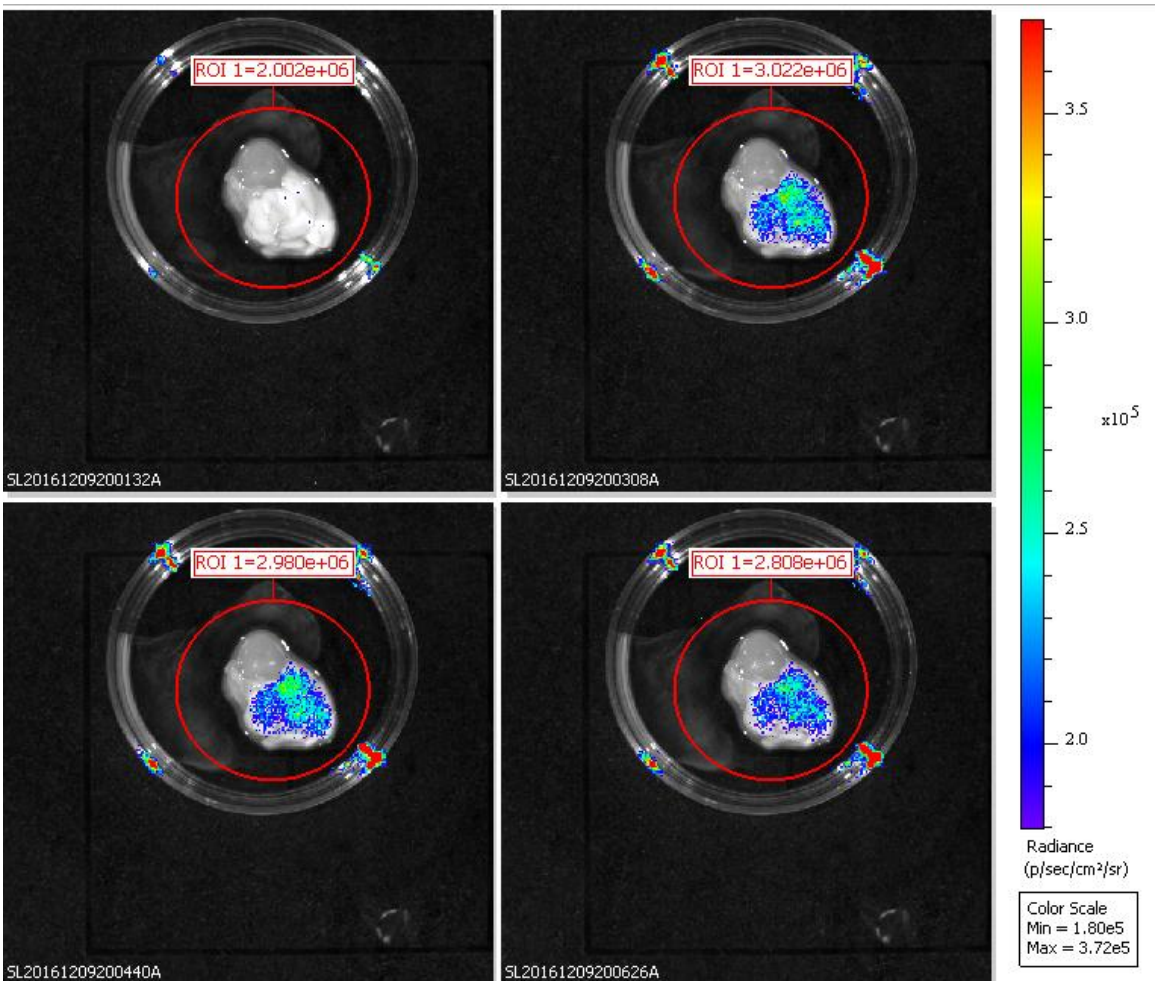

7. Appendix B:

(Information in this section directly refers to *"Modulation of Oxidative Stress Influences Tumor Response to Therapy"*[43], conducted by BOSS, MARY-KEARA)

Radiation Dosimetry:

For the sake of determining the dose delivered to the directly irradiated tissue, blocked ("bystander") tissue, and the surrounding critical organs (lungs and spine), focal dosimetry data for regions of interest within and around the radiation treatment field was obtained by using a nano-crystalline scintillator fiber optical detector (nanoFOD), **as shown in the figure below.** (See BOSS, MARY-KEARA. *Modulation of Oxidative Stress Influences Tumor Response to Therapy*[43].)

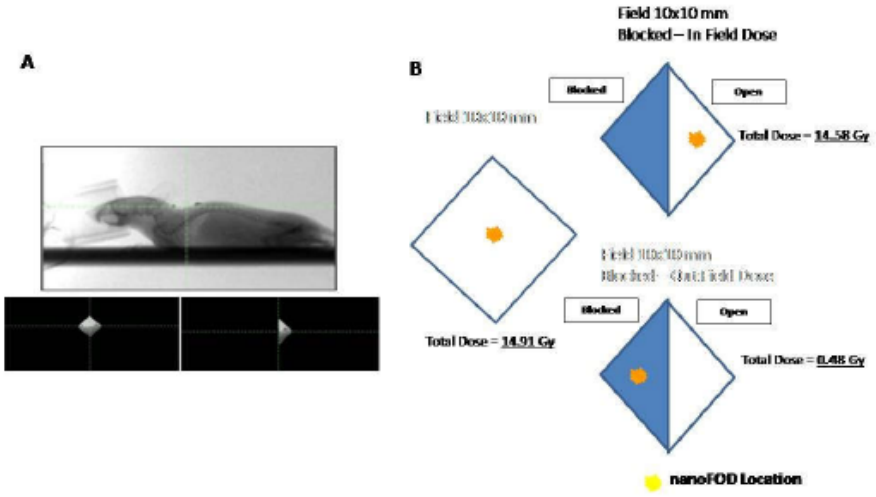

Figure 2.7 Orthotopic dorsal mammary tumor radiation technique and focal dosimetry. (A) A diamond shaped radiation field was used to target the radiation beam to the dorsal mammary tumor while avoiding radiation exposure to the lungs and the spine. (B) Focal dosimetry data obtained using the nanoFOD system defined the radiation dose at the center of the open field to be 14.91Gy, the center of the open portion of the 50% tumor radiation field to be 14.58Gy, and the center of the blocked portion of the 50% tumor radiation field to be 0.48Gy

In Boss' study[43], 15 Gy of single radiation dose was delivered using a micro-CT irradiator. The nanoFOD system determined the dose to the center of the open field to be 14.91 Gy, with a percentage difference of 0.6%. In the current study, 10 Gy of single radiation dose was delivered. It can be, therefore, assumed that the center of the open field received approximately 10 Gy.

Apart from this, in Boss's study[43], regional dosimetry with a rodentmorphic 3D dosimetry system and SmART-Plan small animal radiation treatment planning software were employed to obtain regional dosimetry data in order to create dose volume histograms (DVHs) for tumor, lung, and spinal cord volumes, **as shown in the figure below**.(See BOSS, MARY-KEARA. *Modulation of Oxidative Stress Influences Tumor Response to Therapy.* [43])

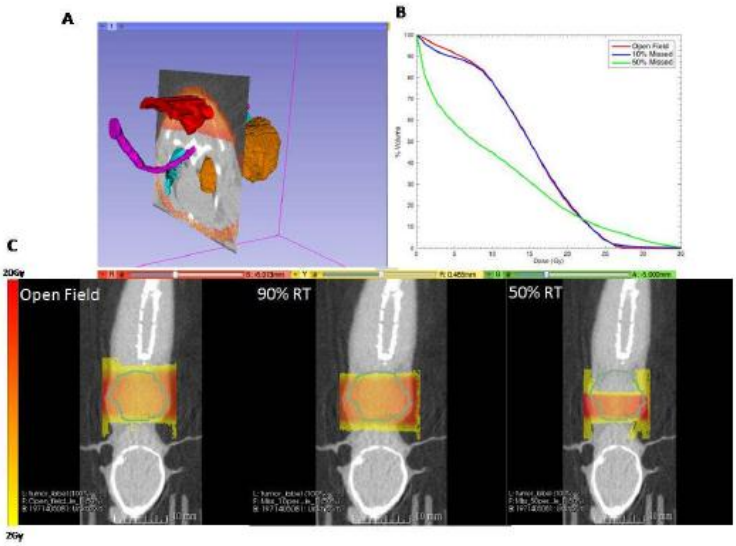

Figure 2.8 Orthotopic dorsal mammary tumor radiation technique and regional dosimetry. (A – C) Regional dosimetry data was obtained using a rodentmorphic 3D dosimetry system and SmART-Plan small animal radiation treatment planning software in order to generate dose volume histograms (DVH) (B) for tumor, lung, and spinal cord volumes (A). The highest 20% of the dose delivered to the tumor volume (D20) was 20.5Gy, 20.3Gy, and 18.9Gy for the 100%, 90%, and 50% irradiated tumors, respectively (C).

8. References:

[1] Douglas H. Weitzel, Chen-Ting Lee, Yulin Zhao et al (2015). Functional imaging of tumor radiation response in combination with immune checkpoint blockade (Unpublished doctoral dissertation). Duke University Medical Center, Durham, NC, USA.

[2] Mellman I, Coukos G, Dranoff G. Cancer immunotherapy comes of age. Nature 2011; 480: 480–9.

[3] Yee C. The use of endogenous T cells for adoptive transfer. Immunol Rev 2014; 257: 250–63.

[4] Maus MV, Grupp SA, Porter DL, June CH. Antibody-modified T cells: CARs take the front seat for hematologic malignancies. Blood 2014; 123: 2625–35.

[5] Rosenberg SA, Restifo NP. Adoptive cell transfer as personalized immunotherapy for human cancer. Science 2015; 348: 62–8

[6] Douglas Hanahan, Robert A. Weinberg. Hallmarks of Cancer: The Next Generation, Cell 144, March 4, 2011 ©2011 Elsevier Inc.

[7] Parisa Momtaz, Michael A Postow, Immunologic checkpoints in cancer therapy: focus on the programmed death-1 (PD-1) receptor pathway. Pharmacogenomics and Personalized Medicine 2014:7 357-365

[8] Ryungsa Kim, Manabu Emi, Kazuaki Tanabe. Cancer immunoediting from immune surveillance to immune escape. Immunology, 2007 May; 121(1):1-14. Doi:10.1111/j.1365-2567.2007.02587.x

[9] David Loose, Christophe Van de Wiele. The immune system and cancer. Cancer Biotherapy and Radiopharmaceuticals. June 2009; 24(3):369-376. Doi:10.1089/cbr.2008.0593

[10] Keishi Adachi, Koji Tamada. Immune checkpoint blockade opens an avenue of cancer immunotherapy with a potent clinical efficacy. Cancer Science 2015 Aug; 106(8): 945-950. Doi: 10.1111/cas.12695.

[11] Micheal A. Postow, Margaret K. Callahan, Jedd D. Wolchok. Immune checkpoint blockade in cancer therapy. J Clin Oncol. 2015 June 10; 33(17):1947-1982. Doi: 10.1200/JCO.2014.59.4358.

[12] Drew M. Pardoll. The blockade of immune checkpoints in cancer immunotherapy. Nat Rev Cancer. 2012 Apr; 12(4): 252–264. Doi: 10.1038/nrc3239.

[13] Daniel Sanghoon Shin, Antoni Ribas. The evolution of checkpoint blockade as a cancer therapy: what's here, what's next? Curr Opin Immunol 2015 Apr; 33: 23–35. Doi: 10.1016/j.coi.2015.01.006

[14] Dana R. Leach, Matthew F. Krummel, James P. Allison. Enhancement of antitumor immunity by CTLA-4 blockade. Science 22 March 1996; Vol. 271, Issue 5256, pp. 1734–1736. Doi: 10.1126/science.271.5256.1734.

[15] Haidong Dong, Scott E. Strome, Diva R. Salomao et al. Tumor-associated B7-H1 promotes T-cell apoptosis: a potential mechanism of immune evasion. Nature Medicine, 2002 Aug; 8(8): 793–800. Doi: 10.1038/nm730.

[16] Helga Schneider, Jos Downey, Andrew Smith et al. Reversal of the TCR stop signal by CTLA-4. Science 29 Sep 2006; Vol. 313, Issue 5796, pp1972–1975. Doi: 10.1126/science.1131078.

[17] Theresa L. Walunas, Deborah J. Lenschow, Christina Y. Bakker et al. CTLA-4 can function as a negative regulator of T cell activation. Immunity August 1994; Volume 1, Issue 5, pp. 405–413.

[18] James P. Allison, Matthew F. Krummel. The yin and yang of T cell costimulation. Science 10 Nov 1995; Vol. 270, Issue 5239, pp. 932–3. Doi: 10.1126/science.270.5238.932.

[19] Y Ishida, Y Agata, K Shibahara, T Honjo. Induced expression of PD-1, a novel member of the immunoglobulin gene superfamily, upon programmed cell death. EMBO J 1992 Nov; 11(11): 3887–3895.

[20] Hiroyuki Nishimura, Masato Nose, Hiroshi Hiai, Nagahiro Minato, Tasuku Honjo. Development of lupuslike autoimmune diseases by disruption of the PD-1 gene encoding an ITIM motif-carrying immunoreceptor. Immunity 1 August 1999; Volume 11, Issue 2, pp. 141–151.

[21] Hiroyuki Nishimura, Taku Okazaki, Yoshimasa Tanaka et al. Autoimmune dilated cardiomyopathy in PD-1 receptor-deficient mice. Science 12 Jan 2001; Vol. 291, Issue 5502, pp. 319–322. Doi: 10.1126/science.291.5502.319.

[22] Clinical Practice Guidelines in Oncology. Melanoma v3. 2014. National Comprehensive Cancer Network. 2014 Retrieved from http://www.nccn.org.

[23] Elad Sharon, Howard Streicher, Priscila Goncalves, Helen X. Chen. Immune checkpoint inhibitors in clinical trials. Chin J Cancer. 2014 Sep; 33(9): 434-444. Doi: 10.5732/cjc.014.10122.

[24] Manish J. Butte, Mary E. Keir, Theresa B. Phamduy et al. Programmed death-1 ligand 1 interacts specifically with the B7-1 costimulatory molecule to inhibit T cell responses Immunity, 2007 July, Volume 27, Issue 1, pp.111-222, CrossRef, Medine. Doi: 10.1016/j.immuni.2007.05.016.

[25] Howard L. Kaufman, Janice M. Mehnert. Melanoma. Cancer Treatment and Research, Series Editor: Steven T. Rosen. Springer, Indexed in PubMed/Medline. Pp.239.

[26] Julie R Brahmer, Scott S. Tykodi, Laura Q.M. Chow, et al. Safety and activity of anti-PD-L1 antibody in patients with advanced cancer. N Engl J Med 2012; 366: 2455-2465, June 28, 2012 CrossRef, Medline. Doi: 10.1056/NEJMoa1200694.

[27] Christina Twyman-Saint Victor, Andrew J. Rech, Amit Maity et al. Radiation and dual checkpoint blockade activates non-redundant immune mechanisms in cancer. Nature. 2015 Apr 16; 520(7547), pp. 373-377. Doi: 10.1038/nature14292.

[28] Tomas Powles, Nicholas J. Vogelzang, Gregg Daniel Fine, et al. Inhibition of PD-L1 by MPDL3280A and clinical activity in patients with metastatic urothelial bladder cancer (UBC). J Clin Oncol 32:5s, 2014 (suppl; abstr 5011).

[29] Neil Howard Segal, Scott Joseph Antonia, Julie R. Brahmer, et al. Preliminary data from a multi-arm expansion study of MEDI4736, and anti-PD-L1 antibody. J Clin Oncol 32:5s, 2014 (suppl; abstr 3002).

[30] Roy S. Herbst, Michael S. Gordon, Gregg Daniel Fine, et al. A study of MPDL3280A, an engineered PD-L1 antibody in patients with locally advanced or metastatic tumors. J Clin Oncol 31, 2013 (suppl; abstr 3000).

[31] Christopher Ryan Heery, Geraldine Helen O' Sullivan Coyne, Ravi Amrit Madan, et al. Phase I open-label, multiple ascending dose trail of MSB0010718C, an anti-PD-L1 monoclonal antibody, in advanced solid malignancies. J Clin Oncol 32:5s, 2014 (suppl; abstr 3064).

[32] Antonin Levy, Cyrus Chargari, Morgane Cheminant et al. Radiation therapy and immunotherapy: Implications for a combined cancer treatment. Critical Reviews in Oncology/Hematology 85 (2013) 278-287.

[33] Raben M, Walach N, Galili U, Schlesinger M. The effect of radiation therapy on lymphocyte subpopulations in cancer patients. Cancer 1976; 37(3): 1417-1421.

[34] Formenti SC, Demaria A. Systemic effects of local radiotherapy. Lancet Oncology 2009;10: 718-726.

[35] Demaria S, Bhardwaj N, McBride WH, Formenti SC. Combining radiotherapy and immunotherapy: a revived partnership. International Journal of Radiation Oncology, Biology, Physics 2005;63: 655-666.

[36] Sandra Demaria, Noriko Kawashima, Anne Marie Yang et al. Immune-mediated inhibition of metastases after treatment with local radiation and CTLA-4 blockade in a mouse model of breast cancer.

[37] Liugu Deng, Hua Liang, Byron Burnette et al. Irradiation and anti-PD-L1 treatment synergistically promote antitumor immunity in mice.

[38] Jing Zeng, Alfred P. See, Jillian Phallen et al. Anti-PD-1 blockade and stereotactic radiation produce long-term survival in mice with intracranial gliomas. Int J Radiat Oncol Biol Phys. 2013 Jun 1:86(2): 343-349. Doi: 10.1016/j.ilrobp.2012.12.025.

[39] Maria Grazia Ruocco, Karsten A. Pilones, Noriko Kawashima et al. Suppressing T cell motility induced by anti-CTLA-4 monotherapy improves antitumor effects. J Clin Invest. October 1, 2012; 122(10): 3718-3730. Doi: 10.1172/JCI61931.

[40] Michael A. Postow, Margaret K. Callahan, Christopher A. Barker et al. Immunologic correlates of the abscopal effect in a patient with melanoma. N Engl J Med 2012; 366: 925-931, March 8, 2012. Doi: 10.1056/NEJMoa1112824.

[41] Roy S. Herbst, Jean-Charles Soria, Marcin Kowanetz et al. Predictive correlates of response to the anti-PD-L1 antibody MPDL3280A in cancer patients. Nature. 2014 Nov 27; 515(7528): 563-567. Doi: 10.1038/nature14011.

[42] Paul C. Tumeh, Christina L. Harview, Jennifer H. Yearley et al. PD-1 blockade induces responses by inhibiting adaptive immune resistance. Nature 515, 568-571 (27 November 2014). Doi: 10.1038/nature13954.

[43] Mart-Keara Boss (2016). Modulation of Oxidative Stress Influences Tumor Response to Therapy (Unpublished doctoral dissertation), North Carolina State University, Raleign, North Carolina, USA .